Preparation and characterization of catalysts

Thesis submitted in accordance with the
requirements of the University of Cardiff
for degree of Doctor in Philosophy
by

Gerolamo Budroni

November 2004

ProQuest LLC
789 East Eisenhower Parkway
P.O. Box 1346
Ann Arbor, MI 48106-1346

Abstract

The preparation of a supported metal catalyst is a complex process where some steps are often not completely understood. The work of this thesis is focused on understanding and improving the processes involved in the preparation of a catalyst, and in particular aims to find a route for the preparation of homogeneous supported alloy catalysts and to establish how particle size can be controlled during the preparation. One of the difficulties preparing homogeneous alloys with traditional methods is the formation of single metal particles. To avoid this, a method based on the selective reduction of a second metal on the surface of a single metal supported catalyst (parent) was chosen. This method has the advantage of producing bimetallic particles where the two metals are in close proximity and can be subsequently alloyed by thermal treatment. Due to the difficulty in characterising supported alloy nano-particles, a combination of different techniques (*in situ* XRD, XPS, temperature programmed reduction, pulse chemisorption, temperature programmed hydrogen desorption etc.) were used to investigate the prepared catalysts and to study the degree of alloying as a function of the reduction temperature. The catalysts were also tested in a fixed bed gas phase reactor for the hydrogenation of crotonaldehyde. To achieve a background of knowledge on the single metal parents used for the selective deposition method, $Pd\text{-}Al_2O_3$, $Ni\text{-}Al_2O_3$, and $Co\text{-}Al_2O_3$ were prepared and characterised. Some important aspects developed in this preliminary work were the solubility of hydrogen in Pd (and its use in characterizing Pd particle size and degree of alloying) and the interaction between Co and Ni with the alumna support. After the single metal study the deposition of Ni over Pd and of Pd over Ni were attempted. The latter system led to the successfully preparation of core-shell particles where the Pd covers the Ni. The $Pd\text{-}Ni\text{-}Al_2O_3$ bimetallic catalyst was then reduced at different temperatures in order to alloy the particles. The results revealed that alloys could be formed at relatively low temperature (300°C). The last part of the work diverged from the main path of my project. It was a work of pure characterisation using *in situ* techniques. An interesting series of XRD and Raman *in situ* experiments on vanadium phosphorus oxide (VPO) catalysts revealed the formation of a metastable phase (ω-$VOPO_4$). The study of the transformation of this phase induced by various reactants under reaction conditions provided useful information in understanding the structure of the active catalyst and cast new light on the on role of the reactant and product gas mixtures in forging the structure of the catalyst.

Microform

This work aims to find a route for the preparation of homogeneous alloy supported catalysts and to establish how particle size can be controlled during the preparation. The chosen strategy for achieving this goal is the selective deposition of a second metal on the surface of a single metal catalyst (parent) and subsequent thermal treatment for the alloying of the particles. In this work, the characterization is crucially important and the catalysts were characterized by a variety of techniques (XRD, XPS, TPR, TPHS, PC, AA etc). The work started with the preparation and characterization of the parents Pd-Al_2O_3, Ni-Al_2O_3, and Co-Al_2O_3 (including the investigation of the hydrogen solubility in Pd and the interaction between Ni and Co with alumina). Pd was then reduced on Ni-Al_2O_3 forming a core-shell bimetallic particle. The characterization revealed that the metals alloying is promoted by reduction treatment at temperatures higher than 300°C. The last part of the work concerns the *in situ* study of the transformation of a metastable phase of a vanadium phosphorus oxide catalyst activated under reaction condition by different reactant.

Dedicadu

a chie a tribagliare m'ada imparadu.

Acknowledgements

I would like to thank my supervisor Professor Graham Hutchings for giving me the chance of doing this PhD. His formidable contagious enthusiasm and the never-ending energy put into the work have been great lessons. Thank also to my other supervisors Stuart Taylor, Albert Carley and Colin Rhodes, for encouraging and supporting me during all this time and for the laborious work of teaching a bit of healthy British optimism.

Thanks to "Johnson Matthey" and especially to Peter Williams for funding this research and for the trust given to me.

Thanks to Pat for the lovely way to cheer up all of us "in front of that door".

Thank to Professor Schlögl and Frank for their collaboration and for the welcome given to me in Berlin.

Thanks to the Italian contingent in Cardiff and especially Luisa, Silvio Andrea and Federica that welcomed me when I first arrived and Fabrizio and Daniele and all the others. Thanks to all the lab members for sharing joy and pain. It has been a pleasure spending my time with you. Thanks to Hongmei for being very close in the moments that most count and to Marco for pleasant and inspiring discussions on chemistry, science and every thing else. Thanks also to special people as Leng Leng, Pablo and Andy whom I have shared some brilliant moments. Thanks to all the people who made for me three fantastic years.

Ringrazio orgogliosamente i miei genitori. Questo traguardo "dottore in filosofia" lo devo ai vostri sacrifici e per questo ve ne saro sempre riconoscente.

The biggest thank is obviously for Maria. You made this real, you made it so beautiful.

Contents

List of abbreviations

AA	Atomic absorption
Abs	Absorption
Ads	Adsorption
ALD	Aldrich
Alu	Alumina
Ca.	Approximately
Sec.	Section
BET	Brunnauer Emmett Teller
Conc.	concentrate
DSC	Differential scanning calorimetric
Et al.	*Et altri*
EPR	Electron paramagnetic resonance
EXAFS	Extended x-ray absorption fine structure
FE	Fraction exposed
FTIR	Infrared Fourier transformed
GC	Gas chromatograph
IWI	Incipient wetness impregnation
MA	Maleic anhydride
MAUD	Material analysis using diffraction
Red.	Reduction
SEM	Scanning electron microscopy
STEM	Scanning transmission electron microscopy
TCD	Thermal conductivity detector
TEM	Transmission electron microscopy
TGA	Thermo-gravimetric analysis
TPD	Temperature programmed desorption

TPHD	Temperature programmed hydride decomposition
TPHS	Temperature programmed hydride sorption
TPR	Temperature programmed reduction
VP-d	VPO prepared via dihydrate
VP-o	VPO prepared via organic route
wt	Weight
XRD	X-ray diffraction
XPS	X-ray photoelectron spectroscopy

Chapter 1

1 Introduction

1.1 Introduction

The wide spread use of catalysts in the chemical industry has contributed to shape the world were we live. Oil derivatives, synthetic materials, fertilisers and medicines that have improved the quality of live could become largely available at low price thanks to industrial production that depends on catalysis. The reduction of polluting gas emissions in the atmosphere in the developed world was also achievable thanks to the development of ever more efficient catalysts. The demand for better catalysts increases constantly for economic and environmental reasons and today catalytic research is promoted and sustained by many developed countries.

From a scientific point of view heterogeneous catalysis is an exciting field. Despite the fact that we produce catalysts able to activate very complex reaction, some extremely simple reactions are still not fully understood. So today catalysis research can be divided in two main parts. The first is empirical research that aims to find the best catalyst for a specific reaction, mainly by testing a large number of them. The second concentrates attention on understanding the principles and mechanisms of catalysis. In recent years this second objective, has reaped the benefit of development of surface techniques, *in situ* analysis, computer simulation, and high-resolution microscopy that reach the point of catching time resolved atomic scale images of surface catalysis.[1] The combination of understanding and testing catalysts (as in most scientific fields) is the route to the improvement of the catalysts and eventually the route to the improvement of our quality of life.

The knowledge we have achieved, already allows us to design many features of a catalyst such as shape, texture, phase and dispersion, but the technology in producing these feature could not

be available. Furthermore it is well known that very small changes in the preparation conditions could lead to dramatic effects on the properties of the catalyst. Preparing a catalyst is a complex process where some steps are not completely understood.

In this context, the work of this thesis is focused on understanding and improving the processes involved in the preparation of a catalyst, and ultimately to develop a preparation method able to control the characteristics of the final catalyst.

Characterisation is a crucial part of this work, and a large number of techniques have been extensively used. For example, in Chapter 6 we can see how more techniques combined together can synergistically support each others results and we were able to provide valuable information about a notoriously "difficult" system such as supported alloy nano-particles. On the other hand, in Chapter 4 it is shown how changing a large number of variables in the preparation can enhanced the value of the results of the analysis and allows us to extract some general conclusions impossible to propose with a limited number of samples.

In order to make the characterisation more effective the catalysts were analysed all throughout the preparation steps. All the characterisation work represents the effort to understand not only the final catalyst but also the role and importance of all the preparation steps.

After the characterisation many catalysts were tested. Well-studied reactions were chosen in order to the able to extract extra characterisation information from the catalytic data.

The last part of my work diverges from the main path of preparation. It is a work of pure characterisation using *in situ* techniques. Today as technology develops, the uses of in situ techniques are acquiring more importance in the context of studying real catalyst under reaction condition. In Chapter 7, an exciting series of XRD and Raman *in situ* experiment on vanadium phosphorus oxide (VPO) catalysts, reveals the formation of a metastable phase (ω-$VOPO_4$) and its thermally-reversible phase transition undetectable at room temperature. Under reaction conditions the reducing atmosphere also decomposes this phase but it can be reformed again by thermal treatments in an oxidising atmosphere. The reversible phase transition and the use of a variety of reducing agents led to useful information in understanding the mechanism of the catalytic reaction.

1.2 The project

This project is a collaboration between Johnson Matthey and Cardiff University and aims to develop a preparation method capable of:

- producing uniform and homogeneous alloy supported catalysts
- controlling the size of the alloy particles
- producing highly dispersed particles (nano-particles)

These general aims underline the fact that we are not limited to any specific catalyst or reaction but that the preparation method is the central focus. Highly dispersed particles are usually obtained using high surface area supports and a specific preparation method, but the real control of the particle size is still a very difficult target. In the case of bimetallic catalysts the system is even more complicated. In fact not only are small and uniform particles desirable but also the composition of the particles should be uniform and the formation of single metal particles avoided. The available technologies that attempt to control the particle size during the preparation have been reviewed and starting from some of those ideas this work has developed.

After the preparation it is necessary to evaluate what really has been prepared and so detailed catalyst characterisation is crucially important and a variety of characterization technique were used. Today characterising alloy nano-particles is still a challenge.

Finally the catalyst is tested. The reaction should be well studied in a way that the catalytic data could also indirectly provide information about the state of the metals in the catalyst and enrich the characterisation data.

The metals proposed for the study were Co, Ni and Pd, chosen because they are commonly used in catalysis. Ideally we should alloy a small amount of the precious metal Pd with a larger amount of Ni or Co. They were also selected because they have a close packet crystal structure (cubic Ni and Pd hexagonal Co) of a similar size and are able to form alloys as a solid solution as reported in the phase diagrams.[2] γ-alumina was chosen as support: it is again largely used both as catalyst and as support and has got a high surface area ideal for depositing high dispersed metal.

1.2.1 Relevance of nano-particles and alloy catalyst

Why is it important to study alloy catalysts compared with the much simple single metal catalyst? There are two main reasons.[3]

The first is to achieve a better understanding of the role and the mechanism of catalysis on metals. In fact the main effect of alloy is to modify the geometric structure and the electronic structure of the single metal respectively called ensemble and ligand effect. The ensemble effect is due to the dilution of active centres with inactive atoms. In this case the metals in the surfaces of alloy keep a certain degree of individuality and are only influenced by the their immediate environment. The ligand effect instead is due to electronic change of the surface atoms either increasing or decreasing the heat of adsorption.[4] The study of the effect of this modification contributes to our understanding of the catalytic mechanism and builds theoretical models.

The second main reason to study alloys is that, despite the effect on the activity of the catalyst is varied and difficult to predict, we often observe an improvement of the efficiency of the catalyst. For this reason and because of the demand of industry, there is much empirical research dedicated to finding the best performing alloy catalyst, and many patents are produced every year.

For example, Pd is incredibly efficient regarding selectivity in hydrogenation of alkynes and alkadienes, achieving without difficulty 100% selectivity. Pd is the most selective single metal catalyst for the hydrogenation of a single double bond. But alloying the Pd with a second metal[3,5] the efficiency may increase and the side reactions reduce. Focusing the attention on Pd-Ni bimetallic alloy, *Bertolini et al.*[6,7] showed that alloying Pd with Ni (in a wide range of concentration) largely increases the activity of Pd for the hydrogenation of 1-3 butadiene despite Ni alone shows a very small activity. In this example the Ni located in the uppermost plane and in the sub layer electronically modified the Pd. *Moss et al.*[8] showed that Pd_{50}-Ni_{50} (surface composition) had almost the same activity for the ethane hydrogenolysis of pure Ni, although pure Pd itself is not very active. This suggested that an ensemble effect is operating.

How difficult is it to prepare supported alloy catalysts? In the literature it is easy to find the word alloy but it is difficult to find a convincing characterisation of the real state of the two metals. Sometimes what is called alloy would be better described simply as "bimetallic catalyst" (where the to metals are not alloyed). The large number of preparation methods used for preparing bimetallic catalysts are based on the common single metal methods such as precipitation or impregnation extended to two metals. However, as a general rule undesired single metal particles are often present and only a fraction of the metal particles exist as alloys.

We have established the reasons for an interest in alloys. The other requirement is to produce small particles in the region of few nanometres in diameter. Small particles are generally desirable in a catalyst because they represent the highest ratio $\frac{active\ sites}{amount\ of\ metal}$. This increased efficiency of the catalyst is particularly important when precious metals are involved. But the increased number of active sites is not the only factor to be considered. By reducing the particle size to the order of few nanometres we change properties of the metal such as the electronic structure, the average co-ordination number and the interaction with the support. Selectivity and activity of the catalyst for a particular reaction are influenced by these "particle size dependent" properties.[9] The class of reaction designed as "structure sensitive" has revealed how the performance of a catalyst could be strongly affected by the dimension of the particles and increased the interest in preparing catalysts with a specific range of particle size.

The study of structure sensitive reactions is also directly relevant to alloy catalysts, since they exhibit different inter-atomic distances and electronic structures as a function of the alloy composition.

1.3 Strategy

We will start reviewing the possible methods for the preparation of supported bimetallic catalysts and selecting the one most appropriate for our tasks. Then are discussed (sec. 1.3.2) the conditions necessary for the alloying of bimetallic particle. In the section 1.3.3 we introduce the preparation and the characterisation of the single metal catalyst that will be used as the starting material for the preparation of the alloy catalyst. Section 1.3.4 explains the difficulties in characterising small supported particles and introduces the techniques we have used.

1.3.1 Preparation methods for supported bimetallic catalysts

To prepare bimetallic supported catalysts three main different groups of methods were identified (Figure 1):

1. Deposition of bimetallic compounds
2. Non-selective deposition methods
3. Selective deposition methods

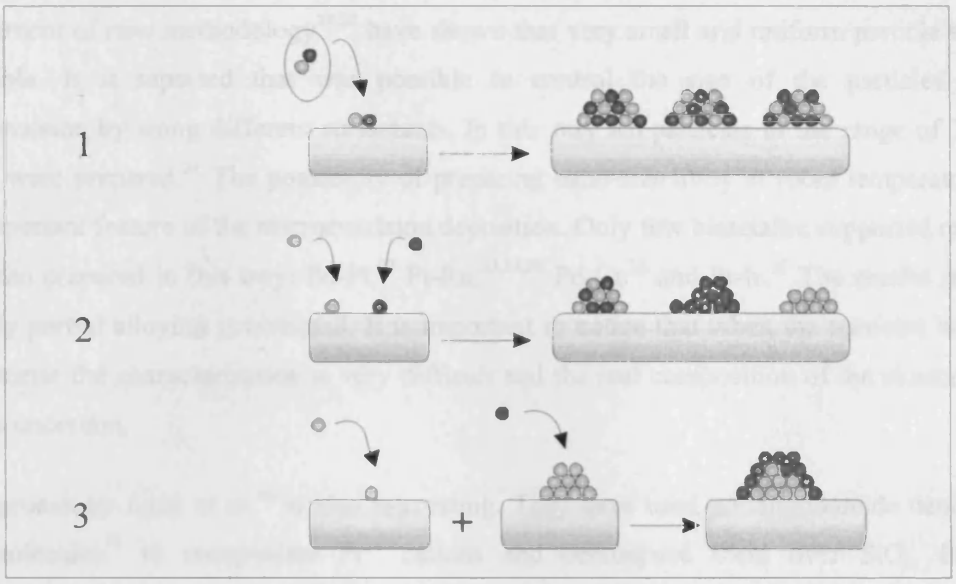

Figure 1. Scheme of the three main categories of methods to prepare bimetallic catalyst: 1) deposition of bimetallic compounds, 2) non-selective deposition methods, 3) selective deposition methods. On the right is reported the type of the metal-metal mixing expected from each method.

The first category includes bimetallic complex decomposition and ion exchange of bimetallic salt.[10] The use of bimetallic molecular compounds to prepare the supported alloy has the strong advantage of the existing interaction between the two metals.[11] The bimetallic organic complex decomposition over the support surface is known to be a powerful way to prepare well-dispersed and homogeneous alloy particles. Unfortunately no simple and convenient bimetallic salts or complexes between Co, Ni or Pd are easily available. The preparation of bimetallic complexes is complicate, expensive and also the storage is problematic. They have found application only on the lab scale. As example is reported the deposition of $[PPh_4]_4[Pd_{13}Ni_{13}(CO)_{34}]$[12] on SiO_2 in organic solvent. The characterization suggests that alloys are formed after calcination at 400°C.

Another developing method is the microemulsion deposition. It consists in pre-forming in solution metal or metal oxide agglomerates stabilised by a shell of organic molecules. *Boutonnet et al.*[13] have recently reviewed the microemulsion nano-particles preparation with emphasis on the application in heterogeneous catalysis. The preparation of supported catalyst via microemulsion is an exciting field as potentially the size, the size distribution and the surface structure could be precisely controlled before the deposition. At the moment it is still a challenge to separate the particles from the constituents of the micro emulsion and to maintain the homogeneity when transferring the particles onto the support. Furthermore the particles should be strongly adsorbed on the support in order to avoid sintering and formation of large aggregate.[14] For these reasons the microemulsion in the past was not much used to prepare

supported catalyst. The progress by *K. Wakabayashi et al.*,[15,16] *Boutonnet et al.*[17,18] and the development of new methodology[19,20] have shown that very small and uniform particle size are achievable. It is reported that was possible to control the size of the particles in the microemulsion by using different surfactants. In this way Rh particles in the range of 3.0 and 8.2 nm were prepared.[21] The possibility of preparing nano-size alloy at room temperature is a very important feature of the microemulsion deposition. Only few bimetallic supported catalysts have been prepared in this way: Pd-Pt,[22] Pt-Ru,[23,24,25] Pd-Cu[26] and Pt-Ir.[27] The results revealed that only partial alloying is obtained. It is important to notice that when the particles have 1-2 nm diameter the characterization is very difficult and the real composition of the clusters often remains uncertain.

The approach by *Lang et al.*[28] is also interesting. They have used poliamidoamide dendrimers macromolecules[29] to encapsulate Pt^{2+} cations and decompose them over SiO_2. Uniform distribution of the particles of about 2 nm were obtained with this method. The ability of the dendrimers to encapsulate a variety of metal cations could be exploit to prepare bimetallic nano-particles.

The second category of method for the preparation of bimetallic catalyst are the "non-selective deposition" methods. They can be considered as a single metal preparation method extended to bimetallic systems. They include co/sub-impregnation,[30,31,32,33] co/sub-ion-exchange,[34] co/sub-precipitation and co-decomposition of metal-organo complex,[35] where "co" indicates that the two metals are deposited together and "sub" indicates that they are deposited sequentially. Some of these methods, such ion exchange, have been shown to be suitable for preparing very small particles by careful control of all the variables (temperature, pH concentration etc). However all the non-selective methods have in common the same weakness: the difficulty in achieving close proximity of the two metals. High reduction temperatures are therefore necessary because we do not have to just alloy the particles but also to induce diffusion (mobility) of the metals on the support and mix them. Sintering and agglomeration are inevitable and the dispersion will deteriorate. Furthermore the total mixing of the metals is normally not achieved[36,37] because single metal particles are often formed. Using this method some bimetallic alloy have been prepared[38] but most of the attempts reveal that only a partial alloying is normally achieved and the formation of single metal particle appear inevitable compromising the uniformity of the catalyst. Despite they provide limited control over particle size, distribution and uniformity such methods are convenient and relatively inexpensive and have been largely preferred in lab scale for the preparation and the study of bimetallic supported catalysts.

The necessity of the two metals to be deposited in close proximity has led to new "selective decomposition methods". First a single metal supported catalyst called "parent" is prepared and

then a second metal (modifier) is added by a reaction on the surface of the first metal. This modification occurs through a selective reaction, which take place exclusively on the monometallic particles of the parent catalyst. There are varieties of reaction that have been used to control surface deposition:

- organo-complex decomposition
- direct redox reaction
- redox reaction of adsorbed reductant

In the first method a metal complex (such as ferrocene, ruthenocene or tetramethyl tin) decomposes selectively on the surface of the supported metal parent[39,40,41,42] depositing the metal. In this context, *Renouprez et al.*[43,44] reported the deposition of Ni over Pd-SiO_2 by reaction of $(C_5H_5)_2Ni$ with H_2[45] selectively adsorbed on Pd. The XRD, STEM and EXAFS results showed that the Ni-Pd particles have a uniform composition and that uniform alloy is obtained after reduction at 450°C.

The second method "direct redox reduction" consists of the reduction of the modifier added as liquid solution in the oxidized state (cation) directly with the metal parent that behave as reducing agent (reductant) following the reaction (1) (Figure 2.

$$Ox_{modifier} + Red_{parent} \rightarrow Red_{modifier} + Ox_{parent} \quad (1)$$

The evolution of the reaction is defined by the electrochemical equilibrium of the reaction that can be calculated from the standard potential of reduction (2).[46]

$$Me^{n+} + ne^{-} \rightarrow Me^{0} \quad (2)$$

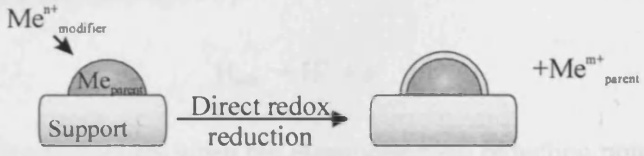

Figure 2. Scheme of direct redox reduction.

When the standard electrochemical potential of the modifier is higher than that of the parent the reaction occurs spontaneously. Therefore the method can be used for the deposition of a noble metal onto a less noble parent. A TEM study on Au-Pt system shows that the reduction proceeds with the formation of metallic modifier distributed on the surface of the parent forming true bimetallic aggregates.[47] *Bonarowska et al.*[48,49,50,51] have studied the direct redox reduction of Au on Pt on different supports and have compared the catalysts with others prepared by co-impregnation techniques. The characterization confirmed that in the case of the direct deposition

the Au was selectively deposited on the Pd and that much stronger metal-metal interaction (with partial alloying) was obtained. The reactivity of the two catalysts was also different and, for example, the uniform particles (prepared by direct reduction) were much more active in the hydrodechlorination[49,51] of CCl_2F_2 to CH_2F_2. *Barbier et al.* [52,53] used Cu as parent for deposition of Ru, Pt, Au, or Pd. It was noted that the extent of the deposition strongly depends on the nature of metal couple. While Ru[54] deposition was limited to 1/3 of the Cu atom on the surface (indicating that the deposition occurs selectively in special site) in the case of Au[55] the reduction proceed in excess of the number of Cu atoms on the surface (oxidation of the Cu sub-layer).

A special case of redox reaction between modifier and reductant is the "under potential reduction".[56,57] It occurs when the electrochemical potential of the modifier is lower than the reductant. The deposition proceeds in different way compared with direct redox reduction as the reduced modifier forms a layer of adsorbed atoms (adatoms) instead of bulk metal. The reduction is possible because the activity of the deposited metal over the parent metal surface is not unitary (due to the free energy of chemisorption). This technique is often used in electrochemistry (using conducting support) where is possible to control the electrochemical potential with an external device.[58] In heterogeneous catalysis where non-conducting supports are more often used (SiO_2 and Al_2O_3), the potential can be only controlled with supplementary redox systems.[59]

The final method for the selective deposition of a second metal is the "redox reaction of adsorbed hydrogen". It consists in adsorbing selectively hydrogen on the parent single metal catalyst and adding a solution of the modifier in an oxidised state. According to *Szabo et al.* (that first studied the process depositing Pd on Pt[60]) the adsorbed H can be considered as a source of electron (3) through which the modifier can be reduced and deposited selectively on the surface of the metal parent (Figure 3).

$$H_{ads} \rightarrow H^+ + e^- \qquad (3)$$

The reaction occurs spontaneously when the electrochemical reduction potential of the modifier is higher than the electrochemical reduction potential of hydrogen (0 eV).

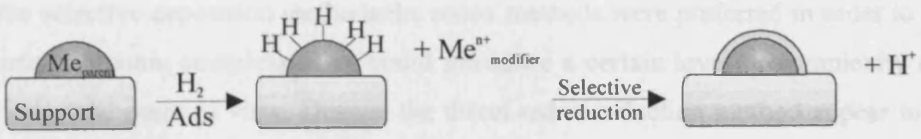

Figure 3. Scheme of redox reaction over adsorbed hydrogen.

The method also requires that the metal is able to adsorb hydrogen and for this reason noble metals are preferred as metal parent. The total amount of second metal that can be deposited is limited by the amount of hydrogen that can be adsorbed on the surface but it can be increased by several repetitions of the deposition process. *Barbier and co-workers* have prepared and characterised various bimetallic catalyst using this method (Au on Pt,[47,61,62] Cu on Pd,[63] Pt on Pd[64,65] and Re on Pt[66,67]). The catalyst prepared by this method compared with the catalyst prepared by co-impregnation consistently showed a different catalytic activity. As expected, the deposition occurred on the surface of the parent forming core-shell particles. AuPt,[61] RePt[66] and PdPt[64] catalysts prepared by reduction over adsorbed hydrogen were compared with those prepared by direct redox reduction. Despite both methods were able to form core-shell bimetallic particles, the deposition in the two methods appears to occur in different ways. The metal deposited by direct reduction occupied uniformly the surface of the metal parent while the reduction over adsorbed H led to the deposition of the modifier preferentially on the low coordination sites (corners, edges, terrace etc). In general a greater mixing of the metals is achieved with direct reduction deposition. In the case the modifier can be reduced by the hydrogen and also by the parent the system is more complex as two redox reactions can occur. Due to the higher velocity of reduction over hydrogen compared with the direct reduction[68] (100 times faster in the Au-Pt system),[69] the modifier is first reduced by the hydrogen. When the hydrogen is finished the reduction continues by direct reduction with the parent.

A special case of selective reduction over adsorbed hydrogen is the reduction of the modifier on the parent under H_2 stream.[68,70] This method, called catalytic reduction has the advantage of depositing larger amount of modifier in a single step. Thermodynamically the reduction could occur with the H_2 in solution but it is kinetically faster on the metal surface as the metal acts as a catalyst.

In this research our attention was concentrated over the selective deposition method. This method ensures the intimate metal-metal contact that is an excellent starting point for the thermal activated alloying of the particles. Differently from the non-selective methods, the selective method does not require surface diffusion and aggregation steps but only intermetallic diffusion. Therefore high reduction temperatures and undesired sintering can be avoided. Among the selective deposition methods the redox methods were preferred in order to avoid the use of metallo-organic complexes that could introduce a certain level of complexity undesired from an industrial point of view. Despite the direct redox reduction method appear to induce a more intimate metal-metal interaction, the "redox reaction on adsorbed hydrogen" was chosen because it appear more versatile, allowing for example the reduction of Pt over Pd and vice-versa.

1.3.2 Alloying of supported bimetallic particles

After the preparation of the core-shell type bimetallic catalyst, a thermal treatment was planned to alloy the particle exploiting the characteristic of Co, Ni and Pd to be soluble in each others lattice forming substitutional[i] solid solutions.[71] In general the degree of solubility of two metals is at a maximum when the following conditions are satisfied:[72]

- the diameter of the solute should not differ by more than 14% from that of the solvent atoms,
- the valences of both types of atom should be the same,
- the difference between the standard electrode potentials of the two metals should not exceed 0.5 volts,
- the two metals should crystallise in the same crystallographic system.

The systems of our interest, Pd-Ni, Co-Ni and Pd-Co, all form substitutional solid solution (Pd-Ni in all range of concentration, Pd-Co for concentrations of Co smaller than 80% and Ni-Co for concentrations of Co smaller than 95%).[2,73] Normally solid solution alloys are prepared at high temperature from the liquid phase, however in the solid-state interphase diffusion occurs and it can lead to the mixing of the metals. The atomic bulk diffusion requires high activation energy and fast diffusion rates are observable only at high temperature.[2,74] In the case of core-shell bimetallic particles, the situation is different from bulk metals because of the very small particles and the large number of surface atoms. It is a situation similar to a layer deposited onto the surface of a bulk metal. Studying the segregation of Pd in Ni, *Bertolini et al.*,[6] showed that diffusion of a layer of Pd into the Ni was activated by annealing at temperature as low as 200°C. *Faudon et al.*[44] showed that core-shell Pd-Ni particles alloyed completely at 450°C. This information reinsure that extremely high temperatures are not necessary to alloy of the bimetallic particles. This is essential in order to avoid sintering[75,76] and other undesired alteration of the catalyst during the final thermal treatment.

The final strategy for the preparation of supported alloy catalysts consists in the preparation of a highly dispersed parent, followed by the selective reduction of the second metal over hydrogen selectively adsorbed on the metal parent and a subsequent thermal treatment.

---

i) Substitutional solid solutions are those in which atoms of the alloy occupy atoms sites previously filled by the atoms of the pure metal whereas interstitial solid solutions are those in which atoms of the alloy occupy the space between the atoms of the solvent element.

1.3.3 Single metal preparation

The preparation of bimetallic catalysts involves the initial preparation of a single metal catalyst. Therefore Pd-Al_2O_3, Ni-Al_2O_3 and Co-Al_2O_3 were prepared and studied in order to achieve a solid background of knowledge necessary to approach the next step of second metal deposition and bimetallic characterisation. The required high dispersion will be directly dependent on the single metal dispersion. Transferring the target from preparing highly-dispersed bimetallic particles to preparing highly-dispersed single metal particles is one of the advantages of the selective deposition method. In this work the second metal deposition study was a priority compared with developing a method for controlling the particle size of the "single" metal catalysts. In future, the development of an efficient single metal preparation method, able to control precisely the particle size, would be adopted and so a precise control of the alloy particles would be achieved.

The Pd-Al_2O_3, Ni-Al_2O_3 and Co-Al_2O_3 catalysts were prepared by the incipient wetness impregnation method. Despite this method does not produce particles of uniform size it is suitable for achieving good dispersion in low metal loading catalysts.[77] Another more elegant method "allyl-Pd decomposition" was also used to prepare Pd-Al_2O_3. This method should provide uniform particles with a diameter smaller than 3 nm.[78,79]

1.3.4 Characterisation of supported alloy catalysts

We have to determine many parameters to characterise supported metal alloy: the average composition, the average size, the degree of alloying, the homogeneity of the particles and possible preferential segregation. Therefore the combination of different techniques is essential.[5,9] A complete characterisation is difficult and most of the publications in the literature report only partial characterisation.

Listed here are the common techniques used in characterising alloys, with particular attention being given to those used in this work.

The total amount of metal present in a catalyst can be measured by X-ray fluorescence, atomic emission or atomic absorption. The latter technique was used to determine the percent of Ni, Co and Pd in the catalysts prepared in this work.

To evaluate the particle size, the most used techniques are chemisorptions analysis and electron microscopy. Many metals are able to chemisorb atoms or molecules such as H_2 or CO. From the number of molecules adsorbed we can calculate the number of metal atoms on the surface and

thus the ratio "fraction exposed" (4) that is a measure of the dispersion and is used to estimate the average particle size. The number of atoms on the surface is also essential for calculating the important catalytic parameter "turnover frequency" (TOF) defined as number of reaction per site per second.

$$FE = \frac{n_{surface\ atoms}}{n_{total\ atoms}} \tag{4}$$

The most used instrumentation is based on volumetric absorption that measures the gas uptake at different pressures. For this work a less common "pulsed technique" at atmospheric pressure was also used. It consists in pulsing known amounts of gas into the stream of inert gas that flows through the sample and measuring the out-coming signal with a TCD detector, revealing quantitatively the amount of adsorbed gas. The limitations of the chemisorption technique are the assumption of a certain value for the ratio $\frac{n_{molecule\ absorbed}}{n_{surface\ atom}}$, the assumption of a constant and regular particular shape of the particles and the possibility of undesired phenomenon such as spillover. Using chemisorption techniques it is also not possible to know the distribution of particle size. To overcome these limitations these measurements are often combined with microscopy measurements that provide an unambiguous identification of the particle size and the possibility to measure the particle size distribution.

The surface composition of supported metals can be investigated by X-ray photoelectron spectroscopy XPS. XPS measures the binding energy characteristic for each electron level of a specific atom. The binding energy depends on the electron environment of the atom and so it can provide information about the oxidation state, the particle size and possible alloying of the metals. The intensity of the signal is proportional to the amount of species so quantitative information could be obtained. In this work the XPS data were often expressed as a ratio of the intensity of the signals from the two metals. This was useful to observe changes of the relative abundance of the metals on the surface as a function of different preparation methods or thermal treatments.

For bulk studies X-ray powder diffraction XRD is a common and powerful technique that allows identification of the different crystal phases. It is also possible to study the degree of alloying of two metals in a solid solution by the shift of the diffraction signals.[44] Unfortunately XRD is limited by in the necessity of a crystal period domain of about 50 Å, essential for the crystal-wave interaction to generate the coherent diffracted beam. The supported metal catalysts analysed were often below this limit. However, by increasing the temperature, re-crystallisation and sintering processes can produce detectable phases. The different responses of the samples to

the thermal treatments were considered evidence of differences in the initial states before the sintering process. The *in situ* X-ray diffraction used in this study was a valuable help in determining the optimum conditions of the thermal treatment leading to the formation of an alloy.

Another technique very useful for bulk studies of alloys is extended X-ray absorption fine structure EXAFS. The energy of a monochromatic synchrotron X-ray beam directed at the sample is gradually increased traversing one of the absorption edges of the element that has to be analysed. When the energy is sufficient to excite the electrons, a large increase in absorption occurs. The emitted photoelectrons have a low kinetic energy and can be backscattered by the atoms surrounding the emitting atom. The backscattering depends from atomic environment of the atom and produce oscillations on the absorption. This oscillation can be used to determine the atomic number, distance and co-ordination number of the atoms surrounding the atom in question. Unfortunately this facility was not available for this study.

Temperature-programmed reduction (TPR) is another bulk technique. It has been extensively used in this thesis especially because the supported metals were prepared by reduction of an oxide precursor. The TPR signals are associated with different reducible species and broadening or shifting of the peak could depend on the interaction of the reducible species with the support or other elements. TPR analysis does not offer as specific information as spectroscopic or diffraction analysis but when the data are supported by other information or when it has used to compare a large number of sample it can become very important in studying alloys.[33] In fact it is very sensitive and a small change in the sample is clearly revealed by a change in the position, shape or intensity of a TPR feature.

Temperature programmed desorption (TPD) of H_2 or CO has been used to correlate the desorption temperature with the metallic[80] species present in the sample. As in the case of TPR analysis we normally obtain information by the comparison of many samples.

"Temperature programmed hydride decomposition" TPHD is based on the property of the Pd to absorb H_2 and form a Pd β-hydride phase containing about a 2/3 of an atom of hydrogen for each atom of Pd. This phenomena is well known and studied but only recently it has been used to characterise bimetallic supported catalysts. The solubility of hydrogen in Pd, (5) is proportional to the amount of bulk Pd and so depend on the particle size but also depends on the degree of alloying with a second metal.[81,82]

$$S = \frac{mol\ H_{absorbed}}{mol\ Pd} \qquad (5)$$

The solubility decreases as the particle size became smaller and it decreases as a second metal alloys. This technique has been used especially by *Karpinski et al.* to characterise Pd based bimetallic catalyst such as Pd-Au,[48,83] Pd-Pt[84] and Pd-Re.[85] In this work the TPHD analysis was used to characterise single metal Pd-Al_2O_3 catalyst and to study the alloying of Pd-Ni-Al_2O_3 bimetallic catalysts.

Other specific techniques that have given a contribution in characterising supported bimetallic nano-particles of Pd, Ni and Co reported in the literature are infrared spectroscopy and magnetic measurements.

"Fourier-transform infrared spectroscopy" (FTIR) has been used to study the vibration of NO absorbed on metal surfaces. It is sensitive to the electron density of the metal and a dependence on the concentration of the alloyed second metal have been found for the Co-Ni alloy.[30,86]

Magnetic analysis has been used for study Co-Pd alloy. Measuring the saturation magnetization as a function of the magnet field is possible to extrapolate the magnetic momentum associated with the "atom of alloy". Comparing the ferromagnetic moment of the catalyst with that of the bulk alloy of the same composition is possible to obtain information about the degree of alloying.[36]

The main conclusion that emerges from this introduction to the "characterization of alloy" is that many analyses together must be used and that a complete characterisation is however difficult to achieve.

1.3.5 Catalytic reaction

The catalytic test reaction measures the efficiency (activity, selectivity and deactivation) of the catalyst but it can also be used to better characterise the catalyst. We need a well-studied catalytic reaction in a way that the catalytic data can be associated with specific properties of the catalyst. Another important features of the reaction is the structure sensitivity, the catalytic results would be thus dependent from the particle size and influenced by alloy formation. In order to study both activity and selectivity a multiple products reaction is also desirable.

Two reactions that meet the request where chosen.

The first is the crotonaldehyde ($CH_3 - CH = CH - CH = O$) hydrogenation. This reaction allows monitoring both activity and selectivity as two different functional groups can be hydrogenated.[87] It is also a structure sensitive reaction as the selectivity to the carbonyl

hydrogenation depends on the particle size of the metal.[88] Figure 1 shows the steps of crotonaldehyde hydrogenation. The two main products are butyraldehyde (I) and crotyl alcohol (II), an inter-conversion is possible between them (III). Butanol can also be formed by a double hydrogenation (IV V).

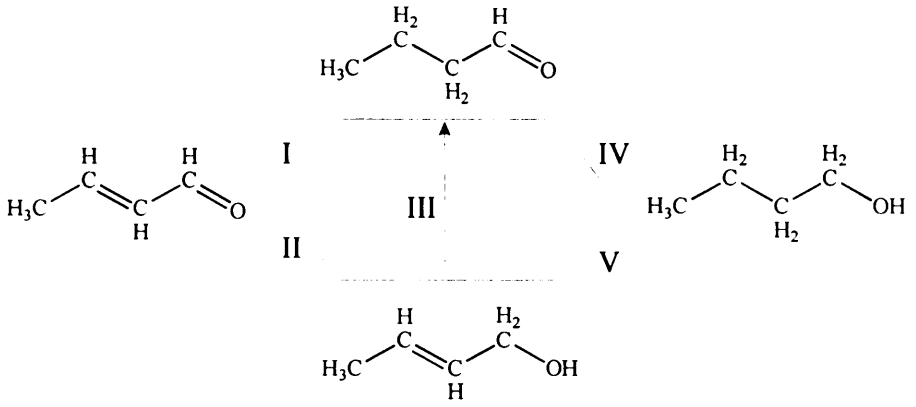

Figure 4. Scheme of the crotonaldehyde hydrogenation .

The alloy catalysts were planned to be tested also in an acetylene hydrogenation reactor. For this reaction the Pd is the most active and selective single metal catalyst but has been reported that some Pd alloy are more stable and efficient.[89] The addition of Co or Ni may thus improve the catalytic performance. This reaction is usually carried out in a large excess of ethylene in condition similar to the industrial process of acetylene hydrogenation in raw stream from a steam cracker.[90] In this condition the acetylene conversion is usually compared with the ethylene selectivity.[89] This reaction has the required characteristic of simplicity, well studied and the selectivity is again structure sensitive.[5]

1.4 *In situ* characterisation of vanadium phosphate oxide catalyst

Since the end of the 1960s when the vanadium phosphates (VPO) were found to be the most efficient catalysts for the synthesis of maleic anhydride from light hydrocarbons[91] there has been a diffuse interest in studying the VPO system.[92,93] Today the production of maleic anhydride using VPO catalyst is a major industrial process with a production of millions of tones per year. Maleic anhydride and its derivates are used for the manufacture of unsaturated polyesters, agricultural chemicals, food activities, lubricating oil additives and pharmaceutical products.

Because of the large number of VPO phases with an intricate net of structural and morphological transformations, three possible vanadium oxidation states and the difficulties in understanding the real form of the active catalyst,[94,95,96] the researchers have found a rich field of investigation with the attraction of industrial catalytic improvements.

The different activity of the VPO catalysts is often associated with the structure and texture of the solid catalyst.[97] $(VO)_2P_2O_7$ is reported to be the most active phase for the synthesis of maleic anhydride from butane and has been broadly studied. Starting from the *in situ* XRD study of $(VO)_2P_2O_7$ preparation steps from the vanadyl hemihydrate precursor, the formation of the elusive ω-$VOPO_4$ phase was observed and a new branch of research dedicated to study this specific phase was started. Many aspects make ω-$VOPO_4$ interesting. ω-$VOPO_4$ is stable in the temperature range of the catalytic process 400-480°C, but is unstable at room temperature making it impossible to detect with *ex situ* characterization. Once decomposed at room temperature it can be reversible recrystallised with a cycle of formation and decomposition. Under reaction conditions, it is also unstable as butane or other molecules can activate a reversible transformation to δ-$VOPO_4$. The *in situ* XRD and Raman study of these transformations provided information useful in understanding the structure of the active catalyst and casts new light on the on the role of the reactant and product gas mixtures in forging the structure of the catalyst.

1.5 Structure of the thesis

The final strategy for the alloys preparation is to start from well-dispersed single metal catalyst and add the second metal with the selective reduction over adsorbed hydrogen. Successive thermal treatment should provide the energy to alloy the particles (Figure 5).

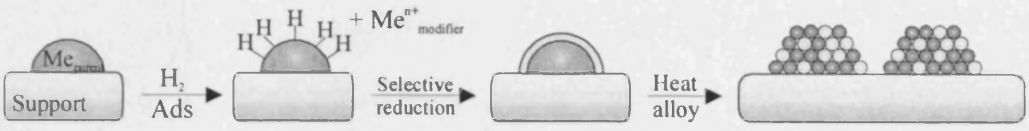

Figure 5. Scheme for the preparation of uniform supported alloy catalyst by selective second metal reduction over adsorbed hydrogen and subsequent thermal treatments.

The first part of the thesis reports the preparation and characterisation of single metal catalyst. This preliminary work aims to achieve a solid background of knowledge necessary for the subsequent alloy preparation. Chapter 3 is dedicated to the study of single metal Pd catalysts.

Pd-Al_2O_3 samples prepared in three different ways were characterised and tested for the hydrogenation of crotonaldehyde. Some aspects of the temperature programmed hydrogen decomposition (TPHD) technique were developed designing a method able to measure accurately both desorption and absorption. The combined use of pulsed chemisorption and temperature programmed chemisorption techniques lead to precise information about the solubility of the hydrogen in Pd that can be used for characterising Pd alloy. Chapter 4 reports the study of Co-Al_2O_3 and Ni-Al_2O_3. In this case temperature programmed reduction analysis offered particularly interesting data about the effect of the preparation conditions on the final catalyst. A model that correlates the metal support interaction as a function of loading and thermal treatments is proposed.

After the single metal study, the deposition of the second metal was approached. The unsuccessful attempts to deposit Ni over Pd in different pH conditions are reported in Chapter 5. Chapter 6 reports the selective deposition of Pd over Ni by reducing the Pd over selectively adsorbed hydrogen. The preparation conditions were optimised before the thermal treatments and the characterisation. The metal-metal interaction and the degree of alloying were studied as a function of the reducing temperatures.

Finally Chapter 7 reports the study of ω-$VOPO_4$ a metastable phase of vanadium phosphorus oxide catalyst. The *in situ* XRD analysis supported by *in situ* Raman analysis revealed the reversible phase transformation of ω–$VOPO_4$ activated by environmental and thermal switcher.

References

1 G. Ertl *J. Mol. Catal. A: Chem.* 182-183 (2002) 5

2 "*Binary alloy phase diagrams*" Ed. T. B. Massalski, Pub. Materials Park, Ohio (1990)

3 V. Ponec *Adv. in Catal.* 32 (1983) 149

4 W. M. H. Sachtler, R. A Van Santen *Adv. in Catal.* 26 (1979) 69

5 V. Ponec, G. C. Bond "*Catalysis by Metals and Alloys*" series *Studies in Surface Science and Catalysis* Vol. 95, Ed. B. Delmon, J.T. Yates, Pub. Elsevier, Amsterdam (1995)

6 J. C. Bertolini, P. Miegge, P.Hermann, J. L .Rousset, B.Tardy *Surf. Sci.* 331 (1995) 651

7 P. Miegge, J. L .Rousset, B.Tardy, J. Massardier, J. C. Bertolini *J. Catal.* 149 (1994) 404

8 R. L. Moss, P. Pope, H. R. Gibbens *J. Catal.* 55 (1) (1978) 100

9 M. Che, C. O. Bennet *Adv. in Catal.* 36 (1989) 55

10 M. Ichikawa *Adv. in Catal.* 32 (1993) 283

11 B. Coq, F. Figueras *J. Mol. Catal.* 173 (2001) 117

12 N. T. Tran, M, Kawano, D. R. Powell, L. F. Dahal *J. Chem. Soc., Dalton Trans.* (2000) 4138

13 S. Ericsson, U. Nylen, S. Rojas, M. Boutonnet *Appl. Catal., A* 265 (2004) 207

14 M. Boutonnet, J. Kizling, V. Mintsa-Eya, A. Choplin, R. Touroude, G. Maire, P. Stenius *J. Catal.* 103 (1987) 95

15 M. Kishida, K. Umakoshi, J. Ishiyama, H. Nagata, K. Wakabayashi *Catal. Today* 29 (1996) 355

16 M. Kishida, T. Hanaoka, W. Young Kim, H. Nagata, K. Wakabayashi *Appl. Surf. Sci.* 121 (12) (1997) 347

17 M. Boutonnet-Kizling, F. Regali, *Stud. Surf. Sci. Catal.* 118 (1998) 495

18 M. Boutonnet, J. Kizling, R. Touroude, G Maire, P. Stenious *Catal. Lett.* 9 (1991) 347

19 P. Sun, P. Atorngitjawt, M. J. Meziani *Langmuir* 17 (2001) 5707

20 M. Bonini, U. Bardi, D. Berti, C. Neto, P. Baglioni *J. Phys.Chem B* 106 (2002) 6178

21 T. Hanaoka, T. Hatsuta, T. Tago, M. Kishida, K. Wakabayashi *Appl. Catal., A* 190 (2001) 291

22 R. Touroude, P. girard, G Maire. J. Kizling, M. Boutonnet, P. Stenious *Colloid Surf.* 67 (1992) 9

23 B. Yang, Q. Lu, Y. Wang, L. Zhuang, J. Lu, P. Liu, J Wang, R. Wang, *Chem. Mater.* 15 (2003) 3552

24 Z. Liu, J. Y. Lee, M. Han, W. Chen, L. M. Gan *J. Mater. Chem.* 12 (2002) 2453

25 X. Zhang, K. Y. Chan *Chem. Mater.* 15 (2003) 451

26 K. Zhang, C. H. Chew, S. Kawi, J. Wang, L. M. Gan *Catal. Lett.* 64 (2004) 179

27 U. Nylen, J. F. Delgado, S. Jaras, M. Boutonnet *Appl. Catal., A* 262 (2004) 189

28 H. Lang, R. A. May, B. L. Iversen, B. Chandler *J. Amer. Chem. Soc.* 125 (2003) 14832

29 A. I. Cooper, J. D. Londono, G. Wignall, J. B. McClain, E. T. Samulski, J. S. Lin, A. Dobrynin, M. Dobrynin, M. Rubinstein, A. L. C. Burke, J. M. J. Frechet, J. M. DeSimone *Nature* 389 (1997) 368

30 T. Ishihara, N. Horiuchi, T. Inoue, K. Eguchi, Y. Takita, H. Arai *J. Catal.* 136 (1992) 232

31 T. Ishihara, N. Horiuchi, F. Eguchi, H. Arai *J. Catal.* 130 (1991) 202

32 W. Juszczyk, Z. Karpinski, D. Lomot, J. Pielaszek, Z. Paal, A. Y. Stakheev *J. Catal.* 142 (1993) 617

33 W. Juszczyk, Z. Karpinski, J. Pielaszek, Z.Paal *J. Catal.* 143 (1993) 583

34 J. S. Feeley, A. Y. Stakeev, F. A. P. Cavalcanti, W. M. H. Sachtler *J. Catal.* 136 (1992) 182

35 A. J. Renouprez, J. F. Trillat, B. Moraweck, J. Massardier, G. Bergeret *J. Catal.* 179 (1998)

36 F. B. Noronha, M. Schmal, C. Nicot, B. Moraweck, R. Frety *J. Catal.* 168 (1997) 42

37 J. Batista, A. Pintar, J. Padeznik, A. Kodre, F. Bornette *Appl. Catal., A* 217 (2001) 55

38 Y. L. Lam, M. Bourdart *J. Catal.* 50 (1977) 530

39 H. Miura *Catal. Today* 28 (1996) 215

40 H. R. Aduriz, P. Bodnariuk, B. Coq, F. Figueras *J. Catal.* 119 (1989) 97

41 E. K. Talas, M. Hegedus, S. Gobolos, P. Szedlacsek, J. Margitfalvi "*Preparation of catalysis IV*" Pub. Elsevier (1987) 689

42 O. A. Ferretti, L. C. B. de Pauli, J. P. Candy, G. Mabillon, J. P. "Bournonville "*Preparation of catalysis IV*" Pub. Elsevier (1987) 713

43 A Renouprez, J. F. Faudon, J. Massardier, J. L. Rousset, P. Delichere, G. Bergeret *J. Catal.* 170 (1997) 181

44 J. F. Faudon, F. Senocq, G. Bergeret, B. Moravueck, G. Glugnet, C. Nicot, A Renouprez *J. Catal.* 144 (1993) 460

45 C. M. Pleass, D. G. Schimmel *J. Catal.* 24 (1972) 424

46 "Handbook of Chemistry and Physics" 82th edition Ed. D. R. Lide, Pub. CRC press (2001)

47 P. Del Angel, J. M. Dominguez, G. Del Angel, J. A. Montoya, E. Lamy-Pitara, S. Labruquere, J. Barbier *Langmuir* 16 (2000) 7217

48 M. Bonarowska, J. Pielaszek, W. Juszczyk, Z. Karpinski *J. Catal.* 195 (2000) 304

49 M. Bonarowska, A. Malinowski, W. Juszczyk, Z. Karpinski *Appl. Catal., B 30* (2001) 187

50 M. Bonarowska, J. Pielaszek, V. A. Semikolenov, Z. Karpinski *J. Catal.* 209 (2002) 528

51 M. Bonarowska, B. Burda, W. Juszczyk, J. Pielaszek, Z. Kowalczuk, Z. Karpinski *Appl. Catal., B 35* (2001) 13

52 J. Barbier, J. P. Boitiaux, S. Leporq, J. C. Menezo, C. Montassier *EU Patent 380 402 1990* Institut Francais du Petroli

53 C. Montassier, J. C. Menezo, J. Naja, P. Granger, J. Barbier, P. Sarrazin, B. Didillon *J. Mol. Catal.* 91 (1994) 119

54 J. Barbier, J. C. Menezo, C. Montassier, J. Naja, G. Del Angel, J. M. C. Dominguez *Catal. Lett.* 14 (1992) 37

55 C. Montassier, J. C. Menezo, J. Naja, J. Barbier, J. M. Dominguez, P. Sarrazin, B. Didillon *J. Mol. Catal.* 91 (1994) 107

56 J. C. Menezo, L. C. Hoang, C. Motassier, J. Barbier *React. Kinet. Catal. Lett.* 46 (1992) 1

57 E. Lamy-Pitara, L. El Ouazzani-Benhima, J. Barbier *J. Electroanal. Chem* 335 (1992) 363

58 E. Lamy, J. Barbier *Appl Catal., A* 149 (1997) 49

59 S. Szabo *Int. Rev. Phys. Chem.* 10-12 (1991) 207

60 J. Margitfalvi, S. Szabo, F. Nagy, S. Gobolos, M. Hegedus "*Preparation of catalysis III*" Ed. C. Poncelet, P. Grange, P. A. Jacobs, Pub. Elsevier, Amsterdam (1983)

61 G. Espinosa, G. Del Angel, J. Barbier, P Bosch, V. Lara, D. Acosta *J. Mol. Catal.* 164 (2000) 253

62 J. Barbier, P. Marecot, G. Del Angel, P. Bosch, J. P. Boitiaux, B. Didillon, J. M. Dominguez, I. Schiftef, G. Espinosa *Appl. Catal., A* 166 (1994) 179

63 R. Melendrez, G. Del Angel, V. Bertin, M. A.Valenzuela J. Barbier *J. Mol. Catal.* 157 (2000) 143

64 C. Micheaud, P. Marecot M. Guerin, J. Barbier *Appl. Catal., A* 171 (1998) 229

65 C. Micheaud, M. Guerin, P. Marecot, C. Geron, J. Barbier *J. Chim. Phys.* 93 (1996) 1394

66 C. L. Pieck, P. Marecot, J. Barbier *Appl. Catal., A 134* (1996) 319

67 C. L. Pieck, P. Marecot, J. Barbier *Appl. Catal., A 141* (1996) 229

68 J. Barbier "*Preparation of Solid catalysts*" Ed. G. Ertl, H. Knoezinger, J. Weitkamp, Pub. Wiley-VCH Weinheim (1999) 526

69 J. Barbier, P. Marecot, J. P. Boitiaux, B. Didillon, G. Del Angel, P. Bosch, M. Dominguez, I. Schiftef *Appl. Catal., A* 116 (1994) 179

70 F. Gauthard, F. Epron, J. Barbier *J. Catal.* 220 (2003) 182

71 R. E. Smallman, R. E. Bishop "*Modern Physical Metallurgy and Material Engineering*" Butterworth Heinemann IV ed. (1999)

72 E. P. Polushkin "*Structural characteristics of metals*" Pub. Elsevier (1964)

73 D. A. Porter "*Phase transformations in metals and alloys*" Ed. David A. Porter, Kenneth E. Easterling, Pub. Van Nostrand Reinhold, New York (1981)

74 H. Mehrer "*Diffusion in solid metals and alloys*" Vol 26 Pub. Springer Velarg (1990)

75 J. Sehested, A. Carlson, T. V. W. Janssens, P. L. Hansen, A. K. Datye *J. Catal.* 197 (2001) 200

76 F. B. Rasmussen, J. Sehested, H. T. Teunissen, A. M. Molenbroek, B. S. Clausen *Appl. Catal., A* 267 (2004) 165

77 M. Legawiec-Jarzyna, A. Srebowata, W. Juszczyk, Z. Karpinski, *Cat. Today* 88 (2004) 93

78 Y. I. Eermackov, B. N. Kuznetov *J. Mol. Catal.* 9 (1980) 13

79 Y. I. Yermackov *J. Mol. Catal.* 21 (1983) 35

80 J. S. Feeley, Alexander, W. M. H. Sachtler *J. Catal.* 131 (1991) 573

81 M. Boudart, H. S. Hang *J. Catal.* 39 (1975) 44

82 A. L. Bonivardi, M. A. Baltanas *J. Catal.* 138 (1992) 500

83 M. Bonarowska, J. Pielaszek, V.A. Semikolenov, Juszczyk, Z. Karpinski *J. Catal.* 209 (2002) 528

84 M. L. Jarzyna, A. Srebowata, W. Juszczyk, Z Karpinski *Catal. Today 88* (204) 93

85 A. Malinowski, W. Juszczyk, M. Bonarowska, J. Pielaszek, Z. Karpinski *J. Catal.* 177 (1998) 153

86 T. Ishihara, K. Eguchi, H. Arai *Chem. Lett.* (1986) 1695

87 M. Albert Vannice, B. Sen *J. Catal.* 115, (1989) 65

88 Z. Rodolfo, L. Catherine, G. Su zanne, T. Raymonde *J. Catal.* 223 2 (2004) 328

89 J. Hwa Kang, E. Woo Shin, W. Jae Duk Park, S. H. Moon *J. Catal.* 208 (2004) 310

90 Q. Zhang, J. Li, X. Liu, Q. Zhu *Appl. Catal., A* 197 I (2000) 221

91 G. Centi, F. Trifiró, J. R. Ebner, V. M. Franchetti *Chem. Rev.* 88 (1988) 55

92 G. Centi *Catal. Today* 16 (1993) 5

93 G. J. Hutchings *Appl. Catal.* 72 (1991) 1

94 G. W. Coulston, S. R. Bare, H. Kung, K. Birkeland, G. K. Bethke, R. Harlow, N. Herron, P. L. Lee *Science* 275 (1997) 191

95 G. J. Hutchings, J. A. Lopez-Sanchez, J. K. Bartley, J. M. Webster, A. Burrows, C. J. Kiely, A. F. Carley, C. Rhodes, M. Hävecker, A. Knop-Gericke, R. W. Mayer, R. Schlögl, J. C. Volta, M. Poliakoff *J. Catal* 208 (2002) 197

96 K. Aït-Lachgar, A. Tuel, M. Brun, J. M. Herrmann, J. M. Krafft, J. R. Martin, J. C. Volta, M. Abon *J. Catal.* 177 (1998) 224

97 G. J. Hutchings, A. Desmartin Chomel, R. Olier, J. C. Volta *Nature* 368 (1994) 41

Chapter 2

2 Experimental

2.1 Introduction

A range of Ni, Co, Pd and Pd-Ni supported on alumina catalysts were prepared, characterized with a variety of techniques and some of them tested for the crotonaldehyde hydrogenation. This Chapter reports: the details of the catalysts preparation, the design of the hydrogenation reactor specifying the reaction conditions, the techniques and the conditions used for the catalysts characterization.

2.2 Catalysts preparation

In section 1.5 has been delineated the strategy for the preparation of bimetallic alloy. It involves the preparation of single metal catalyst (parent) and the successive selective deposition of a second metal. In this section are reported the preparation conditions of the single metal catalysts Ni-Al_2O_3 and Co-Al_2O_3 prepared by incipient wetness impregnation (studied in Chapter 4 and 6) and the preparation conditions of Pd-Al_2O_3 prepared by incipient wetness impregnation and Pd-allyl decomposition (studied in Chapter 3 and 5). The details of the selective metal deposition used for preparing the bimetallic catalyst are reported in Chapter 5 and 6 because this method represents a crucial part of the study and various modifications of the conditions were required in order to improve the method itself.

2.2.1 Ni-Al_2O_3 and Co-Al_2O_3 preparation

The Ni-Al_2O_3 and Co-Al_2O_3 were prepared by incipient wetness impregnation method. This method consists of adding an aqueous solution of metal salt ($Ni(NO_3)_2$ and $Co(NO_3)_2$) to a dry support (alumina) forming a paste without excess of liquid. This was achieved by adding 1.8 ml of solution to 2g of alumina. After carefully mixing the mixture in order to ensure that all the powder is uniformly wet, the samples were dried in air overnight at 120°C. The gradual evaporation of the solvent induces the salt deposition on the surface of the support. Subsequent calcination in air of the sample (normal conditions heating rate 10°C/min top temperature 400°C held for 3 h) leads to the decomposition of the nitrate and formation of the metal oxide. With a subsequent reduction step is possible to reduce the metal oxide and obtain the supported metal catalyst (normal conditions flow 5% H_2 in Ar, heating rate 10°C/min top temperature between 400 and 650°C held for 3h). Using high surface support with this technique is possible to achieve good dispersion with particle size between 5 and 20 nm. However the uniformity of the particles is rarely achieved and the particles are normally formed with a wide range of sizes. The materials used were: $Ni(NO_3)_2$ hexahydrate 99.999% from Aldrich; $Co(NO_3)_2$ hexahydrate 98% from Aldrich; γ-Al_2O_3 neutral Brockman I, STD grade from Aldrich (surface area 165 m^2/g, mesh 150) indicated as **Al_2O_3 ALD**; γ-Al_2O_3 provided by Synetix, ICI (surface area 300 m^2/g, mesh 150-200) indicated as **Al_2O_3 ICI**.

2.2.2 Pd-Al_2O_3 preparation: incipient wetness method

Two series of Pd-Al_2O_3 were prepared by incipient wetness method (above described) using $PdCl_2$ ($PdCl_2$ 99.999% Aldrich) and $PdNO_3$ ($Pd(NO_3)_2$ hydrate 99.999% Strem chemicals) as Pd salts. The support used was high purity γ-Al_2O_3 Puralox SBA–200 from Sasol (Si < 120ppm Fe < 39ppm, Na < 4 ppm, surface area 202 m^2/g, particle size < 90 micron). The catalysts were dried overnight at 120°C and calcined prior to reduction at 300°C for 3 h. The reduction was performed in a 10 ml/min flow of 5% H_2 in Ar with a ramp temperature of 10°C/min.

2.2.3 $Pd\text{-}Al_2O_3$ preparation: allyl Pd complex decomposition method

The Allyl-Pd decomposition method consists in the reaction of the Pd-allyl complex

with the OH groups on the surface of the alumina, and consequent formation of propene and the "anchoring" of the Pd to the oxygen of the alumina as shown in Figure 6.

The Pd complex was prepared by the reaction of the Grignard compound $CH_2CHMgCl$ (prepared with the reaction $Mg + CH_3CH_2Cl \rightarrow CH_2CHMgCl$)[1] with $PdCl_2$ in N_2 atmosphere at -60°C.[2,3] After the reaction, the solvent (diethyl ether) was evaporated at -40°C in vacuum and the Pd-allyl solubilised with hexane. The solution was filtered with a cannula directly into the flask containing the alumina.[4] The white alumina in contact with clear solution became immediately yellow. After 2 h the alumina was filtered using a Whatman number 3 filter and calcined in air at 300°C for 3 h. The sample was then reduced at 300°C in 5% H_2 in Ar (50 ml/min).

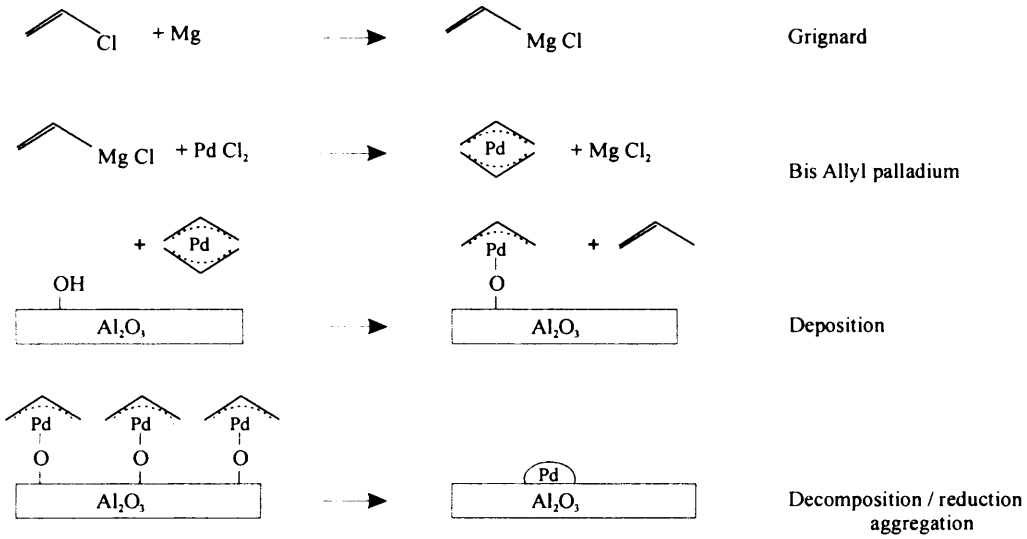

Figure 6. Scheme of $Pd\text{-}Al_2O_3$ preparation by allyl Pd complex deposition.

2.3 Catalytic test

The $Pd\text{-}Al_2O_3$ and $Ni\text{-}Pd\text{-}Al_2O_3$ catalysts were tested in a fixed bed micro reactor optimised for crotonaldehyde hydrogenation.

2.3.1 Reactor

The reactor used for the crotonaldehyde hydrogenation is schematically shown in Figure 7. The catalyst bed is positioned into a micro reactor quartz tube (3 mm diameter) over a layer of packed quartz wool and below a second layer of quartz wool. The temperature of the sample was measured by a thermocouple positioned about 20 mm from the sample and directly connected with the temperature controller of the furnace (Eurotherm 91e). The tube lines between the saturator and the furnace and between the furnace and the gas chromatograph were heated with a heating tape at 120°C in order to avoid condensation of crotonaldehyde and hydrogenated products. The analytical procedure involved the *in situ* reduction of the catalyst with a H_2 flow. The sample was then cooled to the reaction temperature and was ready for test. The H_2 was then passed through the saturator (immersed in a cool bath at 0°C) containing 10 ml of glass beads (used to increase the gas liquid surface contact) and 6 ml of crotonaldehyde (99% predominantly trans from Aldrich). After 30 min, necessary to stabilize the amount of crotonaldehyde in the flow (*ca.* 1.6%), the gas chromatographic analysis of the products was started. Using a loop and a programmable injection system (heated at 120°C) the products were analysed by a gas chromatograph Varian Star 3400 mounting a capillary column CP-wax 52 CB 0.53 mm diameter 30 metres length and an FID detector. The starting temperature of the column during the analysis was 85°C increased after 2 min to 140°C (at 10°C/min) holding this final temperature for 2 min. The injections were performed every 20 min for a time between 2 and 5 h. Blank analyses were regularly performed using the inert support (alumina) instead of the catalyst. The conversion of crotonaldehyde to a certain product was calculated by dividing the area of the product peak with the sum of the areas of the crotonaldehyde and all the reaction products. The response factor was considered unitary because of the similarity between reactant and products.

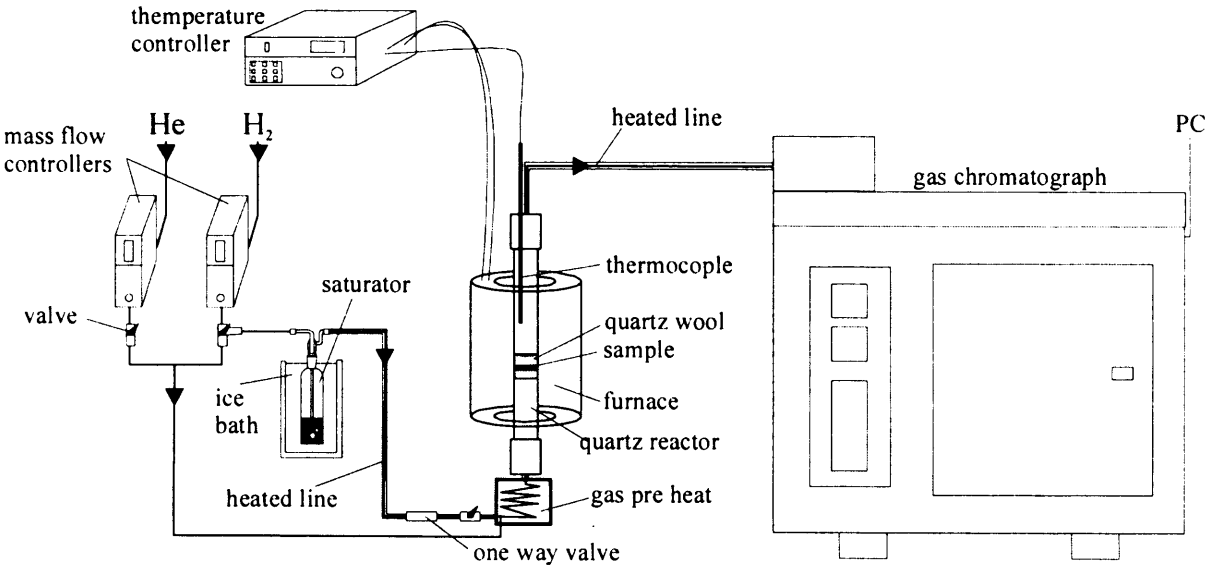

Figure 7. Scheme of the rig for the crotonaldehyde hydrogenation.

2.3.2 Reaction conditions

Two main series of catalytic tests were performed. The first compared the activity of different Pd-Al_2O_3 catalyst prepared in different ways, the second compared the activity of Pd-Al_2O_3, Ni-Al_2O_3 and Pd-Ni-Al_2O_3 during the study for the preparation of the bimetallic Pd-Ni-Al_2O_3 catalyst. Because of the different activity of Pd and Ni (Pd is two order of magnitude more active than Ni)[5] the two series of experiment were performed in different conditions.

2.3.2.1 Reaction conditions for Pd-Al_2O_3 test

The test reactions of Pd-Al_2O_3 (Chapter 3) were performed at 30°C (reaction temperature) with a flow of 50 ml/min H_2 plus 150 ml/min of He and using 6 mg of catalyst diluted with 8 mg of silicon carbide. In this conditions, the space velocity was 1.5 10^6 h^{-1} and the conversion range between 3 and 15%.

2.3.2.2 Reaction conditions for Pd-Ni-Al_2O_3 test

The series of test reaction performed during the study of the Pd-Ni-Al_2O_3 (Chapter 6) were performed in the following conditions: 20 mg of catalyst, H_2 flow 10 ml/min, He flow 10 ml/min, space velocity = 88000 h^{-1}. Each sample was tested at 50°C, 125°C and 200°C. After the reaction at 50°C the temperature was increased at 125°C at about 10°C/min and kept at this temperature for 30 min before collecting the data for 2 h. A similar step was repeated for the test at 200°C. Before such tests, the samples were *in situ* reduced at 300°C for 1h in pure H_2 (heating rate 10°C/min).

2.4 Characterization methods

In this section are reported the techniques used for the characterization of the catalysts specifying the experimental conditions.

2.4.1 Atomic absorption

The atomic absorption (AA) is a quantitative spectroscopy technique based on the absorption of a monochromatic wave by atomised element present in the sample. It provides an elemental

analysis and in this work it has been used for the determination of the metal loading in the supported metal catalysts. The analyses were carried out with a Varian SpectAA 55B atomic absorption spectrometer. The radiation was generated by hollow cathode lamps and the following wavelength, 352.4 nm, 304.4 nm and 244.8 nm were used respectively for the analysis of Ni, Co, and Pd. The samples were atomised using an acetylene-air flame (3.5 bar air and 0.5 bar acetylene). The sample solutions were prepared by acid attack of the catalyst using equal amount of HF 5% and HNO_3 conc. and putting them in the ultrasound bath for a time between 2 and 24 h. After dissolution of the catalyst, the solutions were diluted with water prior to analysis. In the case of Pd analysis EDTA (0.01M) was added to the solution in order to avoid Ni, Co and Al interferences. The calibration curves were constructed using standard solutions purchased from Aldrich.

2.4.2 Thermo-gravimetric analysis

The thermo-gravimetric analysis (TGA) measures the loss of weight as a function of the temperature during a temperature programmed ramp. The derivative of this curve is normally calculated, as the loss of weight can be associated with peaks. The TGA profiles give information on transformation, decomposition or reaction that occur during the temperature ramp. The instrument used for the analysis is a Perkin Elmer TGA 7 Thermogravimetric Analyzer and the analyses were performed in a N_2 flow (50 ml/min) using a ramp temperature from 30°C to 700°C reached at 20°C/min.

2.4.3 Temperature programmed reduction

The temperature programmed reduction analysis (TPR)[6,7] consists in heating slowly the sample under a diluted H_2 flow and records the consuming of hydrogen that react with oxygen present in the sample (forming water) as a function of the temperature. A cold trap is required to avoid the water reaching the thermal conductivity detector (TCD). This technique detects the different reducible species in the sample. In the case of supported catalysts the shape and the position of the reduction signals are very sensitive to the interaction of the reducible species with support and other species present in the catalyst. TPR analysis is often used to study the catalyst during the preparation when they are obtained by oxide precursors. The TPR experiments were performed with a Micromeritics Autochem 2910 equipped with a TCD detector using a flow of 10% H_2 in Ar (50 ml/min) with a ramp temperature of 10°C/min from 25 to a maximum temperature of 1100°C.

2.4.4 Temperature programmed hydride decomposition

The temperature programmed hydride decomposition (TPHD) is a specific technique for the study of Pd sample.[8,9,10] It is based on the characteristic of the Pd which absorbs at room temperature H_2 forming Pd-hydride. Above 70°C, the hydride is unstable and decompose releasing H_2. The analysis consists on a temperature-programmed ramp performed in presence of H_2 similarly to a TPR ramp. At room temperature Pd-hydride is formed. Increasing the temperature it decomposes and the released H_2 is detected by the TCD as a peak. The precise amount of adsorbed H_2 is calculated integrating the signal and using calibration curves obtained by manual injection of H_2. The solubility of H_2 in Pd provides information on the Pd particle size, the interaction with the support and, in the case of bimetallic catalysts, the degree of alloying. The experiments were performed with a Micromeritics Autochem 2910. The Pd-Al_2O_3 samples were reduced *in situ* with a TPR ramp at 300°C and cooled to room temperature. The sample is then heated in 10% H_2 in Ar (50 ml/min) at 10°C/min at 150°C.

2.4.5 Pulse chemisorption

The pulse chemisorption technique is based on the adsorption of molecule such as H_2 (or CO) on metals. Because these gases do not chemisorb on the surface of the support the technique is used to measure selectively the number of the metal atom on the surface in a supported metal catalyst. By dividing this number by the total number of metal atoms (measured for example by atomic absorption) the metal dispersion is obtained.

The analyses were performed with a Micromeritics Autochem 2910. The surface of the supported metal sample was clean *in situ* between 250 and 350°C for 1 h using a 50 ml/min flow of Ar (research grade). The sample is then cooled at 35°C in the case of Pd and 100°C in the case of Co and kept in a 5 ml/min flow of Ar. 0.1 ml of 10% H_2 in Ar is sequentially injected in the system every 12 min using a loop. In absence of sample the pulsed H_2 is recorded by the TCD generating a series of peaks with the same area. In presence of the sample the first pulse produces a small or zero area signal, as the gas is completely adsorbed on the surface of the metal. As the number of pulses increases, the metal surface sites not occupied by a chemisorbed gas atom and thus the amount of adsorbed H_2 in each pulse decrease. After a certain number of pulses no amount of the injected gas is adsorbed and peaks with the same area are recorded. The number of surface metal sites are then calculated assuming stoichiometric factor of absorption equal to 2 for H_2 and to 1 for CO. The loop volume is calibrated by manual injections.

2.4.6 Volumetric chemisorption

Similarly to the pulse chemisorption, "volumetric chemisorption" was also used to measure the metal surface area in supported metal catalysts. The method is based on the measurement of the uptake of H_2 at different pressures. These experiments were performed on Co-Al_2O_3 and Ni-Al_2O_3 samples in the Billingham laboratories of Johnson Matthey.

The analyses were performed in a Micromeritics ASAP 2010 Chemisorption Analyser. The Co samples were *in situ* reduced in pure hydrogen at 650°C for 1 h (heating rate 3°C/min). The sample was then evacuated at a pressure below 10 mmHg for 2 h. Still under vacuum the sample was cooled at 150°C (this temperature was required because of the characteristic activated chemisorption of H_2 on Co). At this point the analysis consists of two stages. First stage is to measure total H_2 uptake (chemisorbed H_2 and weakly bonded physisorbed H_2) at the following pressures: 100, 150, 200, 300, 400, 500, 600, 680 and 760 mmHg. The sample is then evacuated for 30 min to remove the physisorbed hydrogen and the analysis is repeated at the same pressures as quoted above to measure the uptake of physisorbed hydrogen. The linear region of the data is extrapolated back to zero pressure and the metal area calculated assuming a stoichiometric factor equal to 2 (H_2 molecule is adsorbed on 2 Co sites). The same procedure was used for the analysis of the Ni samples except for the reduction temperature (550°C) and the temperature of analysis (35°C).

2.4.7 BET

The BET method is commonly used for determine the total surface area. The measurement is based on multilayer adsorption of molecule over a solid first described by Brunauer, Emmett, and Teller (Equation 1).

$$\frac{P}{V(P_0 - P)} = \frac{1}{V_m C} + \frac{(C-1)}{V_m C} \times \frac{P}{P_0} \qquad (1)^{i}$$

The analyses were performed using a Micromeritics Gemini 2360 surface analyser. The uptake of N_2 is measured at different pressures. A theoretical straight line is obtained plotting $P/V(P_0-P)$ versus P/P_0. Slope and intercept of the line can be used to calculate V_m from which the surface

[i] V = volume of gas adsorbed at pressure at pressure P. V_m = volume of gas adsorbed in a monolayer. P_0 = saturation pressure of adsorbate gas at the experimental temperature. $C = e^{(q_1 - q_L)RT}$ where q_1 = heat of adsorption of the first layer and q_L heat of liquefaction of adsorbed gas on all other layers.

area of the sample can be calculated. The samples were dried at 150°C under H_2 flow for 1h before the analysis.

2.4.8 X-ray powder diffraction

X-ray diffraction is based on the elastic scattering of monochromatic X-ray photons by atoms ordered in a crystalline structure. The diffraction is originated from the constructive interference of the scattered photons that satisfy the Bragg law (2):

$$n\lambda = 2d_{hkl}\sin\theta \qquad (2)^{ii}$$

This phenomenon is exploited to calculate the distance between the lattice planes and thus for phase identification. The XRD patterns of a powdered sample are normally acquired by scanning the intensity of the diffracted peaks as a function of angle 2θ between the incoming and diffracted beam. A limitation of the technique is that long-range order (about 5 nm) is required for the generation of the diffraction signals. However using the Scherrer equation (3) the broadening of the peak can be used for the calculation of the average size of the diffracting crystal. In catalyst characterization XRD provides a powerful bulk analysis method for identification of the crystallographic phases present in the catalyst and for the measurement of the average particle size (between 100 and 5 nm) of supported particles.

$$L = \frac{K\lambda}{\beta\cos\theta} \qquad (3)^{iii}$$

In this study the pattern were collected with an Enraf Nonius FR590 Bragg Brentano geometry, with Cu Kα radiation and Ge (111) single crystal monochromator and a curved position sensitive detector Inel CPS 120. The X-ray generator was operated at 1.2 kW (40 mA and 30 kV) and the acquisition time was 1 h. Phase identification was carried out using the JCPDS[11] database.

[ii] λ = X-ray wavelength; d_{hkl} = interplanar space; N = 1, 2, 3...; θ = incident angle

[iii] L=dimension of the particle in the direction perpendicular to the reflecting angle; λ = X-ray wavelength; β = peak width; K = constant often taken as 1, θ = incident angle

2.4.9 *In situ* X-ray powder diffraction

The *in situ* X-ray powder diffraction analysis (*in situ* XRD) allows the study of phase transformations as a function of the temperature, pressure and atmosphere. It is used to study the catalyst during the preparation steps such as calcination or reduction and is very important in studying the catalyst modification under reaction conditions. *In situ* powder X-ray diffraction data were collected using an Enraf Nonius FR591 instrument with a rotating anode Cu X-ray source working at 4.0 kW (100 mA and 40 kV), a Ge (111) single crystal monochromator (used to select the Cu $K\alpha_1$ X-rays) and an Inel 120 position sensitive detector. Differently from a conventional X-Ray tube the rotating anode provides a better dispersion of the thermal energy generated by the electron bombardment of the metallic target. This allows to work with much higher power and to generate more intense X-ray. The combination of the rotating anode and the curved position sensitive detector offers the possibility of acquisition of the entire pattern in a very short time. This makes the apparatus adequate to observe fast bulk transformations that occur in a time scale of minutes. The sample was mounted in an Anton Parr XRK reaction chamber and the temperature was controlled by a thermocouple placed in direct contact with the sample mounting. Gas flow rates to the cell were regulated using electronic mass flow controllers (usually 60 ml/min) and the gas flowed through the sample to exit the chamber. The typical heating profile is characterized by steps of 25/100°C reached at 10°C/min and lasting 25 min.

2.4.10 X-ray photoelectron spectroscopy

The X-ray photoelectron spectroscopy (XPS)[12] provides an elemental analysis of the surface of a solid sample. It measures the kinetic energy of an electron expelled from the atom by the absorption of an X-ray photon. The binding energy E_{bin} is calculated as in equation (4):

$$E_{kin} = h\nu - E_{bin} \qquad (4)^{iv}$$

The binding energy is characteristic for each electron level of a specific atom (for example O_{1s}, C_{1s} and Pd_{3d}) and is used for the identification of the elements present in the sample. Small shifts of the binding energy are associated with different oxidation state of each element. The particle size and the alloying of the metals also influence the binding energy. A fine analysis of the signals can reveal information on these aspects. XPS is generally used in catalysis both for studying the difference between the surface and the bulk composition and for studying the

deposition of residues after reaction. X-ray photoelectron spectra were recorded on a VG EscaLab 220I spectrometer, using a standard Al Kα X-ray source (300 W) and an analyser pass energy of 20 eV. Samples were mounted using double-sided adhesive tape and binding energies are referenced to the C_{1s} binding energy of adventitious carbon contamination taken to be 284.7 eV. The quantitative analysis is based on the integration of the areas under Ni_{2p}, Pd_{3d}, and Al_{2p} peaks after subtraction of a non-linear Shirley background. The integrations were performed with the software Casa.

2.4.11 *In situ* Raman spectroscopy

When a beam of light (in the region of the visible) passes through a molecule it can be transmitted, absorbed or scattered. Most of the scattered radiation has the same energy of the incident beam (elastic or Rayleigh scattering) and a very small amount (about 1%) is scattered with discrete frequency lower and higher of the incident beam (inelastic or Raman Stokes and anti-Stokes scattering).[13] This is due to the collisions where the vibrational or rotational energy of the molecule is changed. A plot of detected number of photons versus Raman shift from the incident laser gives a Raman spectrum. Each signal is associated with different vibrational or rotational motions and often with a specific functional group. This makes Raman spectroscopy a useful technique for material characterization. Because of the weak intensity of the scattered light (about 10^{-8} parts of the incident beam) Raman spectrometers require an intense monochromatic light and normally a laser beam generated by rare gas as Ar^+ or Kr^+ is used. The samples were analysed using a Renishaw system 1000 Raman microscope. An Ar ion laser (514.5 nm green light) was used as excitation source (20 mW). The laser was focused onto the sample, placed in a LinKam TS1500 *in situ* cell, by means of an Olympus BH2-UMA microscope. Spectra were collected, in the range from 200 to 1200 cm^{-1}, using a back scattering geometry with a 180° and an optical system with a CCD camera detector. Typically 30 seconds exposure and 20 accumulations were used in each scan with 100% laser power. The temperature programmed analysis were performed in air with ramp temperature between 25 and 650°C sampling every 25 or 50°C and a heating rate of 5°C/min.

[iv] E_{kin} = measured kinetic energy, $h\nu$ = energy of the incident photon, E_{bin} = binding energy

References

1 E. A. Hill, W. A. Boyd, H. Desai, A. Darki, L. Bivens *J. Organomet. Chem.* 514 (1996) 1

2 M. Guerra, D. Jones, G. Distefano, S. Torroni, A. Fossati, A. Modelli *Organometallics* 12 (1993) 2203

3 J. K. Beccosall, B. E. Job, S. J. O'Brien *J. Chem. Soc.* (1967) 423

4 Y. I. Yermackov *J. Mol. Catal.* 21 (1983) 35

5 M. A. Vannice, B. Sen *J. Catal.* 115 (1998) 65

6 D. A. M. Monti, A. Baiker *J. Catal.* 83 (1983) 323

7 N. W. Hurst, S. J. Gentry, A. Jones *Catal. Rev. Sci. Eng.* 24 (2) (1982) 233

8 M. Boudart, H. S. Hang *J. Catal.* 39 (1975) 44

9 A. L. Bonivardi, M. A. Baltanas *J. Catal.* 138 (1992) 500

10 T. C. Chang, J. J. Chen, C. T. Yeh *J. Catal.* 96 (1985) 51

11 JCPDS-ICDD – PC PDF database, PA 19073 U.S.A.

12 D. Briggs, M. P. Seah "*Practical surface analysis*" Pub. John Wiley and Sons (1990)

13 N. B. Colthup, L. H. Daly, S. E. Wiberley "*Introduction to Infrared and Raman Spectroscopy*" Pub. Academic Press, London (1990)

Chapter 3

3 Pd supported on Al_2O_3

3.1 Introduction

In this Chapter is presented the preparation, characterisation and testing of Pd-Al_2O_3 catalysts. In order to obtain samples with different dispersions they were prepared in three different ways at different loadings. The characterisation has been performed with atomic absorption, temperature programmed reduction, X-ray diffraction, temperature programmed hydride decomposition and pulse chemisorption. Some specifically targeted experiments led to interesting consideration about the last two techniques and their applications. Particular attention has been dedicated to the study of the solubility of hydrogen into Pd and its relation with the particle size. It is also described as this information could be used in characterising the degree of alloying in Pd bimetallic catalysts. The catalysts were finally tested for the hydrogenation of crotonaldehyde. This work is finalised to prepare and study single metal catalysts that could be used as "starting material" for selective deposition of a second metal during the process of preparing supported alloy.

3.2 Results

3.2.1 Atomic absorption

Various Pd-Al_2O_3 catalysts with different loadings were prepared by:

1) incipient wetness impregnation of $Pd(NO_3)_2$ (**N-Pd-Al_2O_3**)
2) incipient wetness impregnation of $PdCl_2$ (**C-Pd-Al_2O_3**)
3) allyl Pd complex decomposition[1] (**A-Pd-Al_2O_3**).

Section 2.2.2 and 2.2.3 reported the details for the preparation. The prepared catalysts are summarised in Table 1 where the loadings measured by atomic absorption,are reported.

N-Pd-Al_2O_3	C-Pd-Al_2O_3	A-Pd-Al_2O_3
9.4%		
1.6%	1.93%	0.9%
0.4%	0.63%	

Table 1. Pd loadings (wt %) in the Pd-Al_2O_3 catalysts.

All the samples were prepared using high purity "Sasol" alumina. Another set of Pd-Al_2O_3 (5.8%, 1.1% and 0.2% Pd) indicated as **NA-Pd-Al_2O_3**, was previously prepared by incipient wetness impregnation with $Pd(NO_3)_2$ using "ICI" alumina. This series was analysed by XRD to study the impregnation and calcination steps (next section).

3.2.2 X-ray diffraction

Preparing Pd-Al_2O_3 by incipient wetness impregnation, the Pd salt is deposited on the support during the impregnation and drying step. In Figure 8a are reported the XRD patterns of the NA-Pd-Al_2O_3 samples after the drying step.

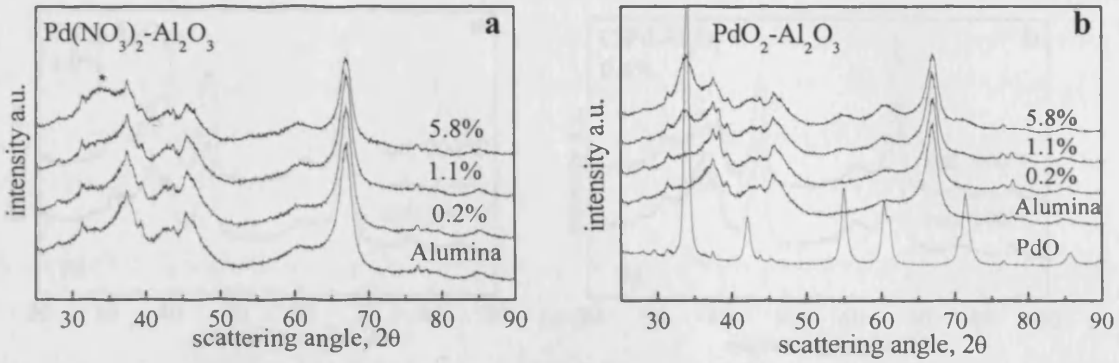

Figure 8. XRD pattern of (a) $Pd(NO_3)_2$-Al_2O_3 and (b) PdO_2-Al_2O_3 at different loading. The pure alumina and pure PdO patterns are reported as reference.

A single broad peak at 36.7°2θ (attributable to PdO) was observed in the higher loading sample. This suggests that the procedure produced a good dispersion of $Pd(NO_3)_2$ particle on the support and that it was partially decomposed to oxide. The subsequent step is the calcination performed at 300°C for 3h. At this temperature the nitrate completely decomposes to PdO. The 5,8% and 1.1% loadings (Figure 8b) showed more intense broad PdO signals. The thermal energy favourited the crystals reorganisation and the growing of the particle by sintering.

After the calcination, the C-Pd-Al_2O_3 and A-Pd-Al_2O_3 samples were reduced at 300°C and analysed by XRD (Figure 9 and Figure 10). The identification of the Pd signals is made uncertain by their low intensity and the overlapping with the alumina peaks. The sample reduced at 900°C revealed an increase of the Pd signals due to the intense sintering. This fact underlines the high sensitiveness of the analysis able to detect the Pd signals for Pd concentration lower than 1%.

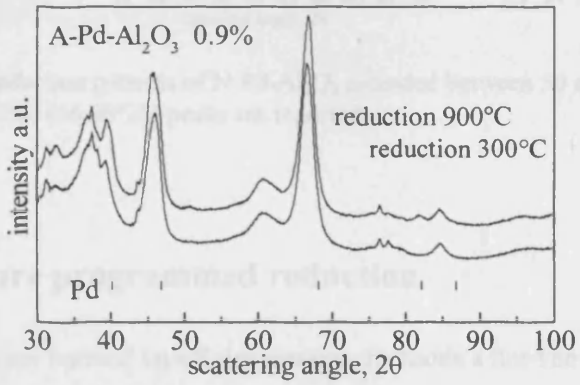

Figure 9. XRD patterns of A-Pd-Al_2O_3 reduced at 300 and 900°C.

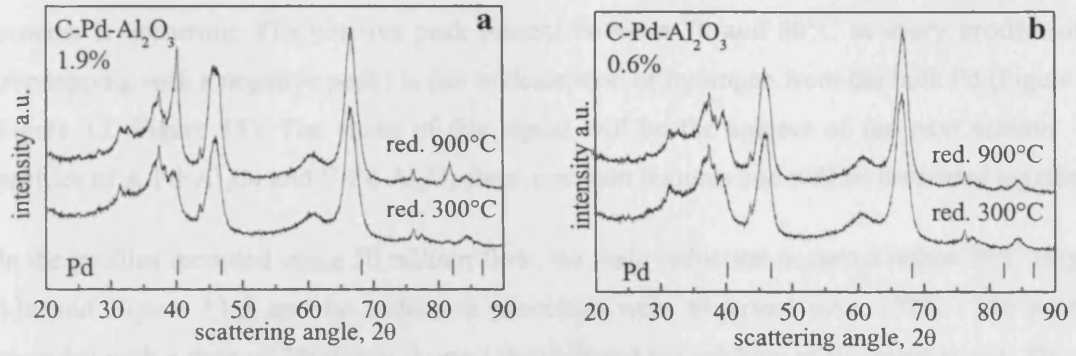

Figure 10. XRD patterns of C-Pd-Al_2O_3 at the specified loading reduced at 300 and 900°C

The N-Pd-Al_2O_3 series was reduced *in situ* in the XRD cell up to 800°C. In Figure 11 is reported the region of the pattern between 32 and 50°2θ containing the two most intense Pd signals. At 100°C the reduction appears to be completed. Following the intensity and the broadening of the Pd signals as the temperature increases it is possible to obtain direct information on the degree of sintering as a function of the temperature. The process appears to proceed gradually up to 500°C when a stronger change is observed in all the loadings.

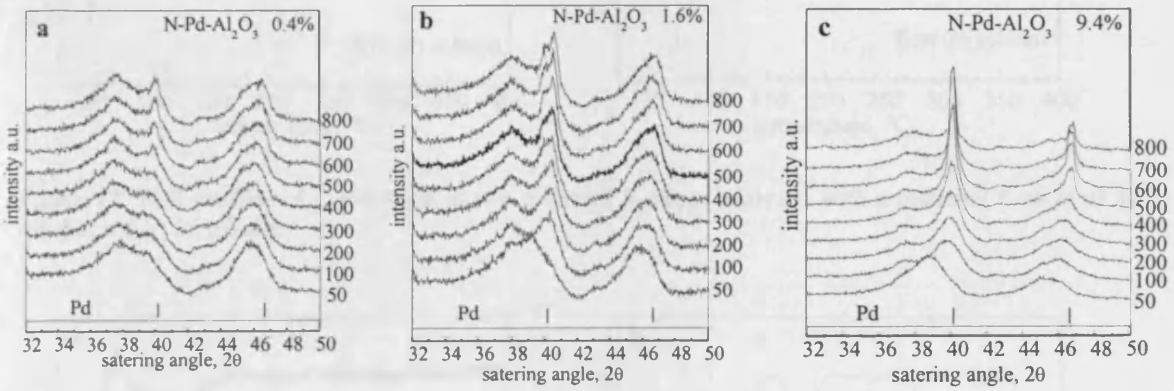

Figure 11. X-Ray *in situ* reduction patterns of N-Pd-Al_2O_3 recorded between 50 and 800°C. The positions of the 111 (40.12°2θ) and 200 (46.66°2θ) peaks are reported.

3.2.3 Temperature programmed reduction

The PdO-Al_2O_3 precursors formed in all preparation methods after the calcination step were analysed by TPR. PdO is an easy reducible species and the analyses were carried out between room temperature and 300/400°C. The analysis were performed using a routine flows of 50 ml/min. 25 ml/min flow was also used and remarkable changes in the patterns were observed.

In the TPR profile, a negative peak represents the consumption of H_2 indicating that a reducing process is occurring. The positive peak present between 70 and 80°C in every profile (often overlapping with a negative peak) is due to desorption of hydrogen from the bulk Pd (Figure 12, Figure 13, Figure 15). The study of this signal will be the subject of the next section. The profiles of A-Pd-Al_2O_3 and C-Pd-Al_2O_3 show common features and will be presented together.

In the profiles recorded using 50 ml/min flow, the main reduction occurred below 50°C (Figure 12a and Figure 13a) and no reduction processes were observed over 150°C. The profiles recorded with a flow of 25ml/min showed the shift and the splitting of the main signal. The less reducing conditions required more energy for the reduction to occur and the main reduction occurred between 50 and 100°C. A second reduction was also observed between 150 and 200°C and a third reduction occurred close to 300°C in the case of the C-Pd-Al_2O_3 samples. The strong effect of the flow on the reduction profiles is surprising.

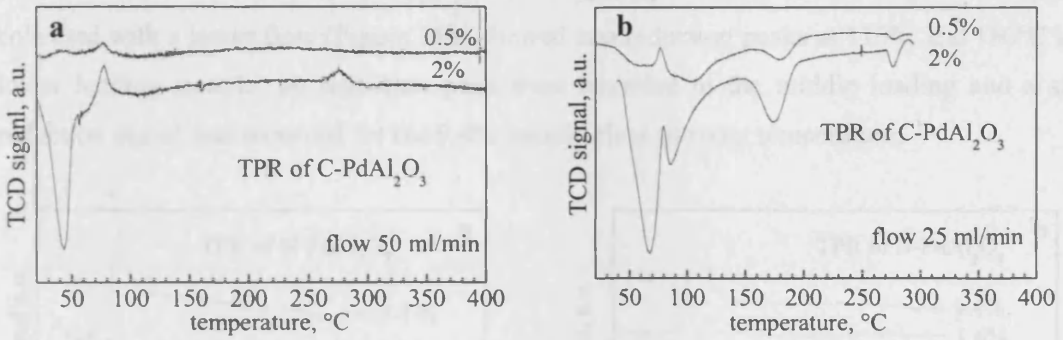

Figure 12. TPR profiles of C-Pd-Al_2O_3 at two different loadings analysed with a reducing flow of a) 50 ml/min and b) 25 ml/min.

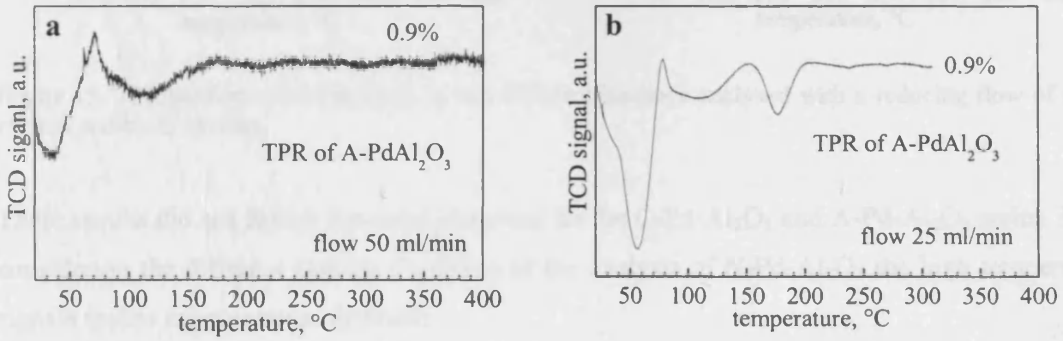

Figure 13. TPR profiles of A-Pd-Al_2O_3 analysed with a reducing flow of a) 50 ml/min and b) 25 ml/min.

The N-Pd-Al_2O_3 catalysts were analysed in slightly different conditions. Before the normal temperature programmed ramp, the samples were held for 10 min at 0°C and the TCD signal recorded. The TCD profiles as a function of the time are reported in Figure 14. These profiles revealed that the reduction can largely occur at zero degree.

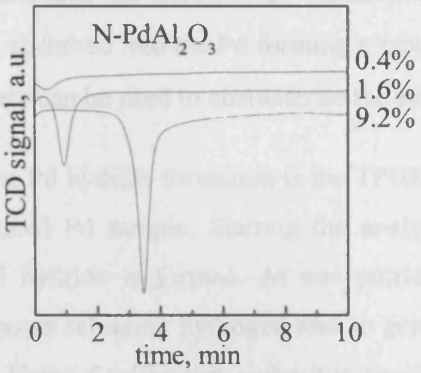

Figure 14. Reduction of PdO-Al_2O_3 performed at the constant temperature of 0°C. The TCD signal is reported as a function of the time.

For the temperature ramp with a flow at 50 ml/min (Figure 15a), the reduction continued for the 9.4% loading at 50°C while for the 1.6% loading two reduction signals were recorded at 80°C and 160°C. The lowest loading sample was completely reduced at zero degree. The profiles collected with a lower flow (Figure 15b) showed two reduction peaks at 110°C and 180°C in the lower loading sample, no reduction peak were recorded in the middle loading and a single reduction signal was recorded for the 9.4% sample close to room temperature.

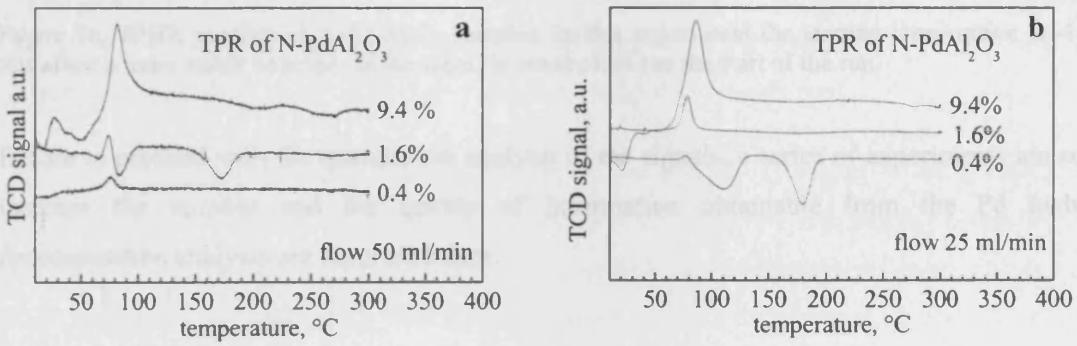

Figure 15. TPR profiles of N-Pd-Al_2O_3 at two different loadings analysed with a reducing flow of a) 50 ml/min and b) 25 ml/min.

These results did not follow the trend observed for the C-Pd-Al_2O_3 and A-Pd-Al_2O_3 series. Even considering the different starting condition of the analysis of N-Pd-Al_2O_3 the high temperature signals makes interpretation difficult.

3.2.4 Temperature programmed hydride decomposition

Introducing this section is useful to define the difference between "absorption" and "adsorption" of gas on metal. Adsorption identifies chemisorption of a molecule or an atom on the surface of

the metal while absorption identifies the sorption of atoms into the bulk of the metal. In particular the hydrogen can be absorbed into the Pd forming a new crystallographic phase β-Pd hydride.[2,3] This peculiar property can be used to characterise the supported Pd catalyst.[4,5,6]

One technique used to study the Pd hydride formation is the TPHD that consists in a TPR ramp performed on an already reduced Pd sample. Starting the analysis at room temperature the hydrogen is absorbed and Pd hydride is formed. At one particular temperature, this phase becomes unstable and decomposes releasing hydrogen and so generating the positive signal in the TCD detector (Figure 16). Using a calibration curve it is possible to measure the amount of desorbed hydrogen.

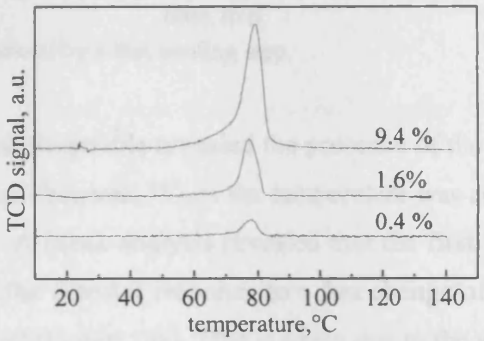

Figure 16. TPHR profiles of N-Pd-Al_2O_3 samples. In this experiment the starting temperature is -10°C this allow a more stable baseline, as the signal is not to close too the start of the run.

Before to proceed with the quantitative analysis of the signals, a series of experiments aimed to increase the number and the quality of information obtainable from the Pd hydride decomposition analysis are reported below.

3.2.5 TPHD development

An interesting work[7] claimed the possibility to measure by temperature programmed hydride desorption and subsequent "sorption" not only the absorbed but also the adsorbed hydrogen. The experiment was so designed. Increasing the temperature up to 400°C first the Pd hydride decomposes and then hydrogen desorbs from the surface in a wide range of temperature producing a very broad positive signal. At this point a fast cooling step should produce the successive re-adsorption and re-absorption, which should be recorded as two negative peaks. It is reported that the experiment has given reproducible results for Pd supported on silica but not for Pd supported on alumina. However we thought it was worth investigating this experiment to evaluate the possible applications.

The 9.4% N-Pd-Al_2O_3 sample was analysed increasing the temperature at 10°C/min (50 ml/min flow of 10% H_2 in Ar) up to 400°C and then the quartz sample tube was cooled rapidly in an ice-water bath. The recorded profile is reported in Figure 17.

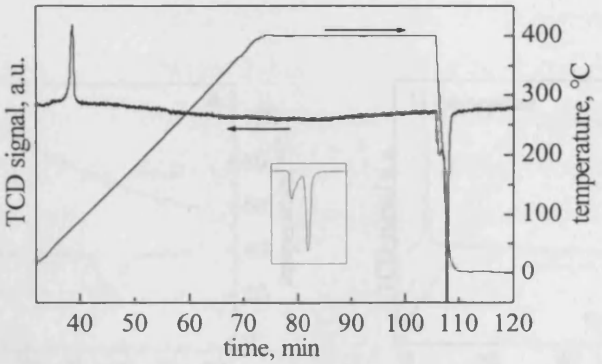

Figure 17. TPHD analysis followed by a fast cooling step.

As the temperature increased the profile revealed the presence of the hydride decomposition but no broad positive peaks were observed. When the temperature was cooled down fast, two peaks were observed as expected. A blank analysis revealed that the first peak is actually an artefact instrumental signal. In fact the detector responds to a fast change of temperature in the sample tube generating a sharp signal (Figure 18a). This is likely due to the sensitivity of the detector to the sudden change of the temperature (and pressure) in the system. In Figure 18b this phenomenon was also observed for more gradual changes of temperature.

This instrumental effect made the observation of the adsorption signal, when present, very difficult. Nevertheless the second signal clearly started when the temperature reached about 80°C and so can be attribute to hydrogen re-absorption. This new type of ramp that presents both desorption and adsorption will be more generally called temperature hydride sorption (TPHS). Different cooling rates were tested in order to obtain a neat absorption signal.

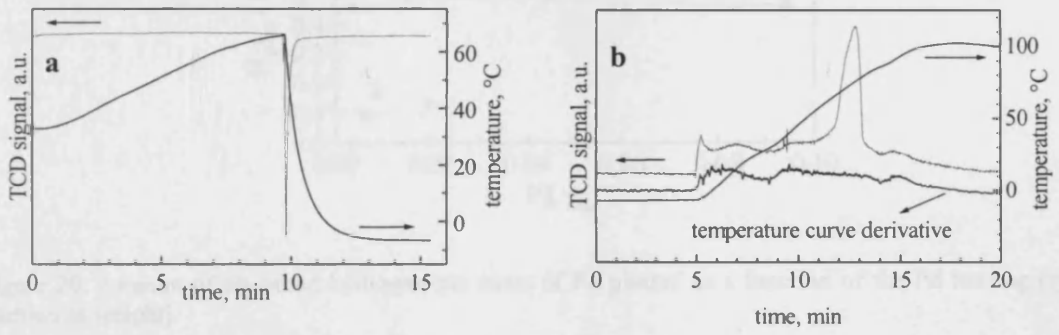

Figure 18. a) A fast change of the temperature of the sample holder generates a sharp signal. b) TPHD trace. At the start and the end of a heating ramp the heating rate can be not constant as revealed by the sinusoidal shape. The changes of heating rate were detected by the detector and generated a "not straight" baseline. This was confirmed by the precise fit of the baseline itself with the first derivative of the temperature ramp.

In Figure 19a a TPHS analysis with a slow cooling ramp is reported. Decomposition and reformation of the Pd hydride phase are clearly observed as positive and negative peaks. The slow cooling ramp resolved the second signal in two components revealing that two sites with different energy are available for the hydrogen when absorbed into the Pd bulk.

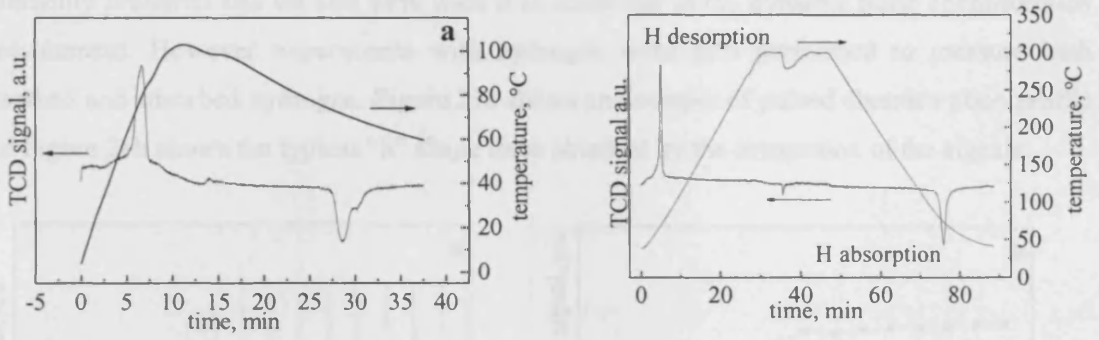

Figure 19. Two examples of temperature ramp for the temperature programmed hydride sorption (TPHS) analysis.

Figure 19b shows a TPHS analysis performed with a similar heating and cooling rate. There was a good quantitative correspondence between the areas of peaks of the two signals but the absorption signal offered the advantage of a more precise integration as it appeared in a region where the baseline is better defined. The ramp program in Figure 19b was finally adopted to measure the amount of absorbed hydrogen in the Pd-Al_2O_3 catalyst. The results of the measurements, expressed as mole of absorbed hydrogen per mole of Pd, are plotted as a function of Pd wt% in Figure 20.

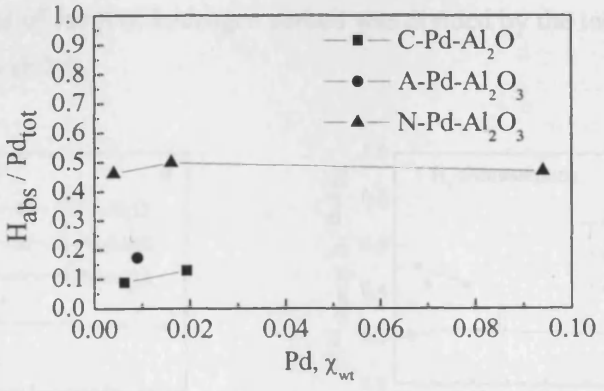

Figure 20. Amount of absorbed hydrogen per atom of Pd plotted as a function of the Pd loading (χ_{wt} = fraction in weight).

3.2.6 Pulse chemisorption

Selective hydrogen and carbon monoxide chemisorption are normally used to measure the dispersion of a supported metal catalyst. In the case of Pd, a problem emerges for the hydrogen chemisorption because the total uptake of hydrogen is affected by hydrogen absorption. CO is commonly preferred and we also have used it as adsorbent in the dynamic pulse chemisorption measurement. However experiments with hydrogen were also performed to measure both absorbed and adsorbed hydrogen. Figure 21a shows an example of pulsed chemisorption profile and Figure 21b shows the typical "S" shape trace obtained by the integration of the signals.

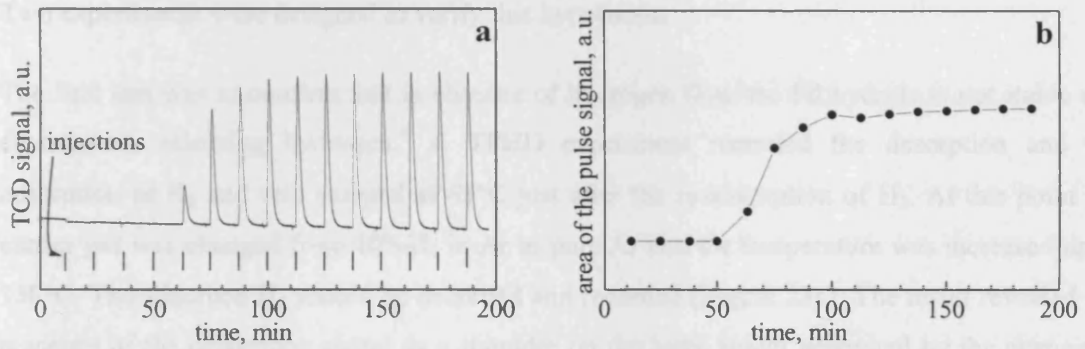

Figure 21. a) H_2 pulsed chemisorption profile for 1.6% N-Pd-Al_2O_3 sample. b) Integration of the PC signals reported as a function of the time.

Assuming that each atom of CO is adsorbed to one atom of Pd, the measured number of adsorbed CO molecules corresponds to the number of Pd atoms on the surface. Dividing this value by the total atom of Pd we obtain the fraction exposed of Pd (FE) (Figure 22a). In a similar way the number of atom of hydrogen sorbed was divided by the total number of atom of Pd and reported in Figure 22b.

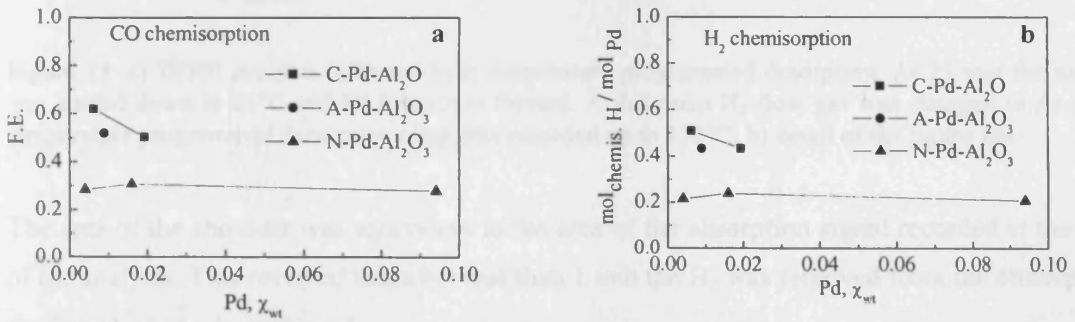

Figure 22. a) Fraction exposed of the Pd measured by CO pulse chemisorption plotted as a function of the Pd loading (χ_{wt} = fraction in weight). b) Number of sorbed hydrogen per atom of Pd.

3.2.7 Consideration over hydrogen pulse chemisorption

The measured amount of sorbed hydrogen is too low to be derived by the measure of both adsorbed and absorbed species. These facts led us to investigate more in detail the technique in order to reveal the real nature of the measurement. It was possible that in this experiment the H_2 absorption into the bulk was not measured. In fact after each injection of H_2 from the loop into the sample there were 12 min of pure argon flow. The starting conditions were appropriate for hydrogen absorption but, as the ratio of hydrogen in the atmosphere decreased, the absorbed H_2 may be desorbed and reach the detector.

Two experiments were designed to verify this hypothesis.

The first aim was to confirm that in absence of hydrogen flow the Pd hydride is not stable and decomposes releasing hydrogen.[8] A TPHD experiment recorded the desorption and the adsorption of H_2 and was stopped at 65°C just after the re-absorption of H_2. At this point the carrier gas was changed from 10%H_2 in Ar to pure Ar and the temperature was increased up to 150°C. The adsorbed H_2 should be desorbed and recorded (Figure 23a). The result revealed the presence of the desorption signal as a shoulder on the large signal generated by the change of gas[i] (Figure 23b).

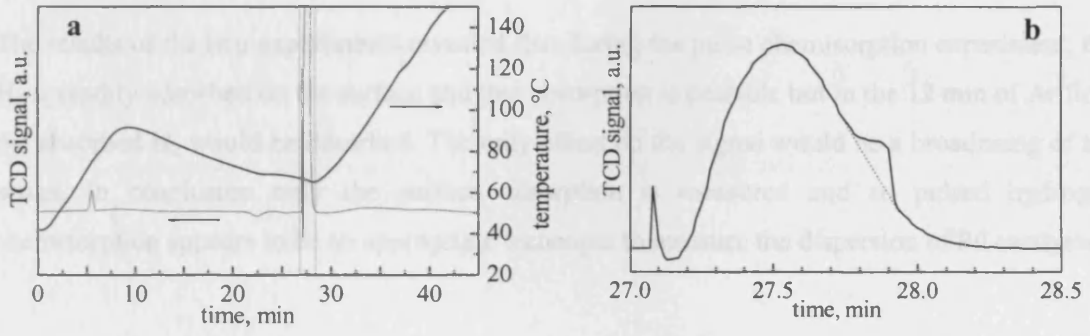

Figure 23. a) TPHR analysis followed by a temperature programmed desorption. At 25 min the sample was cooled down to 65°C and Pd hydride is formed. A this point H_2 flow gas was changed to Ar and a temperature programmed desorption ramp was recorded up to 150°C. b) detail of the figure 16a.

The area of the shoulder was equivalent to the area of the absorption signal recorded at the start of the analysis. This revealed that after less than 1 min the H_2 was removed from the atmosphere the β-Pd hydride decomposed.

[i] The change of the carrier gas produced two signals (Figure 23b). The first is a spike generated by the valve turning. The second is a large signal generated by the temporary large difference of gas composition of reference and carried gas into the Wheatstone bridge circuit of the TCD detector and due to the difference in the length of the two paths.

The second experiment measured the chemisorption of hydrogen at different temperatures (Figure 24).

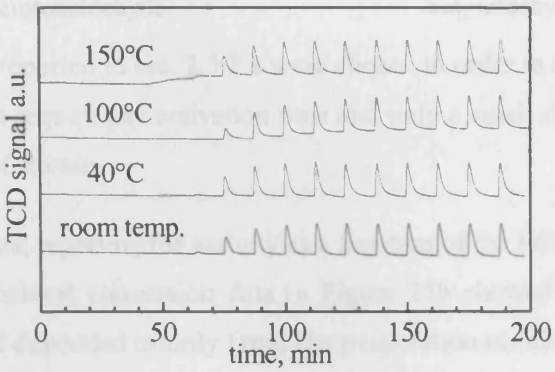

Figure 24. Pulse chemisorption profiles of 1.6 % N-Pd-Al_2O_3 recorded at different temperatures.

We know that above 80°C the absorption does not occur since the Pd hydride is unstable. So if the hydrogen chemisorption at room temperature measured both absorbed and adsorbed atoms at higher temperature we would expect smaller amounts of sorbed hydrogen. The integration of the signals revealed that there were no differences between the amount of chemisorbed hydrogen below and over 80°C. It has to be noted that a change in the baseline occurs but this phenomenon was observed in other samples also at room temperature.

The results of the two experiments revealed that during the pulse chemisorption experiment, the H_2 is readily adsorbed on the surface and that absorption is possible but in the 12 min of Ar flow the absorbed H_2 would be desorbed. The only effect on the signal would be a broadening of the peaks. In conclusion only the surface adsorption is measured and so pulsed hydrogen chemisorption appears to be an appropriate technique to measure the dispersion of Pd catalysts.

3.2.8 Catalytic test

The Pd-Al_2O_3 catalysts were tested for the hydrogenation of the crotonaldehyde ($CH_3-CH=CH-CH=O$). The crotonaldehyde has two double bonds that can be hydrogenated producing three possible products[9] (sec. 1.3.5). The Pd catalysts were strongly selective to the hydrogenation of the carbon-carbon double bond[10] and negligible amount of C=O bond hydrogenation was observed. Therefore in this section is monitored the activity of the catalyst to the hydrogenation of crotonaldehyde to butyraldehyde (1).

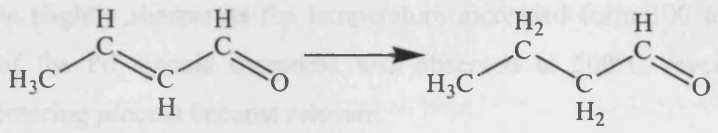

crotonaldehyde butyraldehyde (1)

The reaction conditions reported in sec. 2.3.2.1 were chosen in order to obtain a low conversion. The conversion does not require any activation time and only a small deactivation (about 10%) was observed after 8 h of stream.

The results of the analysis, reporting the activity as a function of the Pd loading, are summarised in Figure 25. The normalised conversion data in Figure 25b showed that the activity of the catalyst per mole of Pd depended mainly from the preparation method. A-Pd-Al_2O_3 was the most active and N-Pd-Al_2O_3 was the less active. The activity of the sample prepared with the same method seems to depend from the particle size: bigger particles are more active than smaller one.

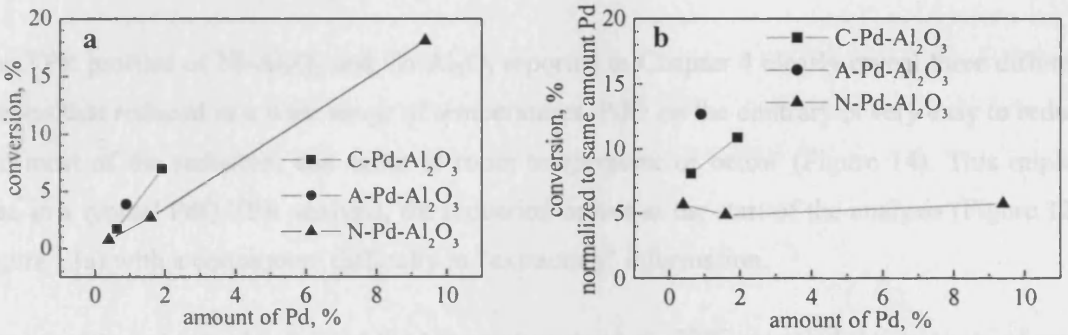

Figure 25. a) Conversion of crotonaldehyde to butyraldehyde reported as a function of the Pd loading. b) Conversion data normalised for 3% Pd loading.

3.3 Discussion

3.3.1 Sintering

The Pd signals in the XRD patterns of the low loading samples showed small signals that overlapped with the alumina signals. The *in situ* XRD temperature programmed reduction used for the characterization of N-Pd-Al_2O_3 revealed to be an efficient technique in studying the thermal effect on the supported Pd. From the sequence of the patterns it was possible to observe the change of the broadening of the Pd signals directly related with the Pd crystallites size. The

Pd signals became slightly sharper as the temperature increased form 100 to 400°C. A more marked change of the Pd signals sharpness was observed at 500°C revealing that at this temperature the sintering process become relevant.

A more detailed analysis of the pattern was attempted using MAUD[11] a simulation program based on "Rietveld" method. Unfortunately the high surface area of the alumina implies a structure rich in defects and strain that produce a pattern with very broad and "distorted" peaks that made the simulation very difficult. A good fitting was never obtained. Comparing visually the patterns of the various series reduced at 300°C, we observed more intense signals for the N-Pd-Al_2O_3 series in agreement with the dispersion measurement. Furthermore, the extent of sintering at high temperature was larger for the N-Pd-Al_2O_3 samples suggesting that larger particle sintered more easily.

3.3.2 Reducibility of palladium oxide

The TPR profiles of Ni-Al_2O_3 and Co-Al_2O_3 reported in Chapter 4 clearly reveal three different species that reduced in a wide range of temperatures. PdO on the contrary is very easy to reduce and most of the reduction can occur at room temperature or below (Figure 14). This implies that, in a typical PdO TPR analysis, the reduction occurs at the start of the analysis (Figure 12a, Figure 13a) with a consequent difficulty in "extracting" information.

Some instruments capable to start the temperature ramp at -70°C revealed the presence of more than one reducible species.[12] In attempt to increase the quality of the information of our TPR profiles, the analysis were performed with the routine flow of 50 ml/min and with a smaller flow of 25 ml/min.

Comparing the profiles recorded at 25 ml/min with those recorded at 50 ml/min (Figure 12 and Figure 13) we observed that the milder conditions induced the splitting of the signal revealing the presence of different reducible species not observed in previous works.[13] The main peak is also shifted at higher temperature. Using only TPR analysis, the identification of the species reduced at higher temperature appeared to be a difficult task. The TPR of N-Pd-Al_2O_3 unfortunately did not help us to understand as the trend observed for C-Pd-Al_2O_3 and A- Pd-Al_2O_3 is not confirmed. The alternation of the position of the high temperature reduction signal and the anomalous high intensity of the peak at 110°C and 180°C recorded for the 0.4% loading (Figure 15) led us to consider with more attention the possible origin of the signals observed at high temperature.

3.3.3 The hydrogen-palladium system

The hydrogen interaction with metal Pd is characterised by the possibility of both adsorption and absorption (Figure 26).

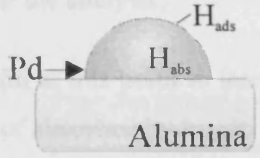

Figure 26. Hydrogen adsorption (Hads) and hydrogen absorption (Habs) on supported metal Pd.

Measuring the hydrogen chemisorption in a "volumetric" apparatus, the absorption process affects the total uptake of hydrogen and a back sorption is necessary to calculate the adsorbed hydrogen.[14,15] In the literature the Pd hydride formation has been avoided,[16,17] when using a dynamic pulsed apparatus, setting the sample temperature at 70°C (Pd-H decomposition). The consideration in section 3.2.7 demonstrates that this technique can selectively measure the chemisorbed hydrogen also when performed at room temperature.

From the number of adsorbed hydrogen (and assuming that one adsorbed hydrogen occupies a Pd surface site) the Pd fraction exposed was calculated. The FE was also measured by CO adsorption generally considered a reliable method as it is not absorbed into the Pd.

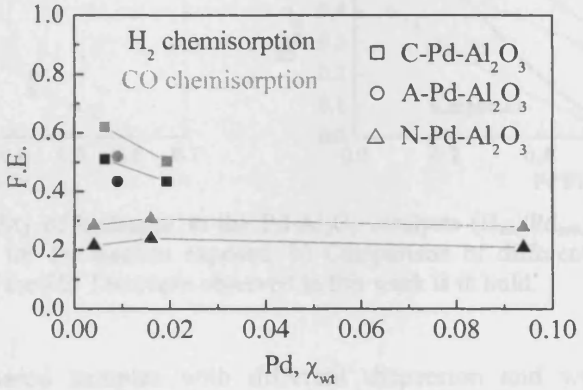

Figure 27. Comparison of the fraction exposed of the sample measured by H_2 and CO pulsed chemisorption.

The comparisons of the H_2 and CO measurement reported in Figure 27, showed that they were in good qualitative agreement. The FE measured by CO is about 20% higher compared with that measured with H_2. The constant difference suggested that some systematic process might have affected one of the two measurements. This could depend from instrumental or physical reason. In the second case the assumption adopted in the calculation that one atom of Pd interact with only one atom of CO or one atom of H could be not correct. Furthermore the spillover of adsorbed species may affect the measurement.

Continuing the analysis of the Pd-hydrogen system, we have seen that the amount of absorbed hydrogen was measured by a temperature programmed sorption technique (section 3.2.5). The TPHS ramp developed in this work appears to be an elegant way to observe quantitatively the reversible absorption desorption process. The consistent double measurement reinsures on the quality of the analysis.

It is useful at this point to introduce the new quantity "solubility of hydrogen in Pd" defined as number of absorbed hydrogen per atom of Pd (1).

$$\text{Solubility of H in Pd} = \frac{H_{abs}}{Pd_{total}} \qquad (1)$$

It is directly dependent on the amount of "bulk" Pd and, more specifically, it can be affected by three main factors. The first is the particle size: small particles can absorb less hydrogen as they are composed by more surface and less bulk Pd. The second is the alloying with other metals: the solubility decreases as the concentration of the second metal increases. The last factor that could influence the solubility of hydrogen in Pd is the support interaction.

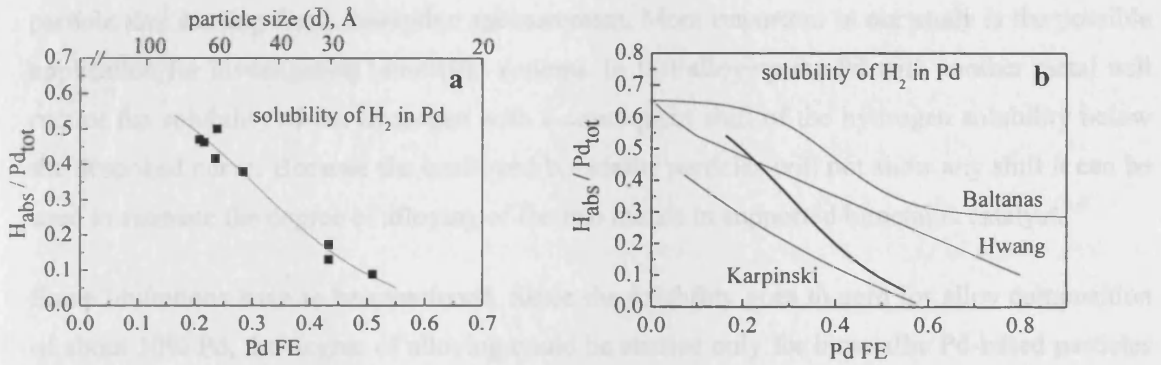

Figure 28. a) The solubility of hydrogen in the Pd-Al_2O_3 catalysts (H_{abs}/Pd_{total}) measured by TPHS is plotted as a function of the Pd fraction exposed. b) Comparison of different study of the hydrogen solubility as a function of the FE. The curve observed in this work is in bold.

Because we had prepared samples with different dispersion and we had measured both solubility of hydrogen and dispersion we were able to verify their relationship. The hydrogen solubility as a function of the FE calculated by hydrogen chemisorption is plotted in Figure 28. On the top axes is also reported the average particle size ($\bar{d}$) estimated assuming spherical particle shape, by the equation $\bar{d} = \frac{11.2}{FE}$.[18] The fitting curve clearly underlines the expected correlation between the solubility and the fraction exposed. This correlation was previously studied for pure Pd by *Boudart and Hwang*[3] and for supported metal Pd by *Baltanas et al.*[19] (who reviewed previous studies) and *Karpinski et al.*[6] (Figure 28b).

The first two authors, who used an isothermal apparatus for the measurement of the absorbed hydrogen, did not find much agreement for high dispersion samples. The differences were attributed to the different pre-treatment of the sample. The hydrogen solubility observed by Baltanas reaches a plateau for FE higher than 0.5. This was explained by dividing H_{abs} in two components, H_β (β-hydride adsorbed into the bulk) and H_{ss} (hydrogen sorbed in surface below the first few layer of Pd), and considering that the second component becomes very important at higher FE. The deviation from the main fitting line observed in other works[20,21] was also considered and correlated with strong interaction with the support induced by prolonged reducing process. In the present and in Karpinski's work, that used a temperature programmed technique, a lower solubility curve was observed. Support interaction could have played a role, but the absence of the plateau at high dispersion suggested that the divergence is mainly due to the different techniques used. In particular the H_{ss} may be not detectable by the TPHD measurement. At low dispersion the curve measured in this work approached the Baltanas curve and correctly aimed the value of 0.66 typical of pure bulk Pd.

The knowledge of the H_{solub}/FE curve is relevant as it could be used for the study of the average particle size starting from absorption measurement. More important in our study is the possible application for investigating bimetallic systems. In fact alloying the Pd with another metal will reduce the solubility of the hydrogen with a consequent shift of the hydrogen solubility below the described curve. Because the unalloyed bimetallic particles will not show any shift it can be used to estimate the degree of alloying of the two metals in supported bimetallic catalyst.[4,6]

Some limitations have to be mentioned. Since the solubility goes to zero for alloy composition of about 50% Pd, the degree of alloying could be studied only for bimetallic Pd-based particles containing more than 50% Pd. Moreover, as we can see in figure 22a, when the dispersion increases the solubility goes to zero and so there is a limit to the detectable size of the particles.[22]

Another result that worth some comments is the splitting of the TPHS signal observed in Figure 19 when a slow cooling rate was used. It is easily reproducible in the desorption step using a low rate heating ramp. This splitting, not reported in the literature, may be originated by two different types of site were the Pd is allocated. TPHD analysis performed with a low rate heating ramp could provide additional information useful to investigate the solubility of hydrogen in Pd and thus the particle size and the degree of alloying.

3.3.4 Reaction

The reaction results showed that the activity of the catalyst per mg of Pd mainly depends on the preparation method. The dependence of the activity from the particle size observed for the samples C-Pd-Al_2O_3 and N-Pd-Al_2O_3 is interesting but should be confirmed with a larger number of samples. This reaction was chosen because the selectivity to the C-O hydrogenation is structure sensitive.[23,24] Since all the Pd catalysts were 100% selective to the C-C double bond we could not investigate this aspect. When a second metal will be added to form the alloy catalysts some selectivity to the double C-O double bond could be induced and studied.

3.4 Conclusions

From a general point of view the single metal Pd study was planned to acquire a background of knowledge necessary for the next step: the preparation of uniform alloy particle by the selective reduction of a second metal.

From the *in situ* XRD, we have obtained precise information about the sintering process that will be useful for the thermal treatment needed for the alloying of the bimetallic particles after the deposition of a second metal. In fact marked sharpening of the peaks observed above 500°C will set a limit temperature for the thermal treatment needed for the alloying of the two metals in order to avoid large sintering.

The preparation of Pd-Al_2O_3 in different method produced a series of samples with different dispersion. The combination of chemisorptions and adsorption measurement allowed to well define the solubility property of the hydrogen into the bulk Pd. This achievement is particular relevant as leads to a method that will be very useful for difficult task of measuring the degree of alloying of Pd bimetallic particles.

The exclusive hydrogenation of C-C double bonds in the test reaction precluded the study of the selectivity. The deposition of a second metal planned to prepare the alloy catalyst could induce a certain degree of selectivity to the C-O bond allowing the study of the structure-sensitivity of the reaction.

Three other achievements can be mentioned.

The TPR analysis performed at low flow revealed the possibility to resolve the Pd signal in different components. Despite a complete understanding of the origin of the signal was not achieved, this could be an information source to differentiate the various Pd catalysts.

The TPHD analysis was developed in a more complete TPHS that allowed the precise measurement of the amount of absorbed hydrogen. The use of slow heating (and cooling) rate in the temperature ramp revealed the presence of different sites where the Pd could be absorped.

It has been showed that the dynamic pulsed hydrogen chemisorption measures selectively the adsorbed hydrogen also when performed below the decomposition temperature of β-Pd hydride.

References

1 Yu. I. Ermackov *J. Mol. Catal.* 21 (1983) 35

2 D. M. Nace, J. G. Aston *J. Amer. Chem Soc.* 79 14 (1957) 3619

3 M. Boudart, H. S. Hwang *J. Catal.* 39 (1975) 44

4 M Bonarowska, J. Pielaszek, W. Juszczyk, Z.Karpinski *J. Catal.* 195 (2000) 304

5 A. Malinowski, W. Juszczyk, M. Bonarowska, J. Pielaszek, Z. Karpiski *J. Catal.* 177 (1998)153

6 M. Bonarowska, J. Pielaszek, V. A. Semikolenov, Z. Karpiski *J. Catal.* 209 (2002) 528

7 T. C. Chang, J. J. Chen, C. T. Yeh *J. Catal.* 96 (1985) 51

8 J. A. Konvalinka, J. J. F. Scholten *J. Catal.* 48 1-3 (1977) 374

9 M. A. Vannice, B. Sen *J. Catal.* 115 (1998) 65

10 M. A. Vannice *Topics Catal.* 4 (1997) 241

11 L. Lutterotti, S. Matthies, H. R. Wenk "Proceeding of the Twelfth International Conference on Textures of Materials" (ICOTOM-12) 1 (1999) 1599

12 K. Muto, N. Katada, M. Niwa *Appl. Catal., A* 134 (1996) 203

13 L. W. Konopny, A. Juan, D. E. Damiani *Appl. Catal., B* 15 (1998) 115

14 A. M. Sica, I. M. Baibich, C. E. Gigola *J. Mol. Catal. A: Chem.* 195 1-2 (2003) 22

15 A. M. Eberhardta, E. V. Benvenutti, C. C. Morob, G. M. Tonetto, D. E. Damiani *J. Mol. Catal. A: Chem.* 201 1-2 (2003) 247

16 M. Bonarowska, B. Burda, W. Juszczyk, J. Pielaszek, Z. Kowalczyk, Z.Karpinski *Appl. Catal., B* 35 (2001) 13

17 S. Ordóñez, H. Sastre, F. V. Díez *Thermochimica Acta* 379 1-2 (2001) 25

18 J. R. Anderson "Structure of metallic catalyst" Academic Press, London 1975

19 A. L. Bonivardi, M. A. Baltanas *J. Catal.* 138 (1992) 500

20 P. Chou, M. A. Vannice *J. Catal.* 104 (1987) 1

21 R. T. K. Baker, E. B. Prestige, G. B. McVicker *J. Catal.* 89 (1984) 422

22 M. Legawiec-Jarzyna, A. Rbowata, W. Juszczyk, Z. Karpiski *Catal. Today* 88 (2004) 93

23 E. Martin, J. Andreas, L. A. Johannes *J. Catal.* 166 1 (1997) 25

24 N. Yuriko, U. Kenji, I. Toshinobu *Appl. Catal.* 56 1 (1989) 9

Chapter 4

4 Comparative study of Ni and Co supported on Al_2O_3

4.1 Introduction

In this Chapter is presented the study of the single metal catalysts Co-Al_2O_3 and Ni-Al_2O_3 prepared by incipient wetness impregnation under different conditions. The characterisation, performed mainly by XRD, TPR and dispersion measurement, aimed to study the effect of the preparation conditions on the final catalyst. The effect of the calcination temperature, the calcination time, the loading and the support surface area were investigated. Thanks to a large number of samples analysed a good understanding of the effect of these variables on the catalyst is achieved and a model is proposed.

The TPR analysis, in particular, revealed to be very useful in this study. It was possible to identify and investigate three different species of metal oxide precursors from which the final properties of the metal catalyst depend.

This study was designed to acquire basic knowledge of the single metal catalyst necessary for the subsequent "selective second metal deposition" planned for the preparation of bimetallic alloy catalyst. Ni-Pd-Al_2O_3 (and Co-Pd-Al_2O_3) will be in fact used as "parent" (Chapter 6) for the deposition of a second metal Pd.

4.2 Results

4.2.1 Sample range

Two series of $Ni\text{-}Al_2O_3$ and $Co\text{-}Al_2O_3$ catalysts were prepared by incipient wetness impregnation (IWI) of the nitrate salt using two different types of γ-alumina. They were identified as **$Ni\text{-}Al_2O_3$-I**, **$Ni\text{-}Al_2O_3$-A**, **$Co\text{-}Al_2O_3$-I**, and **$Co\text{-}Al_2O_3$-A** were "I" and "A" identifies the origin of the support, respectively "ICI" and "Aldrich". The surface areas of the supports, measured by the BET method, are 165 m^2/g for "A" alumina and 295 m^2/g for "I". Samples with various metal loadings (from 0.2 wt% to 22 wt%) were prepared for each series (sec. 2.2.1). After the impregnation, the metal nitrate on alumina samples were calcined at 400ºC for 3 h and characterised in order to study the effect of support and loading on the particle size. Four samples (5.6-0.5% $Ni\text{-}Al_2O_3$-I and 7.5-0.5% $Co\text{-}Al_2O_3$-I) where also prepared using different calcinations temperature and calcinations time. Figure 29 summarises the collection of samples prepared specifying the preparation condition.

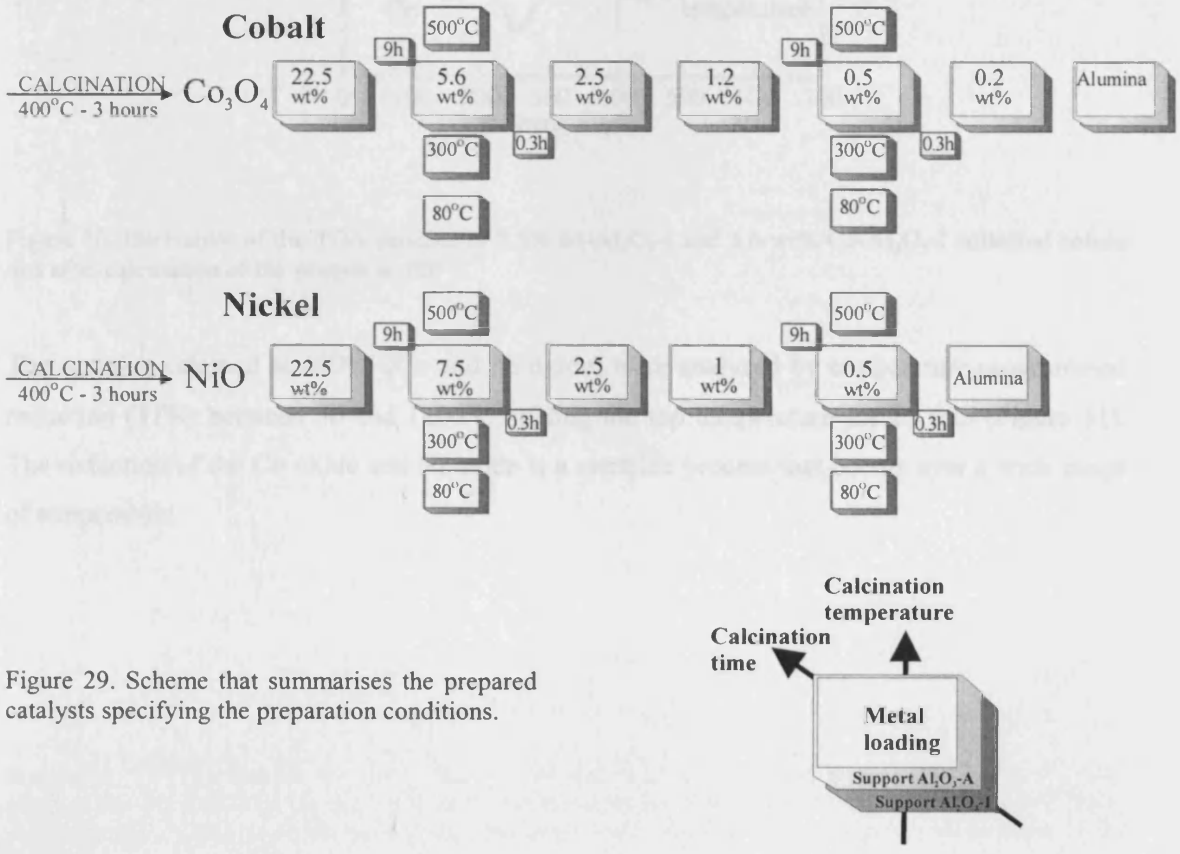

Figure 29. Scheme that summarises the prepared catalysts specifying the preparation conditions.

4.2.2 Temperature programme reduction

After the impregnation (and the drying) the samples were calcined at 400°C for 3 h. This temperature was selected after thermo-gravimetric analysis (TGA). The traces of the dried sample in Figure 30 showed that after the water desorption at about 100°C two more peaks were observable at about 250°C and 400°C. They were due to the nitrate decomposition. The presence of two decomposition signals was probably due to different interactions of the nitrate with the support. After calcination at 400°C the TGA profiles, apart for the water desorption, appeared flat confirming that the nitrate decomposition was complete.

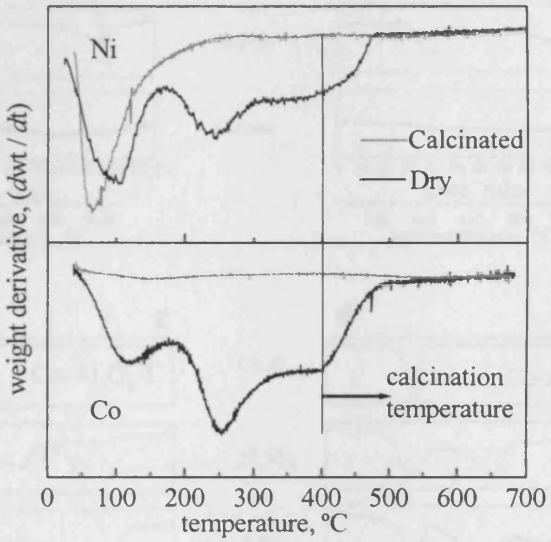

Figure 30. Derivative of the TGA profiles of 7.5% Ni-Al_2O_3-I and 5.6 wt% Co-Al_2O_3-I collected before and after calcination of the sample at 400°C.

The samples calcined at 400°C (Co and Ni oxide) were analysed by temperature-programmed reduction (TPR) between 30 and 1100°C holding the top temperature for 15 min (Figure 31). The reduction of the Co oxide and Ni oxide is a complex process that occurs over a wide range of temperature.

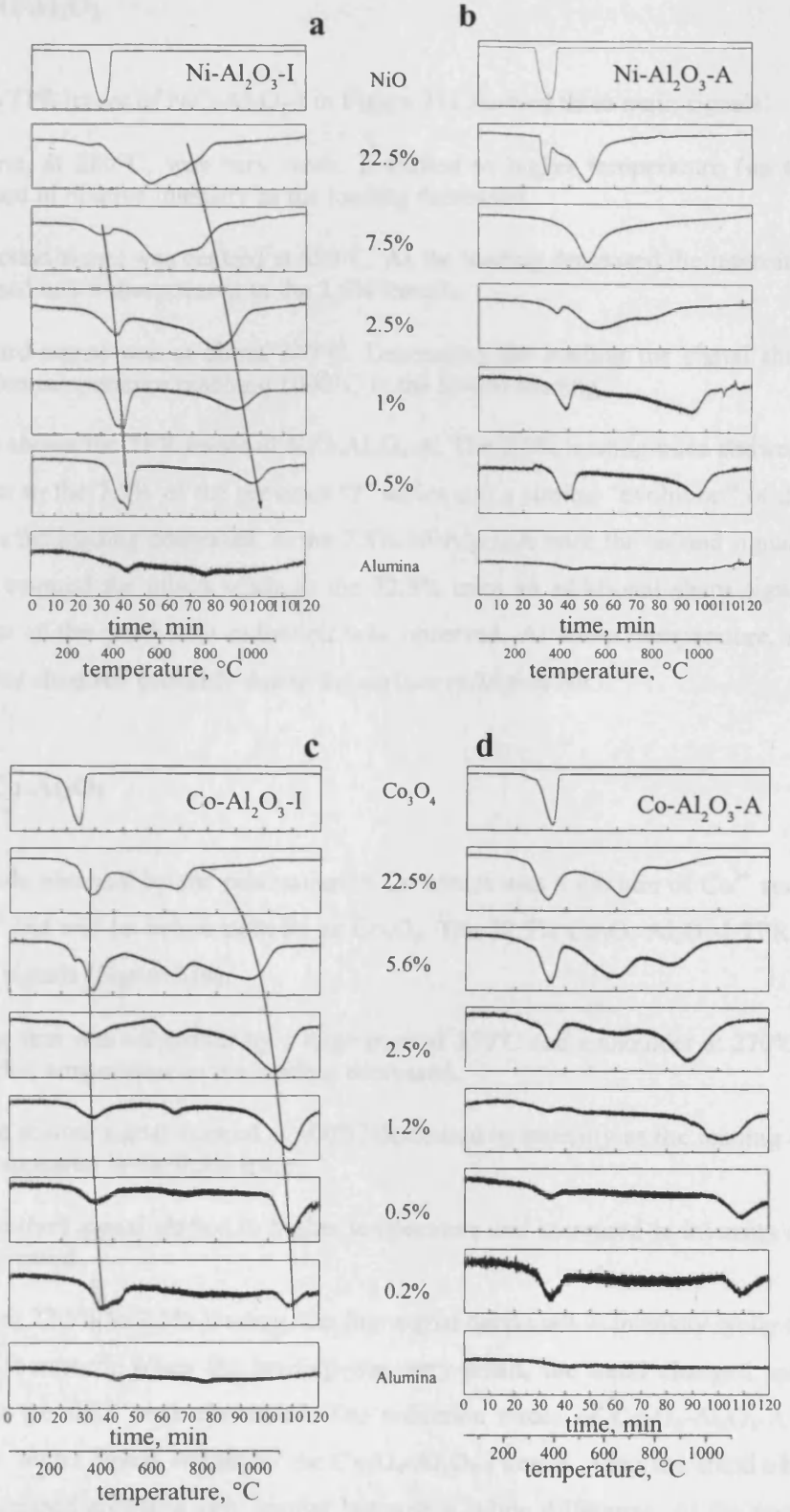

Figure 31. TPR profiles of the four series of samples. The samples prepared by IWI were previous calcined for 3 h at 400°C. On the top of each series the profile of the pure metal is reported as reference. Note that the profiles were not plotted with the same scale in order to allow a better comparison of the signals.

4.2.2.1 Ni-Al_2O_3

The 22.5% TPR traces of NiO-Al_2O_3-I in Figure 31a showed three main signals.

- The first, at 280°C, was very weak. It shifted to higher temperature (up to 420°C) and increased in relative intensity as the loading decreased.
- The second signal was centred at 550°C. As the loading decreased the intensity of the signal decreased and it disappeared in the 2.5% sample.
- The third signal was at about 770°C. Decreasing the loading the signal shifted to higher reduction temperature reaching 1000°C in the lowest loading.

Figure 31b shows the TPR traces of NiO-Al_2O_3-A. The 2.5% loading trace showed three signals very similar to the 7.5% of the previous "I" series and a similar "evolution" of the signals was observed as the loading decreased. In the 7.5% Ni-Al_2O_3-A trace the second signal was the main one and it covered the others while in the 22.5% trace an additional sharp signal at the same temperature of the pure NiO reduction was observed. At lower temperature, a small broad shoulder was observed probably due to the surface reduction NiO.

4.2.2.2 Co-Al_2O_3

The Co oxide obtained by the calcination of Co nitrate was a mixture of Co^{3+} and Co^{2+} (Co_3O_4 and CoO_2)[1] but will be below indicate as Co_3O_4. The 22.5% Co_3O_4-Al_2O_3-I TPR trace showed three main signals (Figure 31a).

- The first was composed by a large peak at 350°C and a shoulder at 270°C. It shifted to higher temperature as the loading decreased.
- The second signal centred at 600°C decreased in intensity as the loading decreased and disappeared in the 0.5% trace.
- The third signal shifted to higher temperature and increased in intensity as the loading decreased.

Passing from 22.5% to 2.5% loading, the first signal decreased in intensity while the area of the third peak increased. When the loading was very small, the trend changed and the relative intensity of the third peak decreased. The reduction traces of Co_3O_4-Al_2O_3-A (Figure 31b) presented a set of signal similar to the Co_3O_4-Al_2O_3-I series. Also the trend observed as the loading decreased appeared very similar but with a subtle difference. At the same loading the shift of the third peak and the "disappearing" of the second peak was less marked.

4.2.3 Effect of calcination temperature and calcination time

The 0.5/7.5% Ni-Al_2O_3-I and the 0.5/5.6% Co-Ni-Al_2O_3-I samples were calcined at 300°C for 20 min, 3 h and 9 h (Figure 29) and analysed by TPR (Figure 32).

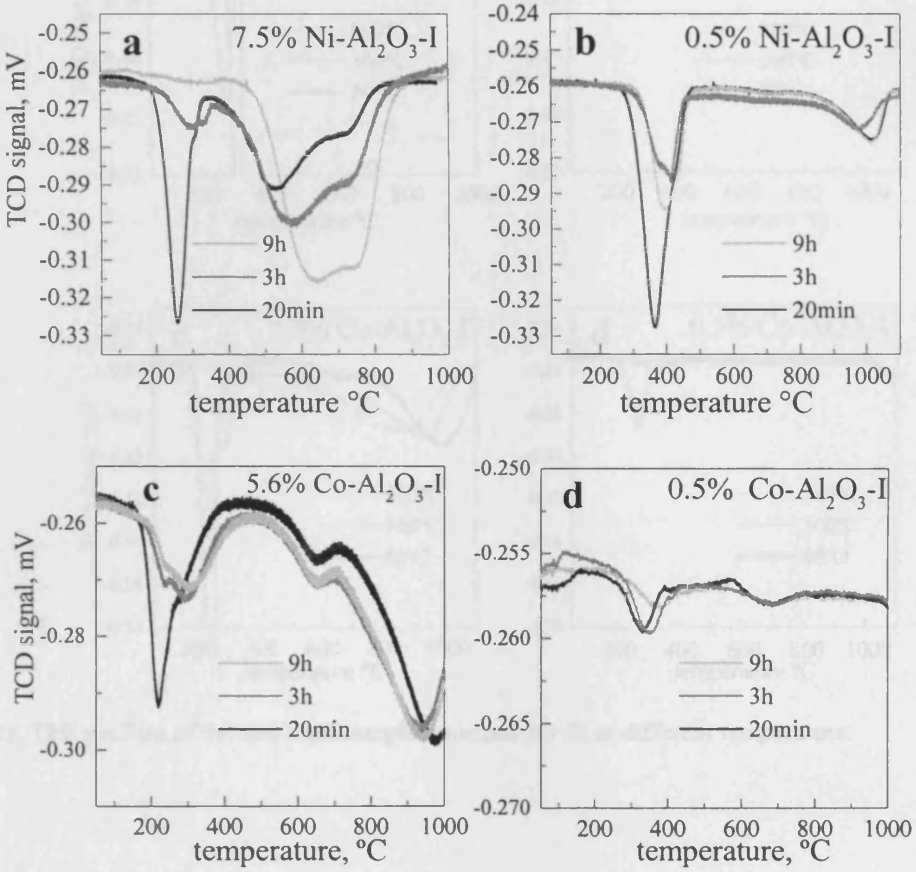

Figure 32. TPR profiles of the specified samples calcined at 300°C for different time.

In all the cases longer calcination time produced the decrease of the intensity of the low temperature signal. The signals at high temperature did not change much in the low loading samples while in the higher loading samples longer calcination time produced the increase of their intensity. This was particularly evident in the 7.5% Ni-Al_2O_3-I profile.

The same set of samples (0.5-7.5% Ni-Al_2O_3-I and 0.5-5.6% Co-Al_2O_3-I) were calcined for 3 h at different temperatures and analysed by TPR (Figure 33). For the 0.5% loading samples higher calcination temperature led to the decrease of the low temperature signal. In the case of 7.5% Ni-Al_2O_3-I and 5.6% Co-Al_2O_3-I was also observed the increase of intensity of the high temperature signals.

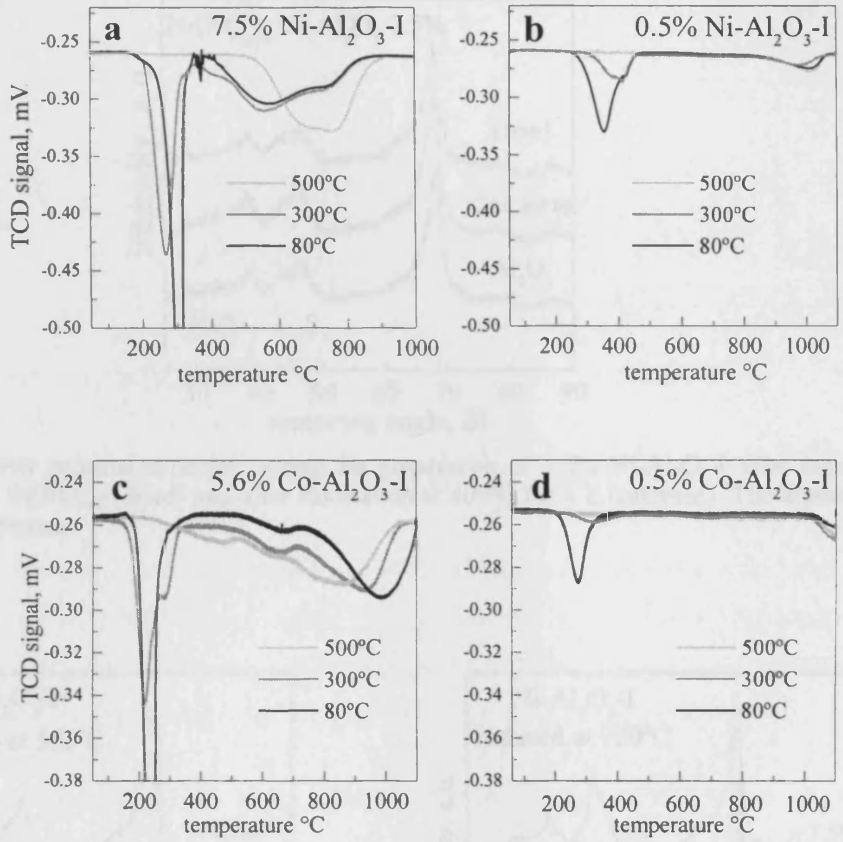

Figure 33. TPR profiles of the specified samples calcined for 3h at different temperature.

4.2.4 XRD study

The 7.5% Ni-Al_2O_3-I sample was analysed by XRD during the preparation. The patterns were collected after impregnation of $Ni(NO_3)_2$ on Al_2O_3 and after calcination at 400°C for 3 h (forming NiO-Al_2O_3) (Figure 34). No $Ni(NO_3)_2$ and NiO signals were observed suggesting that the deposition produced a good dispersion of the particles and that the calcination at 300°C did not promote sintering.

The XRD analysis of the 2-7.5% samples of the Ni-Al_2O_3-I series reduced at 400°C did not show the presence of any crystallised (XRD detectable) Ni. The analysis of the 7.5% sample reduced at 550°C showed only weak Ni signals, while reducing the samples at 750°C more intense signals are observed (Figure 35).

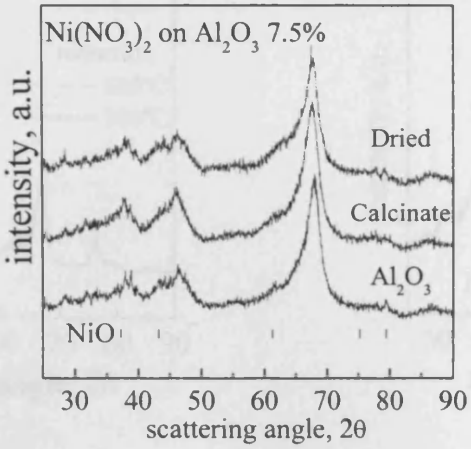

Figure 34. XRD patterns collected during the preparation of 7.5% Ni-Al_2O_3-I after impregnation of alumina with $Ni(NO_3)_2$ (dried) and after calcination at 400°C for 4 h (calcined). The alumina pattern is reported as reference.

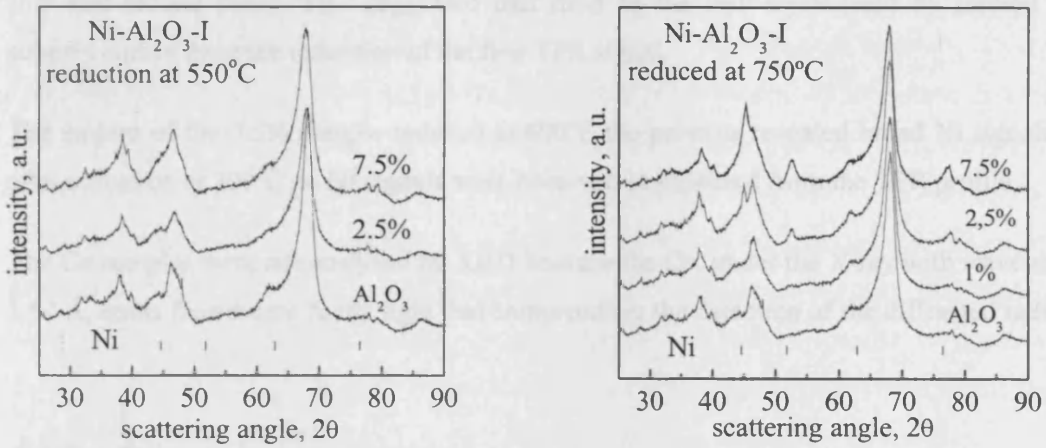

Figure 35. XRD patterns of Ni-Al_2O_3-I at the specified loading after reduction at 550 and 750°C.

The TPR traces showed that the total amount of reduced oxide strongly depend on the reduction temperature. The best reduction temperature will be then a compromise between reducing large amount of Ni and avoiding strong sintering of the particles.

Two Ni-Al_2O_3-A samples (22.5 and 5.6%) were analysed by XRD after reduction at 300°C and 600°C (Figure 36). These temperatures were selected on base of the TPR results and aimed to investigate the reducible species associated with the TPR signals.

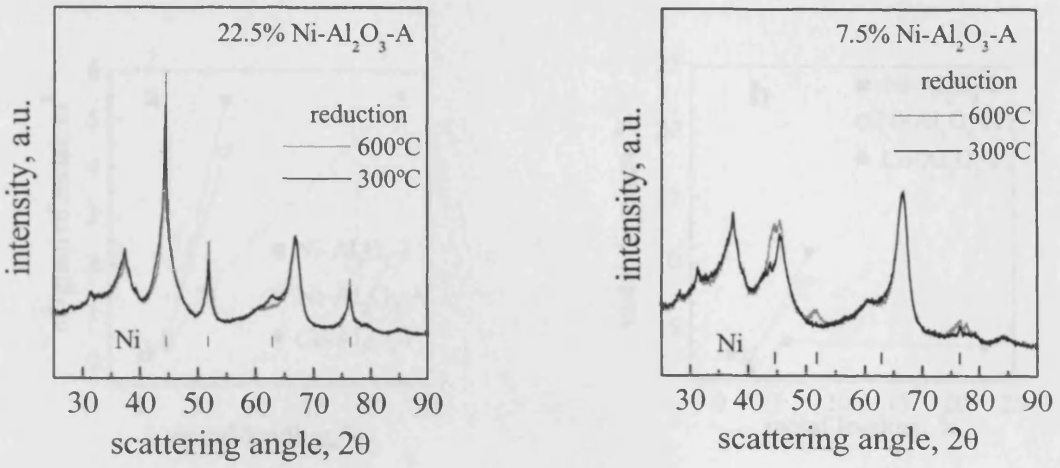

Figure 36. XRD patterns of 22.5 and 7.5% Ni-Al_2O_3-A after reduction at 300 and 600°C.

In the 22.5% pattern the sample reduced at 300°C (reduction of the first peak) showed intense and sharp Ni peaks very similar to those from the sample reduced at 600°C (reduction of the first and second peak). This suggested that most of the well-crystallized Ni formed on the support comes from the reduction of the first TPR signal.

The pattern of the 7.5% sample reduced at 600°C the patterns revealed broad Ni signals while after reduction at 300°C no Ni signals were observed as expected from the TPR profile.

The Co samples were not analysed by XRD because the Co, under the X-ray with wavelength of 1.54 Å, emits fluorescent X-ray light that compromises the detection of the diffracted radiation.

4.2.5 Dispersion measurements

The metal surface of the Ni/Co-Al_2O_3 catalyst (reduced at 550/650°C) was measured[i] by a volumetric hydrogen chemisorption (sec. 2.4.5) and the results are reported in Figure 37a.

[i] Experiment performed in the Johnson Matthey laboratory in Billinghan.

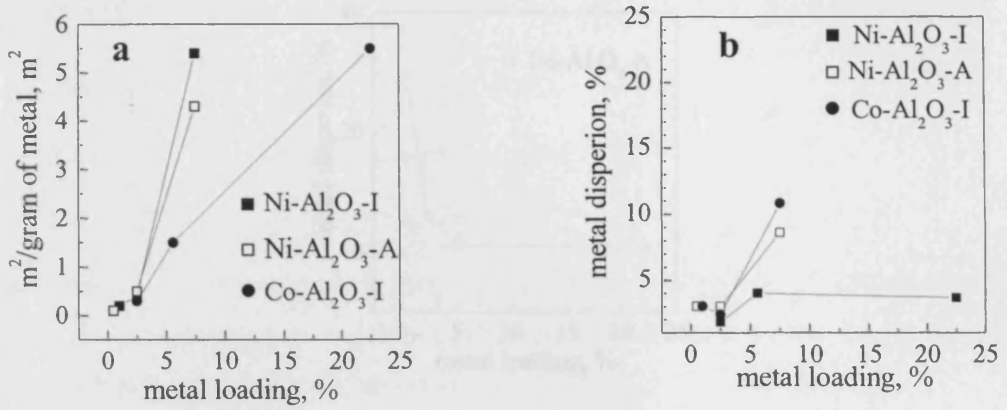

Figure 37. a) Area of surface metal per gram of catalyst expressed as a function of the loading, measured by hydrogen volumetric chemisorption. b) Dispersion of the sample calculated assuming that all the metal was reduced.

From the area of the metal surface is possible to calculate the number of atoms on the surface. The dispersion is then obtained by dividing it by the total number of metal atoms in the sample (Figure 37b). Catalysts prepared by incipient wetness impregnation normally have higher dispersed particles in low loading sample. Remarkably the results did not follow this trend. At high loading we observed relatively high dispersion. At 2.5% loading the dispersion reach a minimum and below this loading we observed a slight increase. A possible reason for this is the wrong assumption in the calculation that all the metal was in the reduced state. From the TPR profiles in Figure 31 we observed that the amount of Ni/Co oxide reduced at 550/650°C was close to 100% only at high loading while at low loading only a fraction of metal oxide is reduced. This introduces an error in the calculation of the dispersion that could explain the drop of dispersion below 5% loading (Figure 37b). Another factor that has to be considered is that the accessibility of the H_2 to the metal atoms could be repressed by strong metal-support interaction. The dispersion data in Figure 37b underlined the complexity of the Ni/Co-Al_2O_3 interactions.

The dispersion of Co-Al_2O_3-I was measured by pulsed H_2 chemisorption performed at 100°C (because of the characteristic activated chemisorption[2] of H_2 on Co) (Figure 38). The results showed a decrease of the dispersion as a function of the loading. This is the general trend expected for a series of samples with different loadings but it was in direct contrast with the previous results. Unfortunately the series of experiment performed with the pulsed H_2 chemisorption (with both Ni and Co) did not provide very reproducible results and cannot be considered totally reliable.

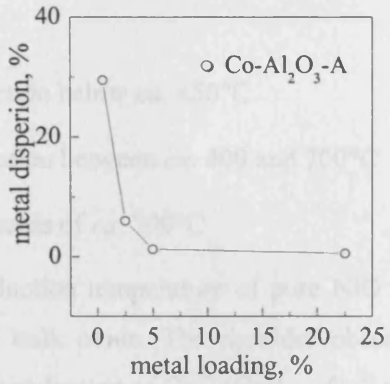

Figure 38. Dispersion of Co-Al_2O_3-A measured by pulsed hydrogen chemisorption.

In conclusion the metal surface measurements provided contradictory results on the metal dispersion. Microscopy analysis appears to be the essential for a direct observation of the particle size.

4.3 Discussion

4.3.1 TPR and reducible species

A supported metal catalyst is often prepared by the reduction of the oxide precursor. In the case of preparation by IWI method, the calcination step, that promotes the salt decomposition and the metal oxide formation, enhances also the metal-support interaction. Different "metal oxide reducible species" are formed as a function of the extent of the interaction. Thus, while the reduction of pure Ni and Co oxide occur at a precise temperature the reduction of supported metal oxide is a complex process and occurs in a wide range of temperature.

In this Chapter we tried to understand the nature and the distribution of the "reducible species" as a function of loading, support and thermal treatment. Comparing the TPR profiles of the Ni and Co oxide (Figure 31) we observed strong differences between the high and low sample loadings. Instead, remarkable similarity emerged for the four series comparing the evolution of the signal as a function of the loading. This observation is very important as suggests that the supported Ni and Co oxide species behave in very similar way under reduction conditions. Thanks to the large number of analysis performed, the complexity of reducing profiles can find

some simplification. In fact three main reduction regimes identifying three different reducible phases were observed.

- Phase I : reduction below *ca.* 450°C
- Phase II : reduction between *ca.* 400 and 700°C
- Phase III : in excess of *ca.* 700°C

Phase I showed the same reduction temperature of pure NiO and Co_3O_4 (Figure 31) and was assigned to the reduction of bulk oxide. The shoulder observed in the Co_3O_4 samples was probably due to the successive reduction of Co^{3+} ($Co^{3+} \rightarrow Co^{2+}$ and $Co^{2+} \rightarrow Co^0$).[1]

Phase II is reported in the literature[3,4,5] to be originated by the reduction of the ionic forms Ni^{2+}, Co^{2+} and Co^{3+} diffused on the surface of the alumina and into the octahedral and tetrahedral interstitial sites present on the surface alumina lattice.[6,7,8,9] It is suggested that for surface and crystalline ion species, the reduction temperature increases as a function of the number of aluminium species that surround the metal. Al^{3+}, in fact, polarizes[10,11] the Co-O and Ni-O bonds increasing the effective charge on the metal and consequently the lattice energy. The XRD analysis of the 22.5% Ni-Al_2O_3-A after reduction at 300 and 600°C showed that the reduction of the second phase did not increase the total amount of "crystallised" Ni. This confirms that Phase II is not a bulk oxide.

Phase III was observed in the region of the reduction temperature of the metal aluminates $NiAl_2O_4$[12,13] and $CoAl_2O_4$[3,14] that reduces respectively at *ca.* 800°C and *ca.* 900°C. The observed reduction temperature in the low loading samples was higher than those expected for the pure metal aluminates. These spinel phases are formed inside the alumina bulk and for this reason to achieve reduction more energy is required.

The three reducible species can thus summarised as following:

- Phase I consists of bulk metal oxide
- Phase II consists of the diffuse metal oxide on the alumina surface and metal ions are occupying interstitial site of the first few layers of the alumina structure
- Phase III consists of metal ions incorporated deep into the alumina structure forming Co and Ni aluminate

In order to visualise the relative change of the reducible species, a semi-quantitative analysis was performed. The areas of the three main signals were integrated and compared with the total area of the peaks of each pattern. Figure 39 shows how the reduction peak areas of the three phases changed as a function of the loading.

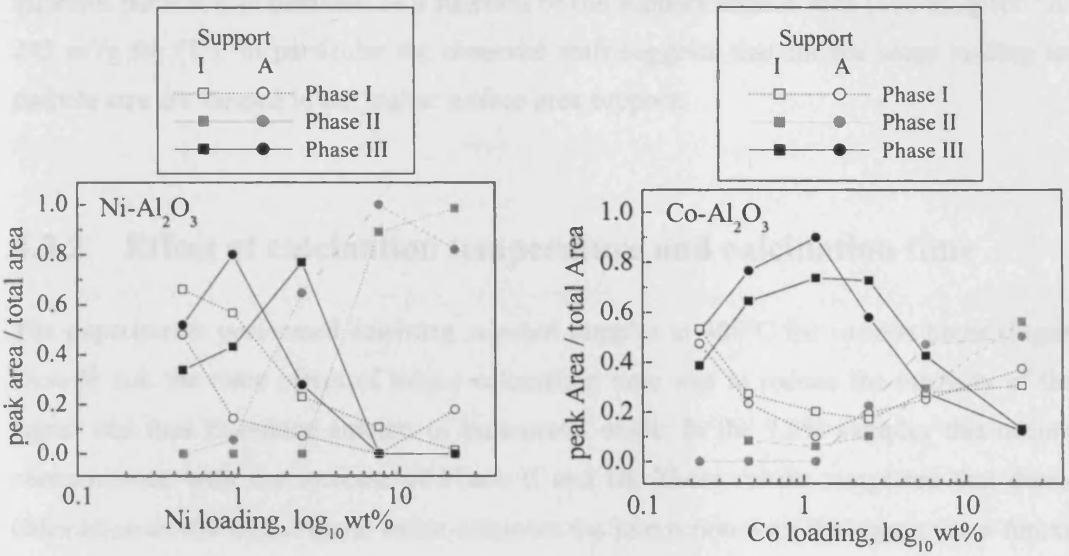

Figure 39. Relative areas of the reduction peaks associated with the three reducible species above specified expressed as a function of the loading.

Analysing the graphs in Figure 39, we can describe the general trend of the relative abundance of the phases as a function of the loading. Phase II showed its maximum intensity at the highest loading and decreased for lower loading disappearing around 2.5-1%. The decrease of Phase II corresponded to an increase of Phase III. This trend was already observed in the literature for both Ni[13] and Co.[15] Phase I appeared to slightly increase for Ni-Al_2O_3 and to slightly decrease for Co-Al_2O_3 as the loading decreased from the highest to about 2.5-1%. Below the 2.5-1% loading, we observe a fast increase of Phase I and a corresponding decrease of phase III.

The relative distribution of the three phases described as a function of the loading could be also expressed as a function of the particle size. The selective hydrogen chemisorption analysis (sec. 4.2.5) could not provide the metal dispersion as after reduction at 500-600°C an unknown fraction of metal has been reduced. The use of higher reduction temperature was not contemplated as the sintering process and the changing of the high surface support would strongly affect the measurement. In the literature,[3,4,6] measurement from the broadening of the XRD peaks showed that smaller particles are formed in the lower loading samples and we expected a similar trend in our samples. This means that the distribution of the three phases can be correlated with different particle size.

Figure 39 offers also the possibility to observe how the surface area of the support has influenced the distribution of the three phases. Following the lines that define the relative intensity of the three phases we observed that the general trend is the same for the two supports (squares and circles) but the lines associated with the support "A" are regularly shifted to the left compared with the "I" support. This result is important as can be associated with the

different particle size obtained as a function of the support surface area (165 m^2/g for "A" and 295 m^2/g for "I"). In particular the observed shift suggests that for the same loading smaller particle size are formed in the higher surface area support.

4.3.2 Effect of calcination temperature and calcination time

The experiments performed calcining selected samples at 400°C for various times (Figure 32) showed that the main effect of longer calcination time was to reduce the intensity of the first signal and thus to reduce amount of bulk metal oxide. In the 7.5% samples this occurred in concomitance with the increase of Phase II and III. These results suggested that during the calcination at 400°C, the metal oxide enhances the interaction with the support as a function of the calcination time.

Calcining the samples for 3h at different temperatures (Figure 33) we observed a similar effect. Higher calcination temperature reduced the amount of bulk oxide and increased the diffusion of the metal ions on the surface, and into the surface, of the alumina. This description was consistent with the XPS analysis of Ni supported on α-Al_2O_3 performed by *Molina et al.*[16] which showed a decrease of the Ni on the surface as a function of the calcination temperature. At 500°C the transformation was complete as no more bulk metal (phase I) was observed. The fact that after calcination at low temperature Phase II and III are however observed suggested that exist a distinction between bulk and diffused particles (Phase I and II) since the nitrate salt is deposited during the impregnation process. This observation founds confirmation in the thermo-gravimetric analysis (Figure 29) that revealed two signals for the decomposition of the nitrates.

4.3.3 Origin of Ni and Co aluminates

An important fact that has to be reminded when presenting TPR results is that it is a destructive technique. When high temperatures are reached (especially above the calcination temperature) the analysis actively modifies the samples. The Tammann temperatures (about 1/2 of the melting point temperature) for Ni and Co are respectively *ca.* 590°C and 610°C. Above these temperatures the metal mobility can be relevant and promote solid-state diffusion. Phase III, the product of solid diffusion of the ion into the alumina, is thus a phases that may not exist before the analysis and be created during the increase of the temperature. The TPR profiles collected in this work offered the opportunity to observe and analyse the evolution of Phase III. In particular it is very interesting to note the shift of Phase III to high temperature as the sample loading

decreased. At the highest loading Phase III may not be present, decreasing the loading first it appeared close to Phase II and then it gradually shifted at higher temperature while Phase II disappeared. In contrast with the reduction of bulk $CoAl_2O_4$ and $NiAl_2O_4$ that occur at a precise temperature, we observed a wide interval of reduction temperatures in the case of supported metal. This suggests that the "degree of incorporation" of the ion play important role in determining the reduction temperature and that there are many degrees of intermediate state between the ion diffused on the surface (Phase II) and those deep into the alumina structure (aluminate).

This brings new light onto the actual formation of the metal aluminate. We are, in fact, able to propose a scheme (Figure 40) that explains how Phase II and III depend from the loading (and from the particle size). Phases I and II reduced at a precise temperature and are represented by a horizontal lines. The intersections with the diagonal line indicate the temperature at which we observed the reduction. Phase III is originated by Phase II and increased its reduction temperature as the temperature ramp proceeds (promoting deeper ions incorporation). It reached a plateau at the reduction temperature of $MeAl_2O_4$ formed into the alumina.

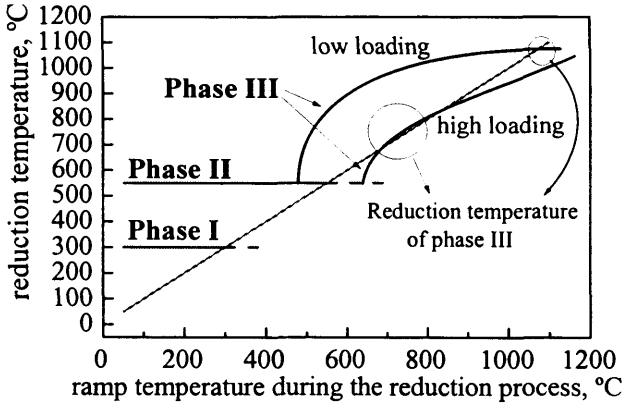

Figure 40. Reduction temperature of the three phases as a function of the temperature during the TPR process. The incorporation process of Phase II occurs more efficiently for the low loading supported catalyst.

We can distinguish three cases. If the reduction of Phase II is complete before the incorporation starts, no Phase III will be formed (the case of higher loading samples) while if the incorporation is complete before the Phase II starts to reduce, no Phase II will be observed (the case of very low loading samples). Between these two cases the incorporation could be in competition with the reduction and both processes occur. In this case the incorporated ions could be reduced before they have completely formed the $MeAl_2O_4$ phase and thus the signal is observed at lower temperature.

4.3.4 Formation and transformation of the reducible species

Organising the information, we can describe the formation and the transformation of the three phases in the various steps of the preparation of the supported metal catalyst (Figure 41).

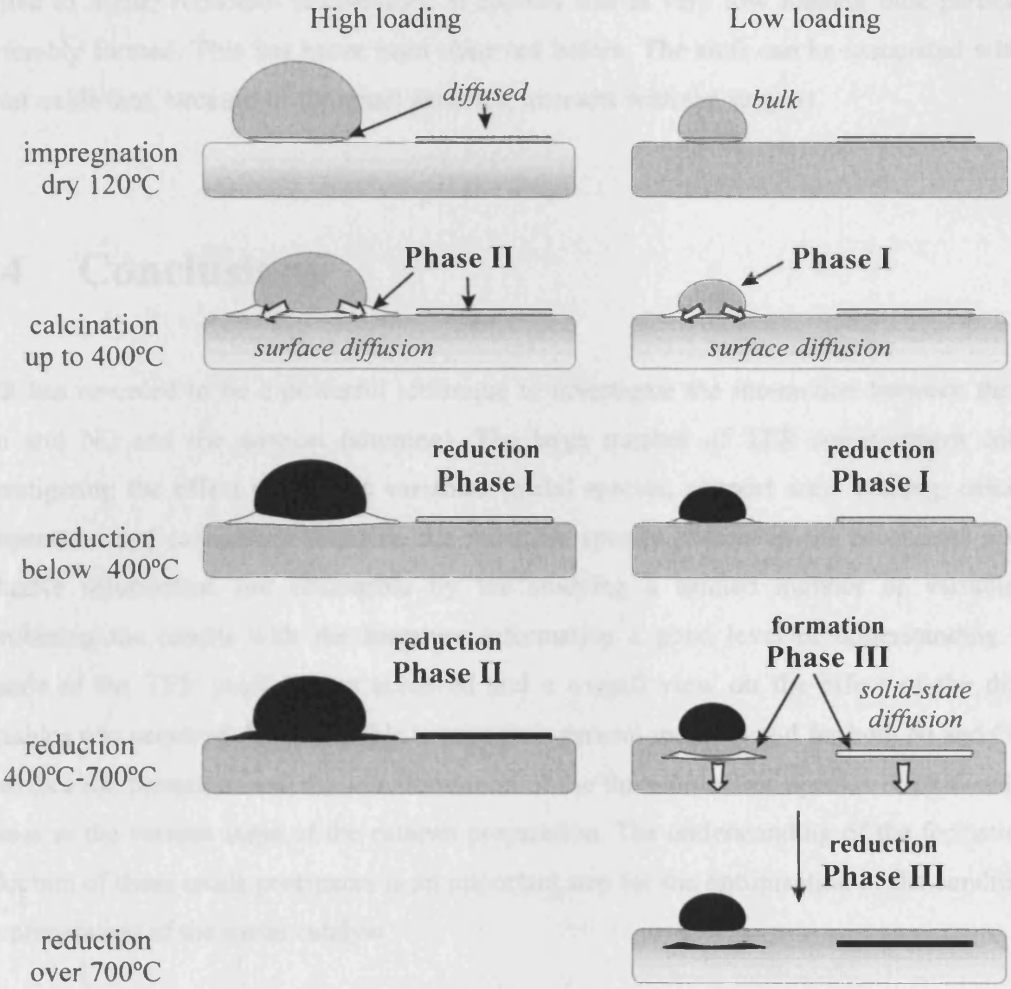

Figure 41. Model that describes the formation and the evolution of the three reducible species during the preparation steps of the metal (Co and Ni) supported catalyst.

After the impregnation mainly Phase I and Phase II (as nitrate particles) were formed. Higher surface area of the support and lower loading favoured smaller particle size. The calcination step decomposes the nitrate into oxides (Phase I and Phase II) and also promotes the metal ion mobility inducing the transformation of Phase I into Phase II. Longer calcination time and higher temperatures favoured this transition. At temperatures below 400°C, the reduction of the bulk metal oxide (Phase I) occurs while the diffuse Ni oxide strongly interacting with the support requires higher temperatures. Above 400°C, Phase II can be reduced but the process is in competition with the solid-state diffusion of the ionic metal species into the alumina structure and consequent formation of a highly stable aluminate (Phase III). Large particle size favoured the reduction of Phase II while smaller particle size more easily can diffuse into the support.

Finally Phase III was reduced above 700°C. Its exact reduction temperature depends on the degree of solid-state diffusion that is favoured for small particle size.

For very low loading, interestingly Phase I increased in relative intensity and at the same time shifted to higher reduction temperature. It appears that at very low loading bulk particles are preferably formed. This has never been observed before. The shift can be associated with bulk metal oxide that, because of the small particles, interacts with the support.

4.4 Conclusions

TPR has revealed to be a powerful technique to investigate the interaction between the metal (Co and Ni) and the support (alumina). The large number of TPR measurement collected investigating the effect of various variables (metal species, support area, loading, calcination temperature and calcination time) on the reducible species present in the precursors provided valuable information not obtainable by the studying a limited number of variables.[12,16] Combining the results with the literature information a good level of understanding of the signals of the TPR profiles was achieved and a overall view on the effect of the different variables was acquired. We were able to propose a general model (valid for both Ni and Co) that describes the formation and the transformation of the three reducible species of oxidised metal phases in the various steps of the catalyst preparation. The understanding of the formation and reduction of these oxide precursors is an important step for the optimisation of the condition for the preparation of the metal catalyst.

Regarding more in particular this work, from this study will be determined the conditions for the preparation of the "parent" single metal catalyst (Co-Al_2O_3 and Ni-Al_2O_3) for the selective deposition of the Pd in the process of the alloy preparation.

References

1 P. Arnoldy, J. A. Moulijn *J. Catal.* 93 (1984) 38

2 P. Ferreira-Aparicio, I. Rodriguez-Ramos, A. Guerriero-Ruiz *Appl. Catal., A* 148 (1997) 343

3 W. J. Wang, Y. W Chen *Appl. Catal.* 77 (1991) 223

4 R. Bechara, D. Balloy, J. Y. Dauphin, J. Grimblot *Chem. Mater.* 11 (1999) 1703

5 M. LoJacomo, M. Schiavello, A. Cimino *J. Phys. Chem.* 75 (1971) 1044

6 C. Li, Y. Chen *Thermochimica Acta* 256 (1995) 457

7 P. Turlier, H. Praliaud, P. Moral, G. A. Martin, J. A. Delmon *Appl. Catal.* 19 (1985) 287

8 Y. Chen, L. Zhang *Catal. Lett.* 12 (1992) 50

9 B. Jongsomjit, J. Panpranot, J. G. Goodwin *J. Catal.* 204 (2001) 98

10 H. H. Kung *J. Catal.* 73 (1982) 387

11 P. Arnoldy, J. A. M. Van den Heijkant, G. D. de Bol, J. A. Moulijn *J. Catal.* 92 (1995) 35

12 C. Li, Y. W. Chen *Termochimica Acta* 256 (1995) 457

13 L. Zhang, J. Lin, Y. Chen *J. Chem. Soc. Faraday Trans.* 88 (3) (1992) 497

14 D. C. Puxley, I. J. Kitchener, C. Komodromos, N. D. Parkyns, "*Preparation of Catalysts III*" Ed. G. Poncelet et al., Pub. Elsevier, Amsterdam (1983)

15 P. Arnoldy, J. L. De Booys, B. Scheffer, J. A. Moulijn *J. Catal.* 96 (1985) 122

16 R. Molina, G. Poncelet *J. Catal.* 173 (1998) 257

Chapter 5

5 Selective deposition of Ni over Pd-Al_2O_3

5.1 Introduction

The strategy for the preparation of supported alloy catalysts involves the preparation of a "parent" (single metal supported catalyst), the successive deposition of a second metal and a thermal treatment to promote the alloying of the two metals. Three main selective deposition methods are available: organo complex decomposition, direct redox reduction and reduction over adsorbed hydrogen. This work concentrates the attention on the last technique. Chapter 6 reports the successful deposition of Pd over the Ni parent. This Chapter reports the attempt to deposit Ni on the Pd parent (Figure 42).

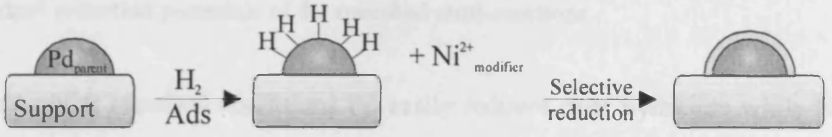

Figure 42. Scheme of redox reaction of adsorbed hydrogen.

The reduction of Ni over adsorbed hydrogen under standard conditions does not occur. However we tested the possibility to reduce the Ni over the hydrogen by changing the reaction conditions (pH, concentrations). XPS, TPR, atomic absorption analysis and the hydrogenation of crotonaldehyde (as a test reaction) were used to characterize the bimetallic catalyst.

5.1.1 Reduction of Ni over adsorbed hydrogen

The "selective reduction over adsorbed hydrogen" method can be used only to deposit metals with reduction potential higher than the reduction potential of the hydrogen. This means that, given the reaction (1), the reaction potential E defined by the Nernst equation (2) must be positive.

$$Me^{2+} + H_2 \leftrightarrow Me^0 + 2H^+ \tag{1}$$

$$E = E^0_{Me} - E^0_{H_2} + \frac{RT}{nF} \ln \frac{|Me^{2+} \,||\, H_2\,|}{|Me^0 \,||\, H^+\,|^2} \tag{2}$$[i]

Under standard condition,[ii] the equation (2) is simplified to the first two terms and it is possible to calculate the reaction potential by the tabled semi reaction standard potentials (Table 2).

Semi-reaction	E^0, V	Semi-reaction		E^0, V
$Ni^{2+} + 2e^- \leftrightarrow Ni_s$	-0.257	$2H^+ + 2e^- \leftrightarrow H_2$	(pH 0)	0.000
$Ni(OH)_2 + 2e^- \leftrightarrow Ni_s + 2OH^-$	-0.72	$2H_2O + 2e^- \leftrightarrow H_2 + 2OH^-$	(pH 7)	-0,415
$Co^{2+} + 2e^- \leftrightarrow Co_s$	-0.28	$2H_2O + 2e^- \leftrightarrow H_2 + 2OH^-$	(pH 14)	-0,828
$Co(OH)_2 + 2e^- \leftrightarrow Co_s + 2OH^-$	-0.73	$Pd^{2+} + 2e^- \leftrightarrow Pd_s$		0.915

Table 2. Standard reduction potentials of the specified semi-reactions.

It is clear that under standard conditions Pd easily reduces over hydrogen while Ni and Co do not. Changing the reaction conditions it is possible to shift the equilibrium in favour of the reduction of the metal. For example at pH 14 the Ni reduction is promoted as E = +0.108. Unfortunately, above pH 7 (for a Ni solution 2 M[iii]) the Ni precipitates as hydroxide[1] and can not participate to the reaction with the adsorbed hydrogen.

---

[i] E is the reaction potential expressed in V. E^0 is the standard reduction potential for a specific semi reaction. T is the temperature in K. R (gas constant) = 8.3145 J/molK. f (Faraday constant) = 96485 coulomb/mol.

[ii] Potential measured at 25°C and 1 atm when all the species have unitary activity (about 1M) and the gases has unitary fugacity (about 1bar).

[iii] Kps of $Ni(OH)_2 = 5{,}48\ 10^{-16}$

Another important consideration has to be done in selecting the pH conditions. Alumina behaves as a weak anion or cation exchanger support as a function of the pH.[2,3] Above pH 7 the cation exchange of Ni on alumina is promoted[4] leading to undesired non-selective metal deposition. For these reason a region of pH below 7 was chosen.

Other factors that influence the redox equilibrium (1) are the concentration of the species and the temperature. Organic solvents[5] also modify the redox equilibrium. The estimation of the reaction potentials is complicated by the formation of the intermediate species $Ni(OH)^+$ for which there is little information.

Despite the limited probability of observing the Ni reduction, we decided to study the deposition process as a function of the pH in a region between 2.5 and 6. Crucial for this choice was the Pd study (Chapter 3) in which the advanced skills in measuring the Pd hydride desorption might have found an important application in measuring the degree of alloying.

5.2 Results

5.2.1 Bimetallic catalyst preparation

The "parents" catalysts, Pd-Al_2O_3, (1.6 wt%) were prepared by incipient wetness impregnation of $Pd(NO_3)_2$ with alumina calcined at 300°C for 3 h and reduced at 250°C for 12 h. The method used to deposit Ni on Pd is similar to that used by *Barbier et al.*[6,7] for the deposition of Pt on Pd. 100 mg of Pd-Al_2O_3 were kept in a hermetic vial, 3 ml of water and nitric acid at known pH were added and He was bubbled (50 ml/min) for 20 min. In these oxygen free conditions H_2 was bubbled (50 ml/min) for 20 min and finally He was bubbled again for 20 min.

The only H_2 present at this point in the reactor is adsorbed on the surface of the Pd. At the same time a solution of $Ni(NO_3)_2$ $2 \cdot 10^{-2}$ M, at the same pH of the parent solution, was prepared and bubbled with He for 20 min. 1 ml of this $Ni(NO_3)_2$ solution was added to the parent solution (Figure 43) and left stirring in He atmosphere for 24 h. The catalyst was then filtered and dried overnight in air at 120°C. The bimetallic catalysts were prepared at pH 2.5, 4, 5 and 6. The sample at pH 5 was also prepared in three different conditions: from a $Ni(NO_3)_2$ solution $2 \cdot 10^{-3}$ M, with a contact time of 2 h instead of 24 h and adding the $Ni(NO_3)_2$ to a Pd not treated with H_2. A complete series of blanks were also prepared in the same conditions at pH 2.5, 4, 5 and 6, adding the $Ni(NO_3)_2$ solution to pure alumina.

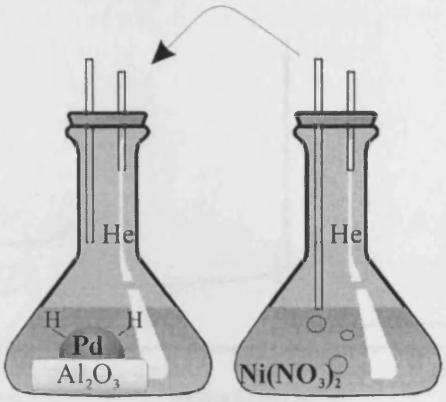

Figure 43. A step of the second metal deposition. The Ni solution is added to the Pd where has been selectively adsorbed hydrogen.

5.2.2 XPS

The four bimetallic catalysts prepared at different pH were analysed by XPS. In Figure 44 is reported, as example, the XPS spectra of the Pd-Ni-Al_2O_3 sample prepared at pH 5. The integration of the Ni, Pd and Al signals are reported in Figure 45. In this graph we can see that there is a strong reduction of the Pd signal after the addition of the Ni suggesting that the Ni could cover the Pd. Because of the nature of the XPS analysis it is difficult to directly compare the absolute area values of different samples. The ratios between the areas of the signals of a specific sample are considered more representative for comparison of different samples. In Figure 46 the Ni/Al area ratios are reported. Assuming constant the total amount of aluminium in all the samples (Al is from the support and so more abundant), the results suggests a larger deposition of Ni at pH 4 and pH 5. At these pHs the Ni/Pd ratio is also larger.

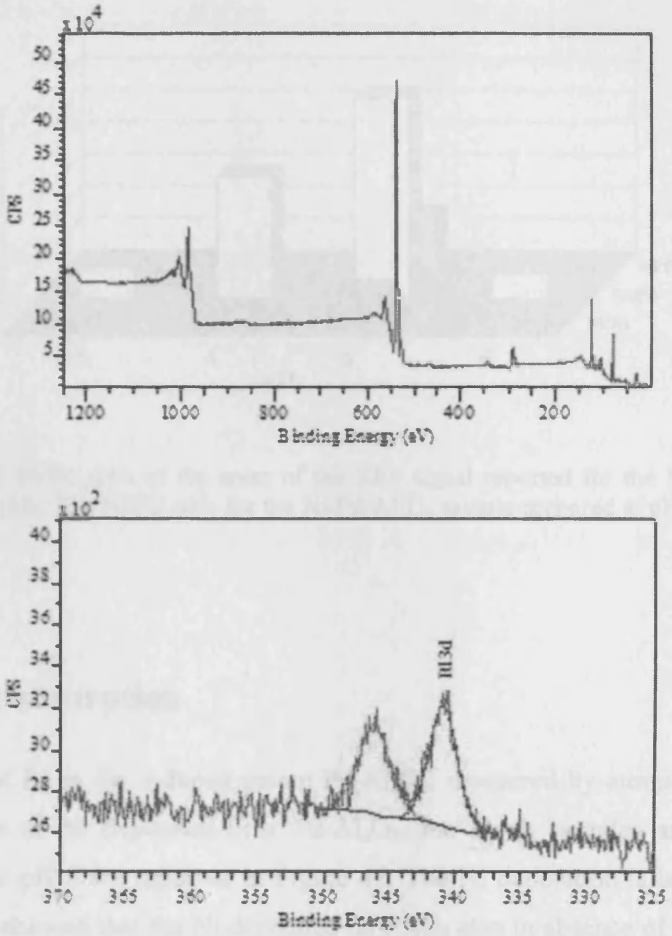

Figure 44. a) XPS spectra of Ni-Pd-Al_2O_3 prepared at pH 5. b) As example is reported the acquisition in the region of the Pd signal. It is shown the fitting and the baseline used for the integration.

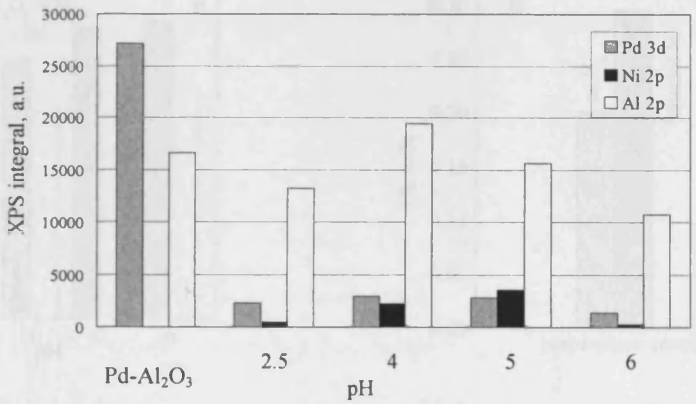

Figure 45. Areas of the XPS signals of Pd, Ni and Al in the Pd-Al_2O_3 sample and the Ni-Pd-Al_2O_3 samples prepared at different pH.

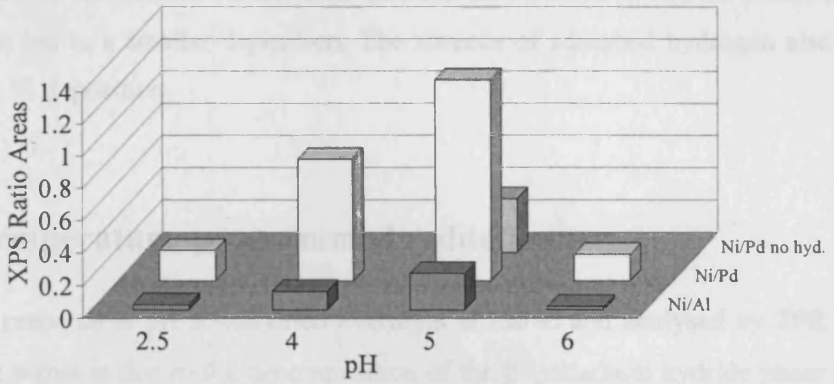

Figure 46. Ni/Al and Ni/Pd ratio of the areas of the XPS signal reported for the Ni-Pd-Al_2O_3 samples prepared at different pHs. The Ni/Pd ratio for the Ni-Pd-Al_2O_3 sample prepared at pH 5 without hydrogen are also reported.

5.2.3 Atomic absorption

The total amount of Pd in the reduced parent Pd-Al_2O_3, measured by atomic absorption is 1.6 wt%. The amounts of Ni deposited over Pd-Al_2O_3, the blank samples and the three extra samples prepared at pH 5 are reported in Figure 47. The Ni deposition is larger at higher pH. The blank analysis showed that the Ni deposited on Al_2O_3 also in absence of Pd. The amount of deposited Ni is as in the previous case dependent from the pH.

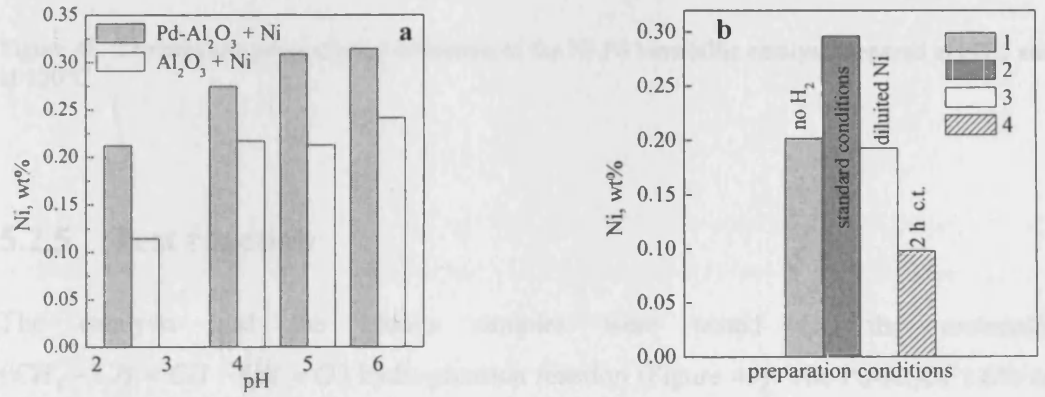

Figure 47. a) Loading of Ni (wt%) in the Ni-Pd-Al_2O_3 catalyst and Ni-Al_2O_3 blanks measured by atomic absorption. b) Ni loading in the sample prepared at pH 5 in various conditions: 1) without the addition of H_2 to the parent, 2) samples prepared in normal conditions, 3) addition to the parent of a $2 \cdot 10^{-3}$ M solution of $Ni(NO_3)_2$ (instead of $2 \cdot 10^{-2}$ M); 4) 2 h contact time (instead of 24 h) between the added Ni and the parent.

Figure 47b shows that shorter contact time between the Ni solution and the parent and lower Ni concentration led to a smaller deposition. The absence of adsorbed hydrogen also reduces the extent of the Ni deposition.

5.2.4 Temperature-programmed reduction

The sample prepared at pH 5 was dried overnight at 120°C and analysed by TPR (Figure 48). The positive signal is due to the decomposition of the β–palladium hydride phase (Chapter 3). The negative signal is a reduction signal. Because the Pd is already reduced the signal has been attributed to the reduction of Ni^{2+} species. This confirms the AA results indicating that non-reductive deposition occurred and so that the Ni nitrate is impregnated in the support.

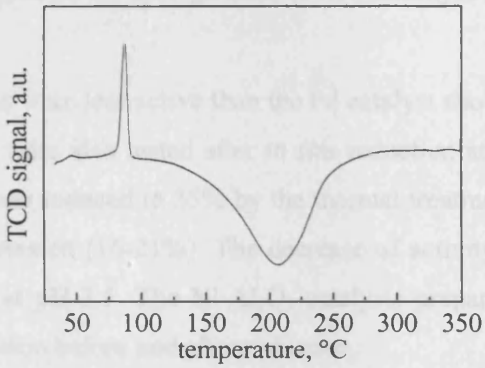

Figure 48. Temperature programmed reduction of the Ni Pd bimetallic catalyst prepared at pH 5 and dried at 120°C.

5.2.5 Test reaction

The catalysts and the blanks samples were tested for the crotonaldehyde ($CH_3 - CH = CH - CH = O$) hydrogenation reaction (Figure 49). The Pd-Al_2O_3 1.6% catalyst under reaction conditions was 100% selective to the butyraldehyde[8,9] (hydrogenation of C=C) and, under reaction conditions, showed a conversion of 86%. After the addition of Ni at different pHs the samples were dried in air at 120°C overnight and tested for the crotonaldehyde hydrogenation.

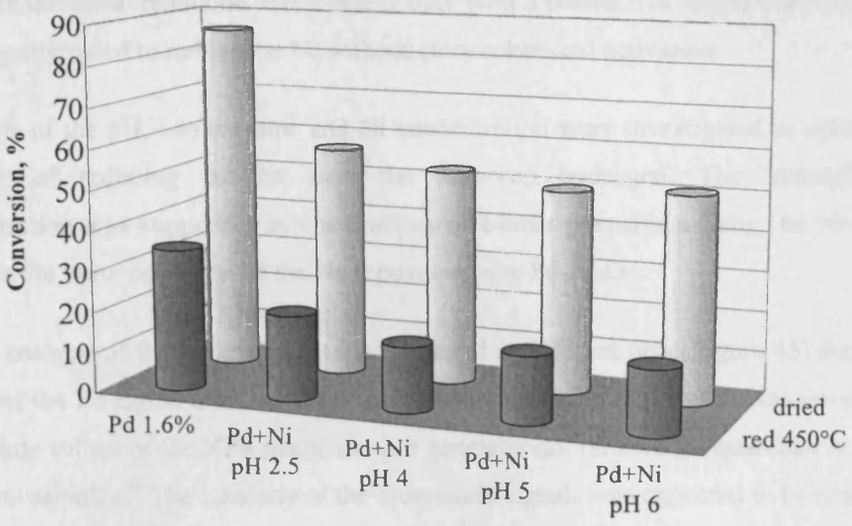

Figure 49. Activity of the catalysts for the hydrogenation of crotonaldehyde to butyraldehyde.

The four bimetallic catalysts were less active than the Pd catalyst showing a conversion between 51 and 57%. The catalysts were also tested after *in situ* reduction at 450°C for 30 min in pure H_2. The activity of the Pd was reduced to 35% by the thermal treatment. The bimetallic catalyst showed again a lower conversion (16-21%). The decrease of activity is less marked in the Ni-Pd-Al_2O_3 sample prepared at pH 2.5. The Ni-Al_2O_3 catalysts prepared as blank (not reported) showed a negligible conversion before and after reduction.

5.3 Discussion

Compared with the traditional co-impregnation methods, the selective deposition methods have the main advantage to obtain close proximity between the two metals avoiding the formation of a single metal catalyst.[10] They are efficient methods in preparing uniform composition bimetallic particles. The formation of partial alloy directly after the deposition has been observed in the case of direct redox reduction.[11,12,13] Thermal treatments can provide energy for the promotion of a more complete alloying of the two metals.[14]

The use of selective reduction methods for preparing bimetallic catalysts today is not widely diffuse[15,16] and the research is still investigating the potentials of this methods.[17] The reduction of Ni was never attempted. A possible method to reduce the Ni would be an under potential reduction (sec. 1.3.1).[18,19] This method would require the use of electrochemical energy in order

to promote the metal reduction and it works only with a conductive support such as graphite.[20] This study attempted to reduce the Ni without electrochemical activation.

The effects of the pH, contact time and Ni concentration were investigated in order to test the possibility of reducing the Ni over the adsorbed hydrogen. The bimetallic catalyst characterization was supported by the analysis of blanks prepared adding the Ni to the pure alumina in the same condition of the Ni deposition over Pd-Al_2O_3.

The XPS analysis of the bimetallic catalyst prepared at different pHs (Figure 45) showed a large decrease of the Pd signal after the deposition of Ni suggesting that the Ni was covering the Pd. The absolute values of the XPS intensities are generally not reliable for quantitative comparison of different samples.[iv] The intensity of the aluminium signals was expected to be nearly constant in all the samples as the aluminium is the most abundant metal. Therefore the fluctuation of the aluminium intensity (±22% around the average) gave a measure of the error for the comparison the signal of different samples. On this bases the larger reduction of the Pd signal in Figure 45 appeared to be due to real change of the amount of Pd on the surface and not to instrumental reason.

A better way of comparing the XPS signals is to eliminate the instrumental error by analysing the ratio of two signal of the same sample. The variation of Ni/Al as a function of the pH (Figure 46b) suggested that larger amount of Ni has been deposited at pH 4 and 5. The Ni/Pd ratio is very important as it gives a direct comparison of the two catalytically active metals. The variation of Ni/Pd as a function of the pH suggests that the Ni deposited at pH 5 cover more efficiently the Pd.

The atomic absorption analysis of the blanks has provided valuable information about the deposition process. The amount of added Ni corresponds to a maximum loading of 2.3 wt% loading. Only a fraction (between 0.21 and 0.31 wt%) was deposited on the 1.6 wt% Pd-Al_2O_3 catalysts. The amount of Ni deposited on the Pd catalyst increases as a function of the pH. The presence of Ni in the alumina blank samples clearly indicated that undesired non-selective deposition is occurring. During the 24 h contact time about 10% of the added Ni remained impregnated on the alumina. The filtration and washing steps were not able to eliminate this weakly adsorbed Ni. The results showed that the impregnation is dependent by the pH, by the Ni concentration and by the contact time.

[iv] The absolute intensity of the XPS signal depends on the amount of the sample on the morphology of the sample and on the intensity of the X-ray radiation. This last is not constant because the relative position of the sample stub and the X-Ray collimator is manually optimised for each sample.

The presence of unreduced species was confirmed by the TPR experiment of the bimetallic sample prepared at pH 5. It showed a large reduction signal attributed to Ni^{2+} reduction derived from impregnation by the nitrate.

The deposition process was thus mainly non-selective. However it is interesting to observe that a slightly higher amount of Ni was deposited on Pd-Al_2O_3. The experiment performed in absence of hydrogen showed that hydrogen is necessary for the excess of deposition. This suggests that the presence of adsorbed hydrogen enhances the Ni deposition. Whether the extra amount of Ni is actually reduced over the Pd or simply impregnated on the alumina cannot be established.

The crotonaldehyde reaction showed that the addition of Ni affects the efficiency of the Pd catalyst. The Pd is an excellent catalyst for the C=C hydrogenation[8,21] and a bad catalyst for C=O hydrogenation due to a weak adsorption of the carbonyl. The C=O selectivity is mainly dependent by the extent of adsorption of the C=O group. The hydrogenation of the C=O group can be promoted by interaction of the Pd with the support (for examples TiO_2[22]) or by doping the Pd with non-metallic species.[21] The Ni is less active than the Pd and it is also selective to the C=C bond.[8] The bimetallic Ni-Pd catalyst for the crotonaldehyde hydrogenation has not been studied. The addition of Ni and the formation of alloy could influence the Pd activity in any direction and possibly promote the hydrogenation of the C=O. The results showed that the addition of Ni repressed the Pd activity. This suggests that the Ni is interacting with the Pd (possibly covering it). After the reduction at 450°C the Pd showed a decrease of the activity. This may depend by some sintering or by stronger support interaction. In the bimetallic catalyst the reduction at 450°C may favourite the reduction of unreduced Ni and the alloying of the two metals. The activity of the bimetallic catalysts is again lower than the pure Pd confirming metal-metal interaction but not adding new information.

The decrease of the activity observed after the addition of Ni could be a consequence of the acid treatment. However the observation that the Ni effect is slightly smaller in the case of the sample prepared at pH 2.5, where the amount of deposited Ni is smaller, suggests that the Ni is influencing the activity. It appears thus that the two catalysts are interacting but this does not prove a selective deposition as metal-metal interaction are normally observed in catalyst prepared by successive impregnation of the two metals.

In conclusion, atomic absorption has shown that the Pd and the adsorbed hydrogen slightly affect the amount of Ni deposited on the parent. It would be interesting to understand the causes of this increase, whether it is due to a Ni reduction or not. The reaction test and the XPS analysis suggest that Pd and Ni are interacting but it is clear that Ni impregnation occurs. The

information collected at this point are not sufficient to establish if the bimetallic catalyst has been formed simply by a subsequent impregnation or a certain amount of Ni has been reduced.

5.4 Conclusions

The overall results underline the interaction between Ni and Pd and show that pre-adsorbed hydrogen influences the amount of Ni deposited over the Pd. On the other hand the total amount of deposited Ni is very small and it is clear that the Ni can be easily impregnated on the alumina. The observation of large amount of non-selective deposition indicates that the preparation method has not provided the ideal conditions for the selective reduction and improvements are necessary. Despite more investigation being required to define the distribution of the two metals on the alumina and the role of the adsorbed hydrogen, it was preferred to move on to the deposition of Pd over Ni (Chapter 6). The Pd reduction over the hydrogen should occur more easily.

As reported in section 1.3.3, the determination of the degree of interaction and alloying between two supported metals is a difficult task that requires the combination of many techniques.[23,24] The quantitative investigation of the Pd hydride formation and decomposition (Chapter 3) was specifically developed in order to study the degree of alloying in Pd based catalysts. Not having selectively deposited the Ni on Pd we have missed the opportunity of using this technique. However it will be useful in studying the deposition of Pd over Ni (Chapter 6).

References

1 *"Handbook of Chemistry and Physics"* 82th edition Ed. D. R. Lide, Pub. CRC press (2001)

2 M. Chem, L. D. Schmidt *J. Catal.* 56 (1979) 198

3 L. Vordonis, P. G. Koutsoukos, A. Lycourghiotis *Langmuir 2* (1986) 281

4 J. A. Moulijn, V. Ponec *"Studies in Surface Science and Catalysis"* vol 79, Pub. Elsevier, Amsterdam (1993)

5 C. Micheaud, P. Marecot, M. Guerin, J. Barbier *J. Chim. Phys.* 171 (1998) 229

6 C. Micheaud, M. Guerin, P. Marecot, C. Geron, J. Barbier *J. Chim. Phys.* 93 (1996) 1394

7 J. Margitfalvi, S. Szabo, F. Nagy, S. Gobolos, M. Hegedus *"Preparation of catalyst III"* Ed. Poncelet, P. Grange, P. A. Jacobs Pub. Elsevier (1983)

8 D. V. Sokolskii, D. V. Zharmagambetova, N. V. Anisilmova *React. Kinet. Catal.* Lett. 30 (1986) 11

9 M. Albert Vannice, D. B. Sen *J. Catal.* 115 (1989) 65

10 J. Barbier, P. Marecot, G. Del Angel, P. Bosch, J. P. Boitiaux, B. Didillon, J. M. Dominguez, I. Schiftef, G. Espinosa *Appl. Catal., A* 166 I (1994) 179

11 M. Bonarowska, J. Pielaszek, W. Juszczyk, Z. Karpinski *J. Catal.* 195 (2000) 304

12 C. L. Pieck, P. Marecot, J. Barbier *Appl. Catal., A 134* (1996) 319

13 P. Del Angel, J. M. Dominguez, G. Del Angel, J. A. Montoya, E. Lamy-Pitara, S. Labruquere, J. Barbier *Langmuir* 16 (2000) 7217

14 F. Faudon, F. Senocq, G. Bereret, B. Moravueck, G. Glugnet, C. Nicot *J. Catal.* 144 (1993) 460

15 R. Mélendrez, G. Del Angel, V. Bertin, M. A. Valenzuela, J. Barbier *Appl. Catal., A* 157 (2000) 143

16 C. Micheaud, P. Marecot, M. Guerin, J.Barbier *Appl. Catal., A* 171 (1998) 229

17 F. Gauthard, F. Epron, J. Barbier *J. Catal.* 220 (2003) 182

18 B. Coq, F. Figueras *J. Mol. Catal.* 173 (2001) 117

19 E. L. Pitara, J. Barbier *Appl. Catal., A* 149 (1997) 49

20 F. Gauthard, F. Epron, J. Barbier *J. Catal.* 220 (2003) 182

21 V. Ponec *Appl. Catal., A* 149 1 (1997) 27

22 M. A. Vannice *Topic Catal.* 4 (1997) 241

23 V. Ponec, G. C. Bond "*Catalysis by Metals and Alloys*" Ed. B. Delmon, J.T. Yates *Studies in Surface Science and Catalysis*, Vol. 95, Pub. Elsevier, Amsterdam (1995)

24 M. Che, C. O. Bennet *Adv. Catal.* 36 (1989) 55

Chapter 6

6 Preparation of Pd-Ni-Al_2O_3 by selective deposition

6.1 Introduction

As introduced in sec. 1.3.1, supported bimetallic catalysts today are prepared mainly by methods used for the preparation of single metal catalysts extended for bimetallic catalysts. This approach does not offer a control of the characteristics of the final catalyst and the exclusive formation of bimetallic entities on the support cannot be guaranteed. In order to have a control on the final composition and distribution of the metals, a surface reaction was used to reduce Pd^{2+} onto the Ni. The formation of bimetallic entities is controlled by the chemical nature of the system itself. This is the first time that Ni-Al_2O_3 is used as a parent as usually noble metals were preferred.[1]

The experimental conditions reported in the literature revealed to be inadequate for the Ni-Al_2O_3 mainly due to the facility of the reoxidation of the Ni surface. In section 6.2 were presented the problems encountered during the preparation and the changes necessary for the optimisation of the method. In section 6.3 the characterization of the bimetallic catalyst prepared with the optimised method showed that the selective deposition was successfully achieved. The bimetallic catalysts were then reduced at different temperature and analysed by XPS, *in situ* XRD and Pd hydride decomposition in order to establish the extent of the alloying as a function of the reduction temperature. The pH conditions during the preparation appeared to be very important in determining the degree of the alloy achievable at high temperature.

6.2 Optimisation of the preparation conditions

Pd-Ni-Al_2O_3 was prepared by reduction of Pd over hydrogen adsorbed over Ni-Al_2O_3 following the method used by *Barbier et al.* for the deposition of Re over Pt Al_2O_3[2] and Pt over Pd-Al_2O_3.[3] The characterization was performed by AA, TPR and XRD. This first preparation can be considered a preliminary experiment where the selective deposition method was tested on a Ni-Al_2O_3 parent. The results showed that a small amount of Pd is reduced and that a certain extent of Pd impregnation occurs. The data also revealed which preparation step promoted the undesired impregnation process. In the conclusions the modifications required to increase the selective deposition of Pd over Ni were identified and an optimised method was proposed.

6.2.1 Preparation conditions

The parent, Ni-Al_2O_3, was prepared by incipient wetness impregnation of $Ni(NO_3)_2$ with Al_2O_3 (sec. 2.2.1), calcined at 400°C for 3 h and reduced at 460°C for 12 h. The Ni loading, measured by atomic absorption was 9.1 wt%.

250 mg of Ni-Al_2O_3 in 5 ml of an HCl solution at pH 4, under continuous stirring, were bubbled (50 ml/min) with He for 20 min in order to eliminate the oxygen. The sample was then bubbled with H_2 for 30 min and He for 20 min. After this treatment H_2 is eliminated from the solution and only the hydrogen adsorbed on the surface of the metallic Ni remains. 1 ml of an oxygen free solution of $PdCl_2$ $1.2 \cdot 10^{-2}$ M in HCl at pH 4 was added to the Ni-Al_2O_3 suspension and stirred for 30 min. At this point the Pd may react with the hydrogen adsorbed on the Ni surface. The catalyst was then filtered and washed with 150 ml of a HCl solution at pH 1 to eliminate the not reduced Pd. The powder was then dried overnight in air at 110°C.

The sample prepared in these conditions was called **d-Pd-Ni-Al_2O_3**. Other 5 samples were prepared as blanks and references.

a-Ni-Al_2O_3 indicates the "non treated" Ni-Al_2O_3 catalyst

b-Ni-Al_2O_3 indicates the Ni-Al_2O_3 catalyst processed for the Pd deposition method but adding an acid solution not containing Pd

c-Pd-Ni-Al_2O_3 indicates the Ni-Al_2O_3 catalyst processed for the Pd deposition method without bubbling the hydrogen

e-Pd-Ni-Al_2O_3 was prepared adding the Pd solution while the hydrogen was still bubbling. This is called "refilling method" and used for deposition of large amount of the second metal.[2,3]

f-Pd-Al_2O_3 indicates the pure support on which the Pd deposition method was applied

6.2.2 Characterization of the bimetallic catalysts

Table 3 summaries the preparation conditions and the colour of the catalysts. It also reports the Pd and Ni loadings measured by atomic absorption.

	Preparation			Atomic absorption		
Sample name	Parent	Added	Colours	Ni wt %	Pd wt %	%Pd deposited
a-Ni-Al_2O_3	Ni Al_2O_3		Black	9.2	/	/
b-Ni-Al_2O_3	Ni Al_2O_3	H_2	Light grey	8.2	/	/
c-Pd-Ni-Al_2O_3	Ni Al_2O_3	+ Pd	Light grey	8.6	0.04	7.3%
d-Pd-Ni-Al_2O_3	Ni Al_2O_3	H_2 + Pd	Light grey	7.9	0.02	4.6%
e-Pd-Ni-Al_2O_3	Ni Al_2O_3	H_2 + Pd H_2	Light grey	8.3	0.09	8.3%
f-Pd-Al_2O_3	Al_2O_3	H_2 + Pd	White	/	0.02	3.3%

Table 3. List of the prepared catalysts. The preparation conditions, the colors of the sample the metal loadings and the fraction of the added Pd deposited on the parent are schematically reported.

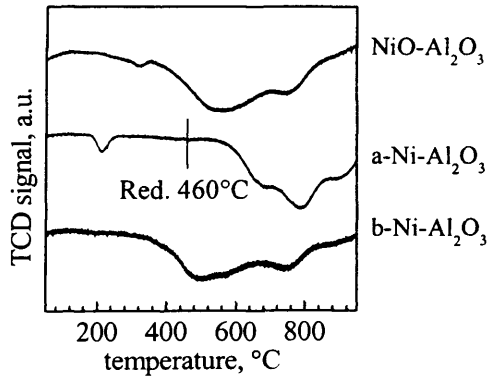

Figure 50. The TPR profiles of the NiO-Al_2O_3 before and after reduction at 460°C (a-Ni-Al_2O_3) are compared with the profile of the blank (b-Ni-Al_2O_3).

The TPR profile in Figure 50 showed that the NiO reduction started at 200°C and presented a small peak at 300°C and two bigger peaks at 550°C and 780°C. From this profile it was decided to reduce the catalyst at 460°C. After the reduction (a-Ni-Al_2O_3) the TPR showed that the NiO species reducible below 500°C has been reduced, except a small peak around 200°C. It could be attributed to a surface oxidation of the Ni due to exposition to the air after the reduction. The TPR of b-Ni-Al_2O_3, showed a pattern similar to the unreduced NiO-Al_2O_3. This indicated that a strong reoxidation of the Ni occurred during the process of depositing the Pd, washing or drying.

The XRD of the 9% Ni-Al_2O_3 catalyst showed only three small Ni signals (Figure 51). After the treatment without Pd (b-Ni-Al_2O_3) the small peaks disappeared. In the Pd-Ni-Al_2O_3 samples (c-Pd-Ni-Al_2O_3 and d-Pd-Ni-Al_2O_3) the Ni signals are also not present.

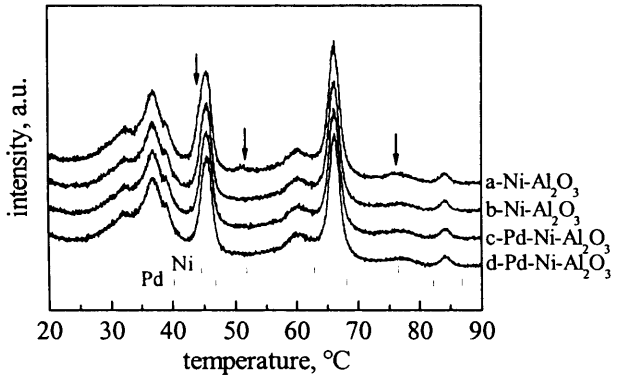

Figure 51. XRD patterns Ni-Al_2O_3 and Pd-Ni-Al_2O_3 prepared as specified above. The position of the Ni and the Pd peaks are reported as references.

6.2.3 Discussion and conclusions on the preparation conditions

The atomic absorption measurements showed that a small fraction of the added Pd is deposited on the catalyst. The maximum deposition is recorded for the catalyst prepared adding Pd^{2+} in a continuous H_2 flow (d-Pd-Ni-Al_2O_3). The preparation of c-Pd-Ni-Al_2O_3 (absence of adsorbed hydrogen) appeared also relatively efficient, suggesting that the direct reduction of Pd over Ni occurred following the reaction (1):

$$Pd^{2+} + Ni^0 \rightarrow Pd^0 + Ni^{2+} \quad (1)$$

The amount of deposited Pd on the alumina samples was 0.02 wt% that corresponds to 4% of the added Pd. This fact is very important because it indicates that impregnation is a relevant

process. 0.02 % was also the amount of Pd deposited on the sample d-Pd-Ni-Al_2O_3 indicating that the selective reduction over adsorbed hydrogen did not occur extensively.

In the TPR analysis the signal at 200°C in the a-Ni-Al_2O_3 profile was attributed to reoxidation of the Ni surface after exposure to air. This is very important as it indicated that the Ni surface, over which the H_2 adsorption should occur, was not "clean", compromising the efficiency of the deposition method. The observation that after the deposition process (b-Ni-Al_2O_3 profile) the Ni is largely reoxidised was also crucial. The analysis of the colours of the samples can be useful to understand at which step of the preparation the oxidation has occurred. NiO-Al_2O_3 is light grey while Ni-Al_2O_3 is black. After the Pd deposition the filtration and the washing, the solution was still black, it turned to light grey after drying overnight at 120°C in air. So the oxidation occurs during the drying step.

In the XRD analysis of the 9% Ni-Al_2O_3 (Figure 51), only weak Ni signals were observed. This could be due to the formation of small metal particles and to the limited amount of reduced Ni. The disappearing of the Ni signals after the Pd deposition process is related with the Ni reoxidation observed during the drying step.

The characterization of the catalysts underlined three main problems of the method used.

- Only a small amount of Pd was reduced during the selective deposition.
- Undesired Pd impregnation on the alumina occurred.
- During the drying step in air of Ni-Al_2O_3 and Ni-Pd-Al_2O_3, the Ni is extensively reoxidised.

The following modifications were adopted to improve the method. To ensure a "clean" reduced Ni surface during the H_2 adsorption Ni-Al_2O_3 was reduced, a second time, *in situ* at 250°C. In order to avoid as much as possible the introduction of oxygen in the system, the He-H_2-He flow sequence described above was performed on a dry sample instead on the liquid suspension.[4,5] This reduced the contact time of the parent with the acid solution, reducing the acid attack to the Ni and the alumina corrosion. The total amount of reduced Ni was enhanced increasing the reduction temperature from 460 to 550°C. The impregnation of Pd salt on the alumina (second point) should be completely avoided. In order to find the best condition to limit the Pd impregnation on the support two different Pd salts, $PdCl_2$ and $Pd(NO_3)_2$, dissolved respectively in HCl at pH 1 and HNO_3 at pH 3, were used for the selective deposition. The low pHs were chosen in order to increase the Pd solubility and promote an efficient action in removing unreduced Pd species during the washing step. The necessity of low pH was confirmed by a blank test where $PdCl_2$ and $Pd(NO_3)_2$ solutions at different pH were added to pure alumina,

stirred for 30 min, filtered and washed with a solution at the same pH. Simply observing the colour of the alumina samples (darker colour indicates more Pd deposition) was possible to determinate that stronger acid condition better prevents Pd impregnation. Finally to avoid the Ni reoxidation during the drying step, it was performed under an inert flow.[4]

6.3 Results

In section 6.2 were delineated the optimised conditions for the preparation of Pd-Ni-Al_2O_3. In this section, those conditions are applied and the Pd-Ni-Al_2O_3 prepared are, firstly, characterised and, secondly, thermally treated at different temperature to promote the alloying. Further characterization and testing of the catalysts will reveal the degree of alloying achieved.

6.3.1 Preparation

The Ni-Al_2O_3 parent was prepared by incipient wetness impregnation as described above but the reduction was performed at 550°C for 10 h (10°C/min flow 5% H_2 in Ar). The samples were then reduced *in situ* in a H_2 flow at 250°C for 1 h. After cooling at room temperature, H_2 was flowed for further 15 min. He was then flowed for 30 min in order to eliminate the H_2 not adsorbed on the Ni surface.

A $1 \cdot 10^{-2}$ M Pd solution at known pH and bubbled for 30 min with He to eliminate the oxygen was added to the Ni-Al_2O_3. The resulting mixture was stirred for 30 min. In these conditions the reaction (2) or (3) could occur.

$$Pd^{2+} + 2H^0 \rightarrow 2H^+ + Pd^0 \quad (2)$$

$$PdCl_4^{2-} + 2H^0 \rightarrow 2HCl + 2Cl^- + Pd^0 \quad (3)$$

Using different Pd solutions, two Pd-Ni-Al_2O_3 catalysts were prepared.

- The first catalyst was prepared by $Pd(NO_3)_2$ dissolved in a solution of HNO_3 at **pH 3**.
- The second catalyst was prepared by $PdCl_2$ dissolved in a solution of HCl at **pH 1**.

The samples were then filtered and washed with 150 ml of acid solution, pH 3 HNO_3 for the first preparation and pH 1 HCl for the second. The samples were then dried overnight in He (60

ml/min) at 120°C and thus ready for characterisation and testing. The two bimetallic samples prepared will be identified as Pd-Ni-Al_2O_3 prepared at pH 3 and pH 1.

Two blank samples were also prepared.

- **Ni-Al_2O_3 treated**, indicates the parent processed under all the steps of the Pd deposition method adding an acid solution not containing Pd. This sample is important to study the effect of the deposition process on the parent.

- **Al_2O_3+Pd**, indicates the Al_2O_3 sample processed for the Pd deposition. This sample is important to monitor the selectivity of the method measuring the undesired impregnation of Pd on the support.

6.3.2 Characterization of Pd-Ni-Al_2O_3

The Pd-Ni-Al_2O_3 samples and the selectivity of the method were studied by AA, TPR, XRD and XPS.

6.3.2.1 Temperature programmed reduction

The reduction of NiO-Al_2O_3 at 550°C was efficient in reducing most of the Ni^{2+} (Figure 52). A small signal, due to the surface oxidation of the Ni was again observed at about 200°C. The "Ni-Al_2O_3 treated" at pH 1 was dried both in air and He. The TPR profiles clearly showed that the drying in an inert flow is necessary in order to avoid extended Ni reoxidation.

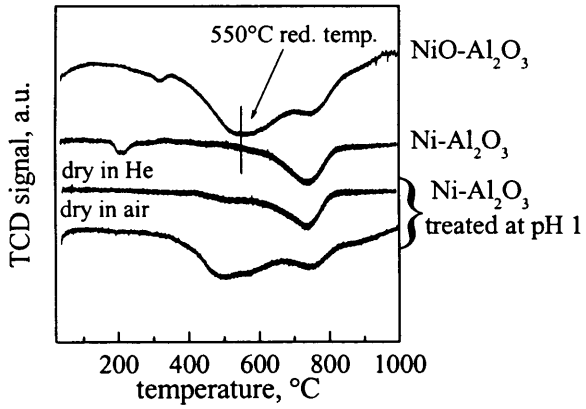

Figure 52. TPR profiles of the specified samples.

While the preparation at pH 1 did not affect the oxidation state of the reduced Ni the treatment at pH 3 induced a partial Ni oxidation as revealed by the peak at 280°C in the profiles in Figure 53.

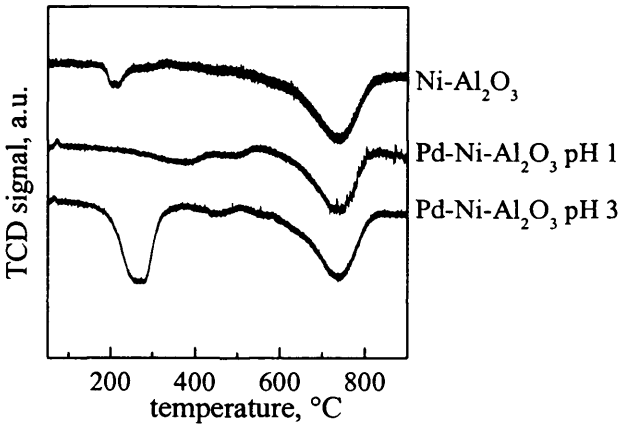

Figure 53. TPR profiles of Ni-Al_2O_3 and Pd-Ni-Al_2O_3 prepared at pH 3 and pH 1.

This is not related with the large re-oxidation observed during the drying in air as it occurs at lower temperature.

6.3.2.2 Atomic absorption

The amounts of Pd deposited on the surface of the Al_2O_3 were measured by atomic absorption. In both cases has been deposited more than the 95% of the added Pd obtaining catalysts with about 1% of Pd. The amount of Pd deposited in the "Al_2O_3+Pd" sample measures the Pd impregnated on the alumina and so it is an indication of the "selectivity" of the method. The analysis of the "treated Ni-Al_2O_3" provided instead information on the effect of the deposition method on the Ni-Al_2O_3 parent.

The results in Figure 54 showed that the deposition of Pd did not occur extensively in the sample without Ni, implying a selective deposition of the Pd over the Ni. The amount of Ni in Ni-Al_2O_3 before the deposition is 4.4 %. After the deposition process at pH 3 this value did not change, while working at pH 1 it decreased to 3.7%. This loss of Ni is probably due to dissolution in consequence of the HCl attack during the deposition and the washing step.

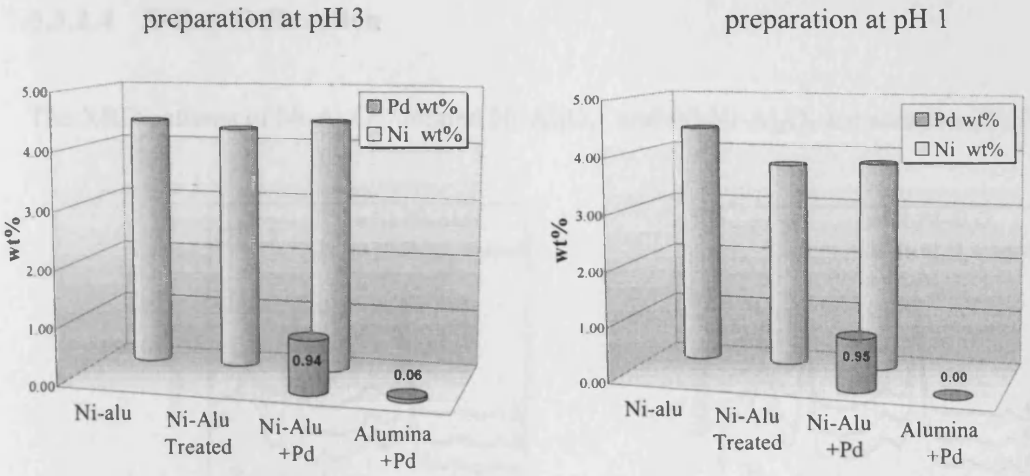

Figure 54. Measurement of the metal loading by atomic absorption. The value "0.00"in the sample "Alumina + Pd" indicated that we are at the limit of sensitivity of the analysis that is about 0.01%.

6.3.2.3 BET measurements

Because the strong acid solution used during the Pd deposition could modify the support property the surface areas of the alumina were measured by BET analysis before and after the acid treatment. The surface area of the Ni-Al_2O_3 and Pd-Ni-Al_2O_3 sample are also reported.

Sample	Surf. area m^2/g
Al_2O_3	202
Al_2O_3 + HCl pH 1 treatment	200
Ni-Al_2O_3	175
Pd-Ni-Al_2O_3 prepared at pH 1	178
Pd-Ni-Al_2O_3 prepared at pH 3	180

Table 4. Surface areas measured by BET.

The results (Table 4) indicate that the acid treatment do not affect the alumina surface area. The reduction of the area observed in the Ni samples (about 10%) is probably due to the occlusion of the smallest pores by the Ni particles.

6.3.2.4 X-Ray Diffraction

The XRD patterns of Ni-Al_2O_3 "treated Ni-Al_2O_3" and Pd-Ni-Al_2O_3 are compared in Figure 55.

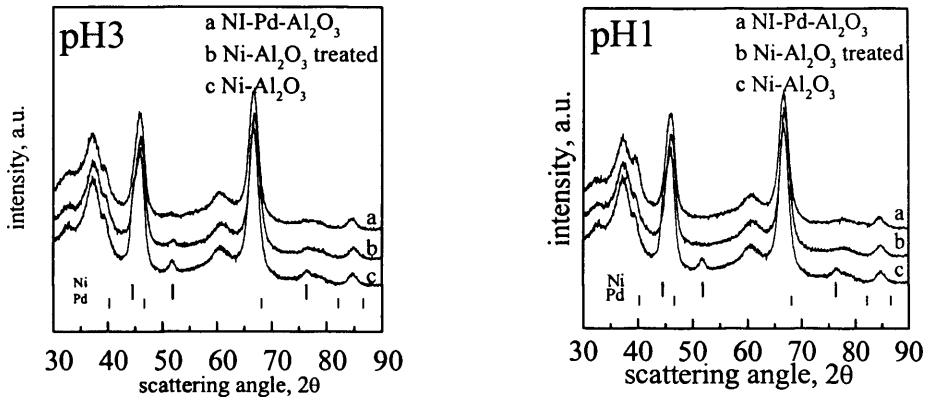

Figure 55. XRD patterns of Ni-Al_2O_3 and Pd-Ni-Al_2O_3. The Ni and Pd position peaks are reported as references.

After Ni-Al_2O_3 was processed for the Pd deposition, with or without adding the Pd, the intensity of the Ni signals decreased. The decrease of intensity was more marked for the samples prepared at pH 1 as in this case the signal practically disappeared. This result indicates that the acid solution induces some modification on the Ni catalyst. In the preparation at pH 3 the decrease is larger for the sample with Pd suggesting Pd-Ni interaction. The Pd signals are not visible and this is consistent with a high dispersion and a loading of wt 1%.

6.3.2.5 X-ray photoelectron spectroscopy

As introduced in Chapter 5, the comparison of the intensity of the XPS signals of different sample is often performed using relative areas. The Al signal was taken as reference. The ratio between Ni and Al is related with the surface concentration of the Ni. In Figure 56, are reported the Ni/Al ratios for the Ni-Al_2O_3 and Pd-Ni-Al_2O_3 samples. In the Ni-Al_2O_3 sample, the Ni/Al ratio is 2.9. After the Pd deposition the values decreased drastically to a range between 0.4 and 0.8. This large decrease occurred also for the blank "Ni-Al_2O_3 treated".

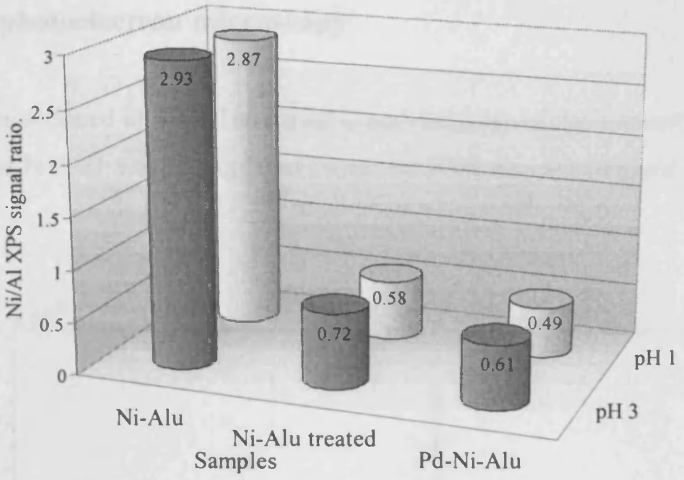

Figure 56. Ratio between the integrated areas of the Ni and Al XPS signals.

The variation of the Ni surface observed with the XPS measurements confirmed that the acid solution had a marked effect on the parent in terms of Ni (or Al) present on the surface. Analysing the Ni/Al ratio of the samples that have been treated with the acid solution with (Pd-Ni-Alu) or without (Ni-Alu treated) Pd, we observed lower Ni/Al values for the samples with added Pd. This supports the fact that the Pd is deposited over the Ni.

6.3.3 Thermal treatments and alloying

In order to promote the alloying of the two metals, the Pd-Ni-Al_2O_3 catalysts were reduced at different temperature between 150 and 950°C. The thermal treatment at high temperature can activate the interphase diffusion of the metals but also the sintering of the particles. We wanted to establish if alloying was possible at reasonable low temperature avoiding strong sintering of the particles. In this section, are reported the characterization (by XPS, XRD and Pd hydride decomposition) and testing (for the crotonaldehyde hydrogenation reaction) of the Pd-Ni-Al_2O_3 samples reduced at different temperature.

6.3.3.1 X-ray photoelectron microscopy

The catalysts were reduced at 550°C and 950°C and the ratio of the intensity of the XPS signals (Ni/Al, Pd/Al and Ni/Pd) were calculated from the XPS spectra (Figure 57) and reported in Figure 58.

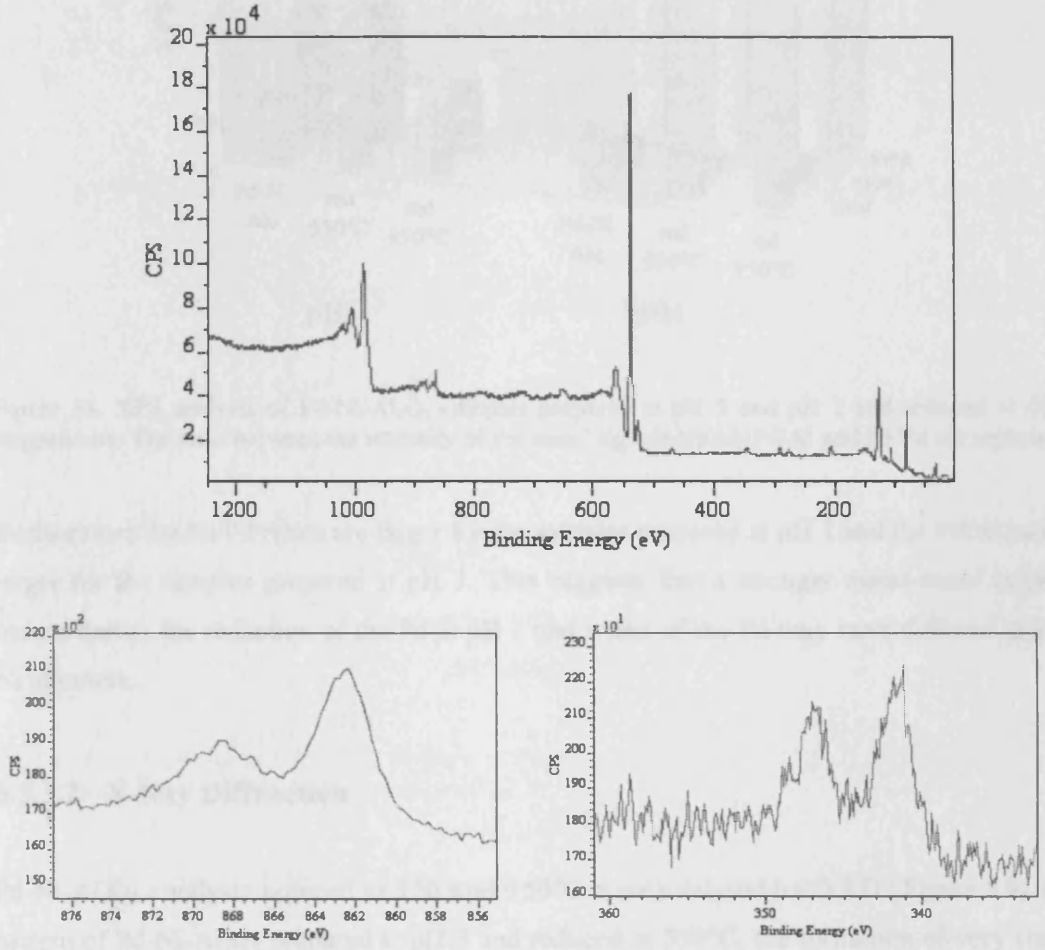

Figure 57. Example of XPS spectra. On the top the entire acquisition of the sample Pd-Ni-Al_2O_3 prepared at pH 1 and not reduced. Below particular of the Ni (left) and Pd (right) signals.

The ratio of the two more abundant metals Ni/Al remained mainly stable after the reductions, while the ratio of Pd/Al and Ni/Pd showed clear trends. Pd/Al decreased as the reduction temperature increased while Ni/Pd increased as the reduction temperature increased. These results showed that increasing the temperature the amount of Pd in the surface decreases. This depends from the sintering and the Pd diffusion the crystal structure of the Ni as explained in the discussion section.

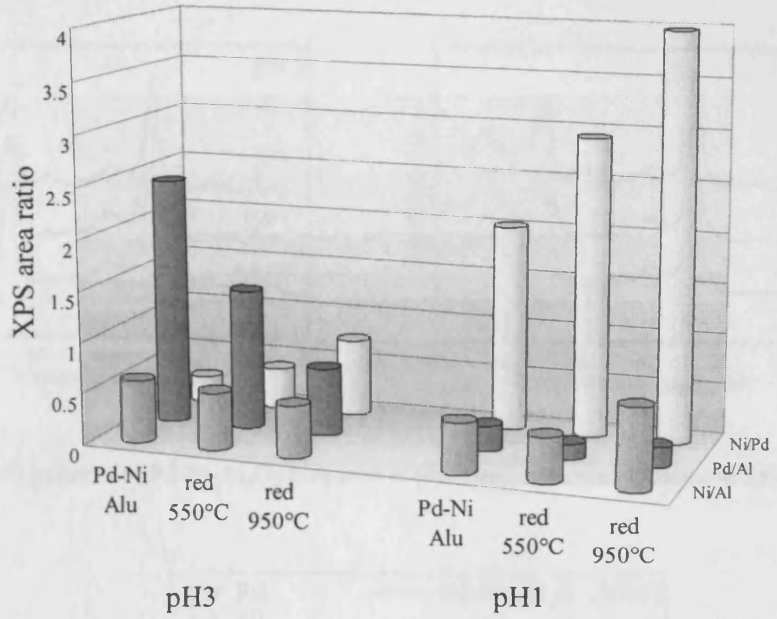

Figure 58. XPS analysis of Pd-Ni-Al_2O_3 samples prepared at pH 3 and pH 1 and reduced at different temperature. The ratio between the intensity of the metal signals Ni/Al, Pd/Al and Ni/Pd are reported.

Furthermore the Ni/Pd ratios are larger for the samples prepared at pH 1 and the Pd/Al ratios are larger for the samples prepared at pH 3. This suggests that a stronger metal-metal interaction occurs during the reduction of the Pd at pH 1 and a part of the Pd may have diffused inside the Ni structure.

6.3.3.2 X-Ray Diffraction

Pd-Ni-Al_2O_3 catalysts reduced at 550 and 950°C were analysed by XRD (Figure 59). In the pattern of Pd-Ni-Al_2O_3 prepared at pH 3 and reduced at 550°C, the formation of very sharp Pd peaks and the increase of the intensity of the Ni signals were observed. Increasing the reduction temperature up to 950°C both the Pd and Ni peaks were more intense but while the Pd signal was very sharp the Ni signal remained broad.

The sample prepared at pH 1 and reduced at 550°C showed a very small increase of intensity of Ni signal and it remained very broad. The main Pd peak (111) at 40.1°2θ was in this case very small and broad and it is shifted at higher 2θ suggesting alloy formation (Figure 60).

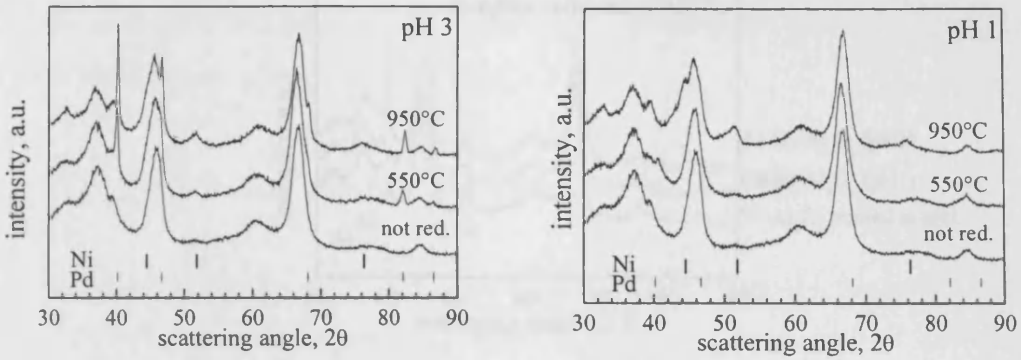

Figure 59. XRD patterns of Pd-Ni-Al_2O_3 prepared at pH 3 and pH 1 and reduced at 550°C and 950°C.

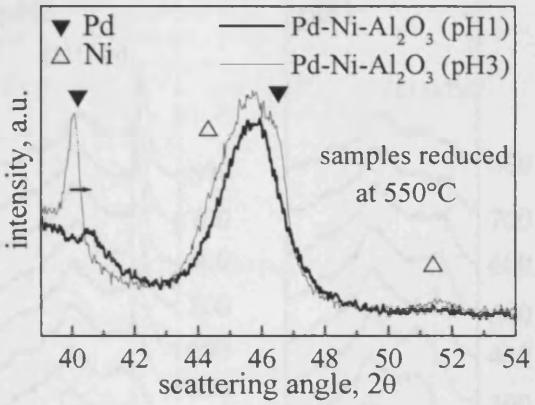

Figure 60. Enlargement of the XRD patterns of Pd-Ni-Al_2O_3 reduced at 550°C. The arrow indicates the shift of the Pd signal in catalyst prepared at pH 1.

Reducing the sample at 950°C the Ni signals were more intense but still very broad and the (200) peak at 51.8°2θ showed a remarkable asymmetry. The Pd peaks were not identifiable. The absence of crystallised Pd after reduction at high temperature is a strong indication that Pd is strongly interacting with the Ni and possibly has formed an alloy.

Ni-Al_2O_3 treated at pH 1 was reduced at 950°C and analysed by XRD (Figure 61). The comparison with Pd-Ni-Al_2O_3 reduced at the same temperature revealed a much sharper Ni signal. This confirmed that the deposited Pd was interacting with Ni as such interaction prevented the formation of large pure Ni crystallite.

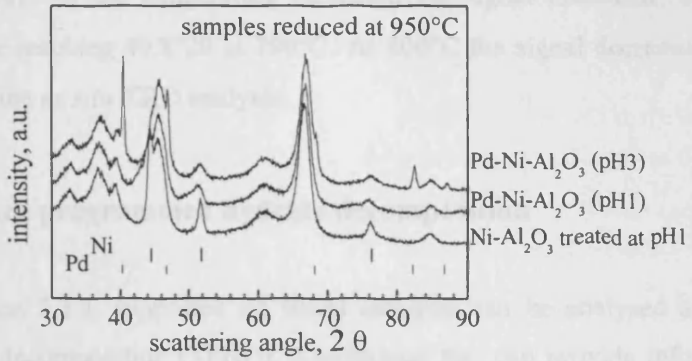

Figure 61. XRD patterns of Pd-Ni-Al_2O_3 reduced at 950°C compared with Ni-Al_2O_3 (treated at pH 1) and reduced at 950°C. The Ni sintering is reduced in the samples containing Pd.

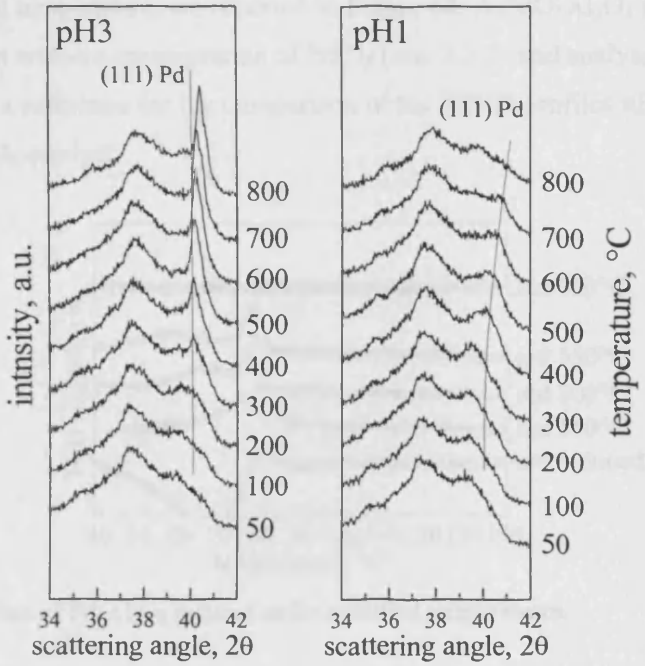

Figure 62. *In situ* XRD of Pd-Ni-Al_2O_3 reduced at pH 1 and pH 3. Enlargement of the region 34-42°2θ where the (311) and (222) peaks of alumina (respectively at 37.6 and 39.5°2θ) and the (111) peak of Pd (at 40.1°2θ) were observable. A line indicates the position of the (111) Pd diffraction.

In order to investigate the shift of the Pd signal observed in the pattern of Pd-Ni-Al_2O_3 reduced at 550°C the Pd-Ni-Al_2O_3, catalysts were analysed by *in situ* XRD. The samples were heated from 50 to 800°C in a 10% H_2 in N_2 flow (60 ml/min). The heating profile is characterized by steps of 100°C reached at 10°C/min and lasting 25 min. Figure 62 reports the enlargement in the XRD region of the patterns containing the (111) Pd signal (40.1°2θ). In the patterns of the sample prepared at pH 3, the Pd signals were observed after reduction at 200°C. It increased in intensity and sharpness as a function of the temperature. In the case of Pd-Ni-Al_2O_3 prepared at pH 1, the Pd signal was observed in the sample reduced at 400°C and its position was shifted to

higher angles (40.3°2θ). As the temperature increased the signal remained very broad and shifted to higher angle reaching 40.8°2θ at 700°C. At 800°C the signal decreased in intensity. These results confirm the *ex situ* XRD analysis.

6.3.3.3 Temperature programmed hydride decomposition

As discussed in section 3.3.3, supported Pd based catalysts can be analysed by temperature programmed hydride decomposition (TPHD), a technique that can provide information about the degree of alloying.

The TPHD profiles of the Pd-Ni-Al_2O_3 catalysts, prepared at pH 3 and pH 1 and collected after reduction at different temperature, are reported in Figure 64. A PdO-Al_2O_3 (2% Pd) sample was prepared by incipient wetness impregnation of $PdCl_2$ (sec. 2.2.2) and analysed by TPHD (Figure 63) in order to have a reference for the comparison of the TPHD profiles of Pd-Ni-Al_2O_3 with a single metal Pd-Al_2O_3 catalyst.

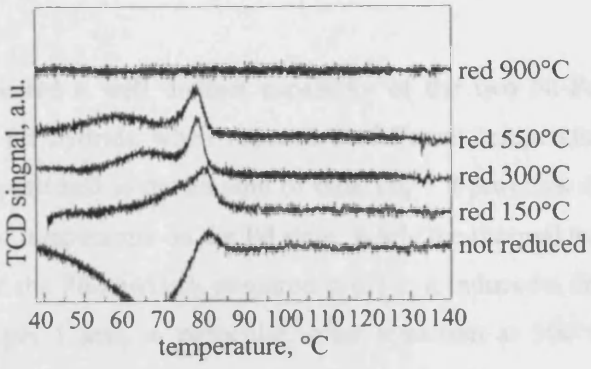

Figure 63. TPHD profiles of Pd-Al_2O_3 reduced at the specified temperatures.

The negative signal at 66°C (Figure 63) in the profile of the not reduced sample was due to the reduction of the PdO. The positive peak at about 80°C and the second smaller signal between 60 and 70°C represented the decomposition of the Pd hydride. The intensity slightly increased as a function of the temperature up to 550°C. This indicated that the amount of bulk Pd did not decrease. *Pinna et al.*[6] found that the temperature of decomposition depends on the particle size. On this base, *Bonarowaska et al.*[7,8] attributed the splitting of the signals in Pd-SiO_2 system to the presence of different particle size. About the splitting observed in our experiment it was unlikely due to the formation of smaller particle size as it is more pronounced at higher temperature. We suggest it was due to the interaction of the Pd with the support. At 900°C the TPHD signal disappeared completely probably because of the strong interaction of the Pd with the support.

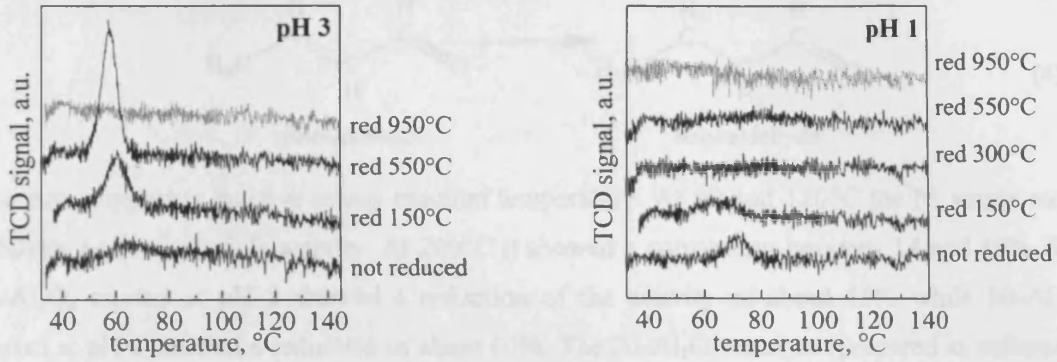

Figure 64. TPHD profiles of prepared at pH 3 and pH 1 and reduced ad different temperature.

The TPHD profile of the not reduced Pd-Ni-Al_2O_3 prepared at pH 3 (Figure 64), showed a broad signal at 66°C. After reduction of the sample at 150° and 550°C the signal was more intense, sharper and shifted at lower temperature. After the reduction at 950°C, the TPHD signal disappeared. In the not reduced sample prepared at pH 1, we observed a TPHD signal at 71°C. After reduction at 150°C, it became broader ed and less intense. The signal totally disappeared at higher temperatures.

The TPHD analysis revealed a well distinct capability of the two Ni-Pd-Al_2O_3 catalysts in adsorbing H_2 and form Pd hydride when reduced at different temperature. Because the Pd hydride formation is proportional to the amount of bulk Pd,[7,9] it provides direct information on the effect of the reduction temperature on the Pd state. While the thermal treatment produced an increase of the bulk Pd in the Pd-Ni-Al_2O_3 prepared at pH 3, it induced a decrease of bulk Pd in the sample prepared at pH 1 and, in particular, after reduction at 300°C any bulk Pd was observed.

6.3.3.4 Catalytic test: crotonaldehyde hydrogenation

The Pd-Ni-Al_2O_3 catalysts, the blanks samples (Ni-Al_2O_3 treated, Al_2O_3+Pd, and pure Al_2O_3) and a reference Pd-Al_2O_3 (0.6 Pd wt% prepared by incipient wetness impregnation method of $PdCl_2$, section 2.2.2) were reduced at 300°C and tested in the crotonaldehyde hydrogenation reaction using the conditions reported in sec. 2.3.2.2. The reaction was carried out at 50, 120 and 200°C in order to find the best condition to compare the Ni, Pd and Pd-Ni catalysts.

All the catalysts were highly selective to the hydrogenation of C=C so the activity for the hydrogenation of crotonaldehyde to butyraldehyde (4) was used to compare the catalysts (Figure 65).

crotonaldehyde butyraldehyde (4)

The pure support is inactive at any reaction temperature. At 50 and 120°C the Ni single metal catalysts had a negligible activity. At 200°C it showed a conversion between 14 and 19%. The Ni-Al_2O_3 treated at pH 3 showed a reduction of the activity of about 15% while Ni-Al_2O_3 treated at pH 1 showed a reduction of about 60%. The Pd-Al_2O_3 catalyst (prepared as reference) shows 100% conversion at all reaction temperatures.

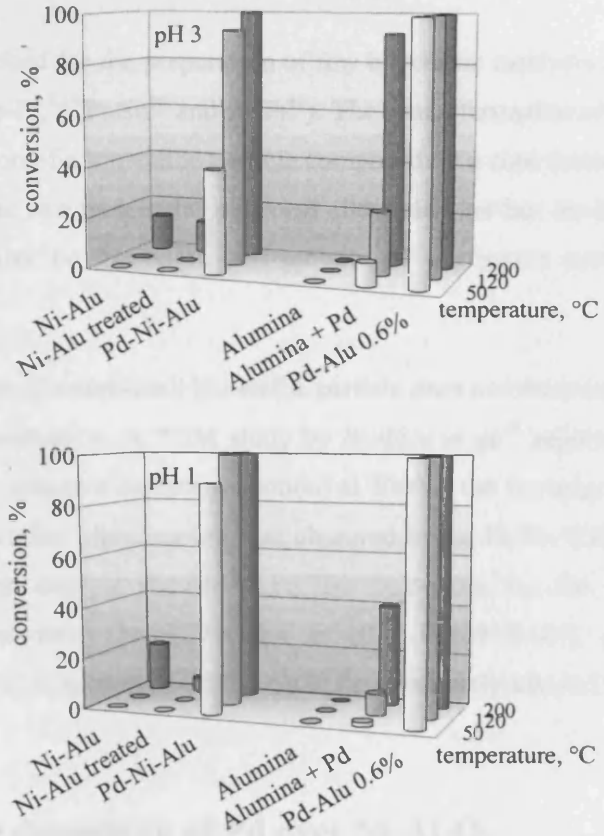

Figure 65. Catalytic test of the pH 3 and pH 1 series performed at 50, 120 and 200°C. In the graph is reported the activity of the specified catalysts (and blank samples) expressed as percent of conversion of crotonaldehyde to butyraldehyde.

At 50°C the two Al_2O_3+Pd blanks (prepared at pH 3 and pH 1 and containing respectively 0.06 and <0.01wt%) of Pd showed respectively 9.1 and 1.8% conversion. The activities increased with the reaction temperature reaching at 200°C respectively 92 and 40% conversion. At 50°C the activity of Pd-Ni-Al_2O_3 prepared at pH 3 was 41% conversion and that of Pd-Ni-Al_2O_3 prepared at pH 1 was 90%. At higher temperature the activity increased reaching conversion near 100%.

6.4 Discussion

The strategy chosen for the preparation of the Pd-Ni-Al_2O_3 alloy catalyst was a controlled surface reaction based on the reduction of Pd^{2+} on H preadsorbed on the surface of Ni (Figure 66) and subsequent thermal treatment.

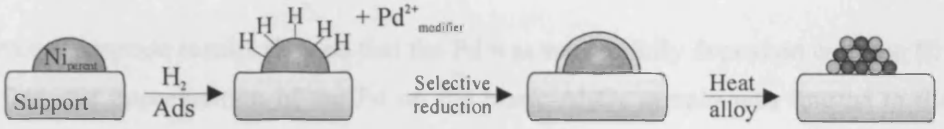

Figure 66. Scheme of the controlled surface deposition.

This method was applied for the preparation of few bimetallic catalysts (for example Au-Pt,[10,11] Cu-Pd,[4] Pt-Pd,[12,13] Re-Pt,[2,14] Pt-Sn[15] and Bi-Pt[16]). The characterization of the bimetallic particles indicated the formation of a bimetallic particle composed by a core (metal parent) and a shell of the second metal. The two metals did not form alloy particles but tended to form single layer aggregates concentrates on the edges and terraces of the parent surface (low coordination sites).[3,17]

The thermal treatment of a core-shell bimetallic particle does not necessarily lead to the increase of the metal-metal interaction. A TEM study by *Barbier et al.*[18] reported that reducing Au-Pt particle (prepared by selective surface reduction) at 300°C, the Au migrates from the Pd to the support (graphite). Similar phenomenon was observed in the Pt-Pt-Al_2O_3 system[13] where after thermal treatment the catalyst showed a Pd like behaviour for the complete oxidation of hydrocarbon. On the other hand, *Faudon et al.*[25] found Pd-Ni, prepared by selective decomposition of $Ni(C_5H_5)_2$ over Pd-Al_2O_3, could be completely alloyed by thermal treatment.

6.4.1 Selective deposition of Pd over Ni-Al_2O_3

In section 6.2, was reported the first attempt to deposit Pd on Ni by selective reduction over adsorbed hydrogen. The characterization of the catalyst showed that the specific conditions led to a very low amount of deposited Pd, comparable with the amount of Pd non-selectively deposited (impregnated) on the support. The reoxidation of the Ni surface before the selective deposition appeared to be the main problem as it reduces the amount of H_2 adsorbed on the Ni surface. An optimised method was formulated to increase the adsorption of H_2 and increase the efficiency of the Pd reduction on the hydrogen. The new method includes a higher reduction temperature of the Ni (to increase the amount of metallic Ni), an *in situ* reduction of the Ni

before the hydrogen adsorption (to eliminate possible surface reoxidation), and a drying step performed in inert gas (to avoid Ni reoxidation). Finally stronger acid conditions were used to increase the Pd solubility during the washing step and reduce the impregnation. In particular two different acid solutions, HCl at pH 1 and HNO_3 at pH 3, were chosen for the Pd deposition. The prepared Pd-Ni-Al_2O_3 catalysts were characterised in order to establish the degree of selectivity obtained.

The atomic absorption results showed that the Pd was successfully deposited over the Ni (Figure 54). In fact, the impregnation of the Pd on the blank Al_2O_3 sample was limited to 6% of the added Pd at pH 3 and below 1% at pH 1 while 95% of the added Pd was deposited on the Ni-Al_2O_3 in both preparation conditions. These strong conditions were necessary because of the note tendency of the Pd to be adsorbed on the alumina.[13] Despite the possibility of anion exchange of $PdCl^{2-}$ on the alumina[2,19] the best result was obtained using an HCl solution at pH 1. These strong acid conditions prevented the Pd impregnation on the support but on the other hand, were responsible for the attack the parent catalyst dissolving 16% of the Ni.

The XRD patterns (Figure 55) also underlined the effect of the pH on the Ni-Al_2O_3 parent. In fact the Ni signals drastically decreased in intensity in the samples prepared at pH 1 and, in smaller entity, in the sample prepared at pH 3. The small decrease of the Ni amount in the catalyst was not enough to explain the decrease of the intensity of the Ni signals. It appeared that the Ni was loosing crystallinity. The origin of this could be due to a higher dispersion, an increased disorder in the structure or a stronger interaction with the support. The XPS (Figure 56) revealed a marked decrease of Ni/Al ratio after the acid treatment indicating that less Ni was on the surface. One possibility was that the alumina support was attacked by the acid conditions destroying the highly porous structure and enclosing the Ni particles. This hypothesis was not supported by the BET analysis that showed that the total surface area of the alumina was not affected by the acid treatment. The two preparation conditions led to different effects on the oxidation state of the Ni. At pH 3 the signal at 270°C indicated a certain amount of Ni re-oxidation, while at pH 1 no relevant re-oxidation was observed. The signal observed in the first case could be due to Ni oxidation promoted by HNO_3. The Pd TPR signals are normally observed below 100°C. The absence of this signal was in agreement with a deposition of Pd involving a reduction process. Moreover the small positive peak at about 70°C due to the Pd-hydride decomposition revealed the presence of the metallic Pd in the sample.

The collected information showed that the selective reduction of the Pd was achieved in both cases and more efficiently in the preparation at pH 1. However, the parent Ni-Al_2O_3 that should remains unmodified was actually affected by the deposition conditions. In fact, were observed

the dissolution of Ni (in the preparation at pH 1), the decrease of the Ni on the surface (XPS), the decrease of the crystallinity of the Ni (XRD) and the Ni partial re-oxidation (in the preparation at pH 3). The acid medium affected in different ways the parent and played a role on how the Pd was deposited on the Ni (as discussed below).[14] The Pd-Ni-Al_2O_3 prepared at the two different pH conditions were ready for the thermal treatments and the subsequent characterization for the determination of the degree of alloying of the two metals. These analyses will also provide some indirect information that may be useful in better define the modification of the Ni during the preparation process and the position of the Pd after the deposition.

6.4.2 Thermal treatment of Pd-Ni-Al_2O_3

The selective Pd deposition had occurred efficiently over the Ni and so it was expected to have obtained a bimetallic catalyst where the Pd is deposited on the Ni particles forming a core-shell bimetallic catalyst.

The Pd-Ni-Al_2O_3 catalysts prepared in this way were a good starting point for the thermal treatment aimed to alloy uniformly the two metals without inducing large sintering. In fact we did not have to activate the mobility of the two metals over the support (as necessary for the bimetallic catalyst prepared with non selective method) but only provide the energy for the interphase diffusion.

As introduced in Chapter 1, Pd can diffuse into the Ni particle (or *viceversa*) and form an alloy solid solution. This means that the alloy is formed by the substitution of an atom of the metal 1 with one of metal 2 in any random position. In order to alloy the two metals is necessary to provide the energy to accelerate the natural movement of the atom in the metallic structure to a rate that would lead in a reasonable time to a complete mixing. Bulk atom diffusion requires high activation energy and is observable only at high temperature[20,21] while diffusion from surface layer of atoms can occur at relatively low temperature.[22]

Often in the alloy the thermodynamically stable energetic state is reached when one of the two metal is more abundant on the surface of the alloy (segregation). This in general is influenced by the releasing of strain due to the different size and compressibility of the atoms. The enthalpy associated with the breaking and formation of metallic bonds (during the segregation) balances the negative entropy.[23]

In particular, the energy of the Pd-Ni system is lowered by Pd-enrichment[22] of the surface since Pd atoms are noticeable larger (larger atoms tend to segregate) than Ni atoms (difference in atomic radii of about 10%) and Pd has lower surface energy than Ni. (Figure 67) reports the segregation behaviour of Pd-Ni.

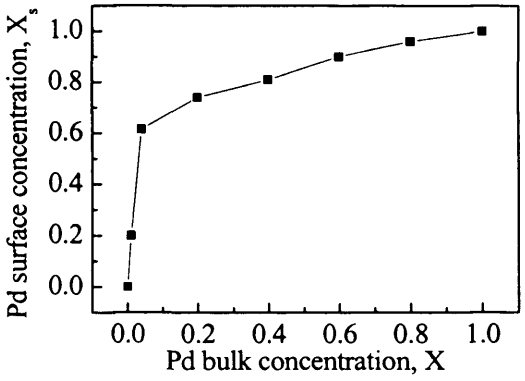

Figure 67. Segregation of Pd in Pd-Ni alloy as predicted by segregation model.[24]

The continuous solid solution formed over the range of composition of Pd-Ni makes the system favourable for a XRD study.[25] The lattice parameter increases continuously by 10% from pure Ni to pure Pd. Therefore from the unit cell parameters (calculated by the position of the (111) diffraction line of the Pd-Ni alloy) and the data of *Bidweel et al.* reported in Figure 68, it is possible to calculate the composition of the alloy.

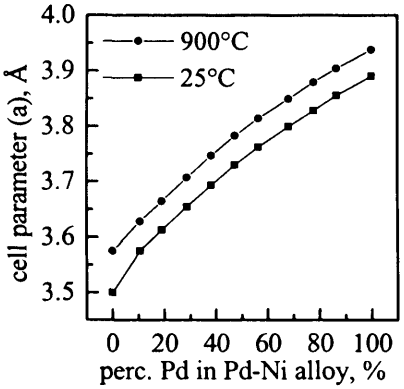

Figure 68. Cell parameter (a) of the Pd-Ni alloy expressed as a function of the percent of Pd in the alloy.[26] The data are measured for 25 and 900°C.

Unfortunately in our Pd-Ni-Al_2O_3 system, the analysis of the peak broadening for the estimation of the particle size is compromised by the overlapping of the (111) signal of the Ni and the (111) signal of the Pd respectively with the intense (400) and (222) signals of the alumina.

In section 6.3.2, the **XRD** patterns of the Pd-Ni-Al_2O_3 samples prepared in different conditions (pH 1 and pH 3) and reduced between 300 and 950°C were reported. In both preparations, the Ni signals increased in intensity at high temperature but remained very broad (Figure 59). When the Pd was absent the Ni signals become much sharper (Figure 61). From this was possible to conclude that the Ni is intensely interacting with the Pd.

At high temperature, the Pd signals of the two samples are different. In the preparation at pH 3 very sharp and intense Pd signals were observed, while in the preparation at pH 1 only small broad signals shifted at higher angles were recorded. This situation indicated that in the first case large particles of pure Pd were formed after reduction while in the second preparation the Pd did not form (large) pure crystallites. The broad signal shifted at higher 2θ angles indicated that the unit cell is decreasing in volume suggesting the alloying of the Pd with the smaller Ni atoms.

The *in situ* XRD analysis (Figure 62) confirmed the formation of alloy particles and showed that it depended from the reduction temperature. The composition of the alloy formed in Pd-Ni-Al_2O_3 prepared at pH 1 was calculated (as describe above) and reported in Figure 69.

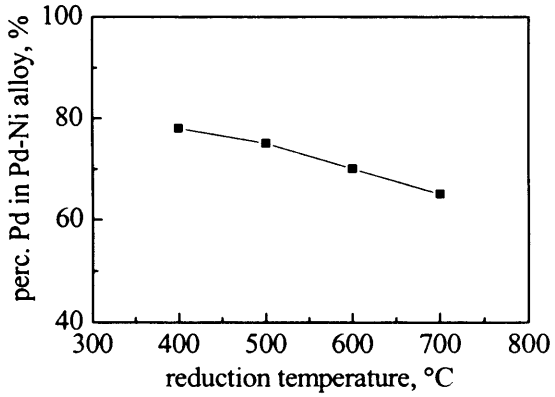

Figure 69. Composition of the Pd-Ni alloy calculated by the position of the position of the (111) signal.

Below 400°C the signal was not observable. At 400°C the reorganization of the atoms in the crystal and sintering process led to the formation of the Pd signal, indicating the formation of alloy containing 80% Pd. Increasing the reduction temperature, the concentration of the Ni in the alloy increased and at 700°C it reached 35%. The presence of the Ni signal after reduction at high temperature indicated that pure Ni was still present in the sample (Figure 59). This could be explained in two ways:

1) the Pd was diffused into the Ni crystal layers without reaching the core of the particles: this would explain the high concentration of Pd in the alloy in a bimetallic system reach in Ni ($Pd_{13}Ni_{87}$)

2) the Pd was deposited selectively only over a fraction of the available Ni.

In Chapter 4 we have seen that reducing NiO-Al_2O_3 two types of Ni were produced, bulk Ni (reduced at low temperature) and Al_2O_3-interstitial Ni (reduced at higher temperature). It is possible that the hydrogen adsorption and so the selective deposition occurs efficiently only on the bulk Ni particles. Figure 70 combines the two hypotheses.

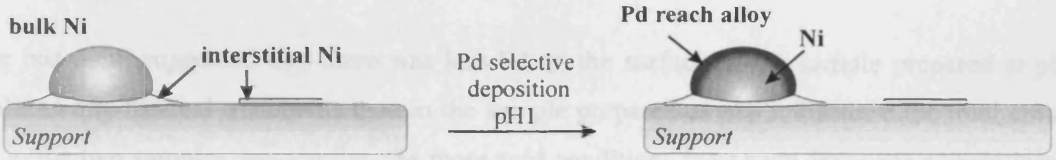

Figure 70. A possible scenario for the selective deposition of Pd over Ni-Al_2O_3 at pH 1. The draw at the left was first presented in sec. 4.3.4. The image at the right is proposed on the basis of the XRD results.

It is important to remember that the picture emerged from the XRD is influenced only by the fraction of phase able to diffract. It does not provide information on the smaller particles.

The **XPS** analysis was used to study the relative atomic abundance on the surface. The ratio of the signals intensity Ni/Al, Pd/Al and Ni/Pd were considered. In particular, the ratio Ni/Pd is very important because it lead to a direct relative relation of the two active metals. The results of the analysis of the Pd-Ni-Al_2O_3 samples prepared at pH 1 and pH 3 and reported in Figure 58 showed that:

- Pd/Al ratio decreased as the reduction temperature increased
- Ni/Pd ratio increased as the reduction temperature increased
- Ni/Al ratio remained mainly stable after the reductions at 550 and 950°C
- Ni/Pd ratios were larger for the samples prepared at pH 1 and the Pd/Al ratios were larger for the samples prepared at pH 3.

The first and the second point indicated that, in both samples, increasing the temperature the amount of Pd in the surface decreased. The decrease of the amount of metal on the surface, measured by the XPS as a function of the temperature is often associated with the sintering of the metal.[27] This was the case of the Pd-Ni-Al_2O_3 prepared at pH 3 as indicated by the XRD.

Another factor that produce the decrease of the amount of Pd on the surface is the alloying process. So the decrease of the surface Pd in the Pd-Ni-Al_2O_3 prepared at pH 1 depended from the diffusion of the Pd from the surface into the Ni lattice.

The fact that the amount of Ni on the surface did not decrease after the treatment at 550°C indicated that Ni sintering did not occur. This is expected for three main reasons: strong sintering of Ni on alumina was observed only at temperature above 600°C,[28] the Ni-Al_2O_3 parent was already reduced at 550°C and the XRD results (Figure 59) showed a small increase of the Ni signal. The fact that the Ni surface area did not decrease but instead slightly increased after reduction at 900°C is possibly connected with increase of Ni due to the reduction of unreduced species of Ni as indicated in the TPR profiles (Figure 52).

The last point suggested that there was less Pd on the surface in the sample prepared at pH 1 (without any thermal treatment) than in the sample prepared at pH 3. Because the total amount Pd in the two samples was similar, the more acid conditions may have favourite a more intense Pd-Ni interaction during the deposition. This stronger interaction may be the main factor that induced the Pd to alloy in one case and to the sintering in the other.

The **TPHD** is the last technique used to characterise the Pd-Ni-Al_2O_3 samples. The phase transformation in (5) has only recently been used (especially by *Karpinski et al.*[29,30]) as characterization technique for Pd base bimetallic catalyst:

$$\beta\text{-Pd-H} \leftrightarrow \text{Pd} + \tfrac{1}{2}\,\text{H}_2 \qquad (5)$$

In Chapter 3, we introduced and improved this technique applying it to the study of single metal Pd-Al_2O_3. Pure bulk Pd absorbs a number of H atoms equal to 2/3 of the number of the atom of Pd[31] but in a supported bimetallic catalyst the H_2 solubility is influenced by:

- the Pd interaction with the support
- the Pd particle size
- the degree of alloying

Working with Pd-based supported catalysts the dependence of the degree of Pd alloying from the extent of the hydride formation, offers an exceptional opportunity to monitor alloying.[30,32]

In particular, the H_2 solubility decreases when the Pd is alloyed with another metal[7,33] and consequently the respective Pd-H hydride decomposition peak decreases in intensity. The temperature of the hydride desorption from a bulk Pd is about 70°C while in a supported catalyst it may change. It depends from the strength of the Pd-H bond and it is also influenced

by alloy formation. Alloying the Pd, a reduction of the Pd-H bond strength and a shift of the peak at lower temperature is expected.[29] However, in the case of Pd-Au[8,34] system an increase of the reduction temperature is observed.

The TPHD analysis confirmed that the Pd in the two Pd-Ni-Al_2O_3 catalysts (pH 1 and pH 3) behaved in a different way when reduced at high temperature. While reducing the sample prepared at pH 3 up to 550°C produced a large increase of the H_2 solubility, the reduction of the sample prepared at pH 1 showed a decrease of the solubility and at 300°C no hydrogen was absorbed. These results were in total agreement with the XRD patterns as they indicated that, in one case the sintering and the bulk Pd formation was promoted by the thermal treatment while in the other case the amount of bulk Pd decreased as a function of the temperature. While the XRD analysis failed in providing direct information on the sample reduced below 400°C the TPHD is sensitive to bulk Pd particle of 2-3 nm[35,36] (sec. 3.3.3, Figure 28) and was able to detect the Pd from room temperature. The presence of the signal after reduction at 150°C indicated that after the deposition the Pd is not alloyed (as expected). The weak signal was probably due to the very high dispersion. The observation that the H solubility is zero after reduction at 300°C of the Pd-Ni-Al_2O_3 prepared at pH 1, indicated that relatively low temperatures were able to activate the metal interphase diffusion decreasing and possibly eliminating the bulk Pd.

Combining the TPHD with the XRD and XPS results emerged that the two preparation conditions (pH 1 and pH 3) had led to two Pd-Ni-Al_2O_3 catalysts that behaved very differently when reduced at various temperatures. The Pd, in the Pd-NiAl_2O_3 prepared at pH 3, formed single metal Pd particles possibly with a similar process of migration from the Ni surface to the support surface described by *Barbier et al*[18] (sec. 6.4). On the other hand Pd-Ni-Al_2O_3 prepared at pH 1 formed Pd-Ni alloy.

In order to acquire more direct evidences on the selectivity of the deposition method, the alloying process and the particle size transmission electron microscopy analysis will be performed on samples reduced at 500°C.

The results of the characterization of the bimetallic catalysts, reduced at different temperature, indirectly provided information on the catalysts before the reduction and thus straight after the deposition. The different behaviour of the catalysts at high temperature was directly connected with the deposition conditions. It appeared that the interaction between the two metals in the sample prepared at pH 1 produced a bimetallic particle not just in close proximity but also with a strong interaction. The understanding of the effect of the acid conditions on the deposition requires more investigation. At the moment on the base of the data we can make the following considerations.

We know that the Pd reduction over adsorbed hydrogen proceed until there is hydrogen available. After that, the direct reduction between Pd^{2+} and Ni^0 can occur. It is possible that the Ni dissolution (due to the HCl medium) may have destabilized the adsorbed H. The Pd deposition would then have proceeded by direct reduction. The direct reduction is reported to induce a stronger metal interaction compared with the reduction over adsorbed hydrogen[3,17] This would explain the differences observed during both the characterization and the thermal treatment.

Another possibility is that after the deposition, the chelating action of the chloride first attacks the deposited Pd (re-oxidising it) and subsequently re-deposits the Pd on the surface of the metal parent following reaction (6) and (7).[37]

$$Pd_{bulk} + 4Cl^- \rightarrow PdCl_4^{2-} + 2e^- \quad (6)$$

$$PdCl_4^{2-} + 2e^- \rightarrow Pd_{ads} + 4Cl^- \quad (7)$$

This mechanism was proposed by *Szabo et al.*[12,38] for the direct reduction of Au and Pd over Pt. They concluded that the chelating power of the chloride ions in the transition metal complexes is critical in deposition and redistribution on the parent catalyst surface. In the case of chloride-free precursors (such $Pd(NO_3)_2$ in HNO_3) the bulk deposition-reoxidation reaction is negligible and the deposition of the additive (Pd) is stable. These differences during the deposition process could explain the differences observed during the thermal treatments.

A final interesting possibility is that the hydrochloric acid attack on the Ni would have "activated" the Ni surface. The dissolution of Ni may have produced a large number of defects and vacancies in the Ni crystal. The Pd interphase diffusion would thus be favourite as it is promoted by the presence of vacancies in the crystal.

6.4.3 Test reaction

The test reaction provides another tool for the characterization of the two Pd-Ni-Al_2O_3 catalysts. Because of the interesting differences observed in the TPHD analysis after reduction at 300°C the catalytic tests were performed on Pd-Ni-Al_2O_3 reduced for 1 h at this temperature. The comparison of the catalytic result of the single metal and the bimetallic catalysts is complicated by the strong difference between the activity of the Ni and the Pd (Pd is two orders of magnitude more active than Ni[39]). Traces of Pd in the alumina have shown activity much higher than the 4% Ni catalyst and the addition of Pd to Ni-Al_2O_3 catalyst drastically increases the

activity of the catalyst. Modifying the reaction conditions was not possible to put in the same scale the activity of the three catalysts without one of them showing 100% or 0% conversion. The best reaction temperature to compare the Pd-Ni-Al_2O_3 catalysts is 50°C. Figure 71 summarises the most relevant information.

At 50°C the Ni was not active, as it requires a temperature of 180°C to activate the reaction. The Pd on the contrary was very active and a small amount of Pd (0.6%) showed a very high activity (100% conversion). The Pd was so active in these conditions that also the trace of Pd impregnated in the blank Al_2O_3 samples (0.06 and <0.01 wt% of Pd) catalysed the hydrogenation of crotonaldehyde. After the addition of Pd to Ni-Al_2O_3, the catalyst became active. Both Pd-Ni-Al_2O_3 catalysts were less active than the catalyst without the Ni and with the same amount of Pd so the presence of the Ni contributes negatively to the activity of the Pd. The role of the Ni in decreasing the Pd activity confirms the Pd-Ni interaction.

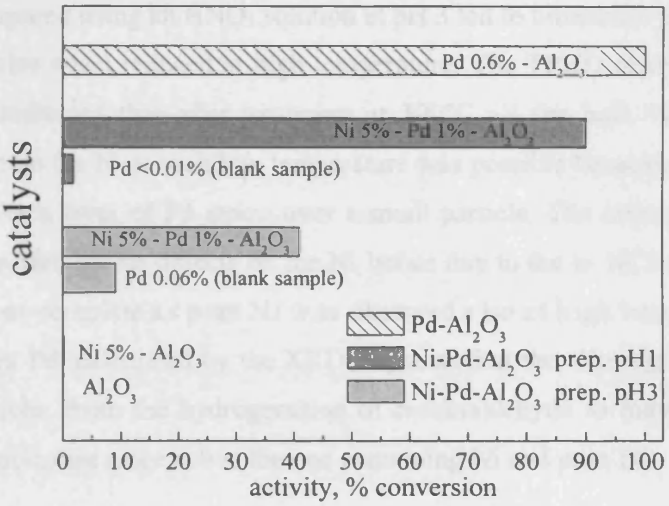

Figure 71. Activity of the specified catalyst reduced at 300°C.

Despite the very similar composition of the two Pd-Ni-Al_2O_3 catalysts the one prepared at pH 1 (in which a better mixing of the metals was achieved) was more active than the one prepared at pH 3 (in which bulk Pd was formed). This is a surprising result considering that we have just asserted that pure Pd is more active than Pd-Ni. In the literature, the most similar system studied is the hydrogenation of butadiene with Pd-Ni catalysts with surface Pd-enriched by segregation. It is reported that the alloy are either equivalent or more active than pure Pd.[40,41] They also proposed an active site made up of ensemble of Pd atoms (two or few more) electronically modified by the surrounding Ni. This information can help to interpret our catalytic data. Considering core-shell (Ni-Pd) particles the presence of the Ni may electronically deactivate the

Pd activity (preparation at pH 3). Only when the particles were alloyed (preparation at pH 1) a synergic effect was observed. In conclusion, the different activity of the Pd-Ni-Al_2O_3 catalysts confirmed the difference observed during the characterization since the greater mixing of the metals coincided with more active catalysts.

6.5 Conclusions

After the optimisation of the condition of the controlled surface reduction, the selective deposition of the Pd over the Ni was achieved. The different acid conditions during the deposition led to the formation of very different core-shell bimetallic particles. The Pd-Ni-Al_2O_3 prepared using an HCl solution at pH 1 produced a bimetallic catalyst with a strong metal-metal interaction that led to the alloy formation when reduced at high temperature. On the other hand the Pd-Ni-Al_2O_3 prepared using an HNO_3 solution at pH 3 led to bimetallic particles that formed large pure Pd particles when reduced at high temperature. The TPHD analysis of Pd-Ni-Al_2O_3 prepared at pH 1 indicated that after treatment at 300°C all the bulk Pd disappeared. The diffusion of the Pd into the Ni at such low temperature was possible because of the nature of the system constituted by a layer of Pd atoms over a small particle. The interphase diffusion may have also been promoted by the defects on the Ni lattice due to the to HCl attack. The alloying of the metal was not complete as pure Ni was observed also at high temperature. The alloy composition reach in Pd, calculated by the XRD, suggests that the alloying did not involve the core of the Ni particle. From the hydrogenation of crotonaldehyde to butyraldehyde emerged that the alloyed particles are more active the one containing Ni and pure Pd.

References

1 F. Gauthard, F. Epron, J. Barbier *J. Catal.* 220 (2003) 182

2 C. L. Pieck, P. Marecot, J. Barbier *Appl. Catal., A* 134 (1996) 319-329

3 C. Micheaud, M. Guerin, P. Marecot, C. Geron, J. Barbier *J. Chim. Phys.* 93 (1996) 1394

4 R. Melendrez, G. Del Angel, V.Bertin, M. A.Valenzuela, J. Barbier *J. Mol. Catal. A: Chem.* 157 (2000) 143

5 F. Gauthard, F. Epron, J. Barbier *J. Catal.* 220 (2003) 182

6 F. Pinna, M. Signoretto, G. Strukul, S. Polizzi, N. Perticone *Reac. Kinet. Catal. Lett.* 60 (1997) 9

7 M. Bonarowska, J. Pielaszek, W. Juszczyk, Z. Karpinski *J. Catal.* 195 (2000) 304

8 M. Bonarowska, J. Pielaszek, V. A. Semikolenov, Z. Karpinski *J. Catal.* 209 (2002) 528

9 M. Boudart, H. S. Hwang *J. Catal.* 39 (1975) 44

10 J. Barbier, P. Marecot, G. Del Angel, P. Bosch, J. P. Boitiaux, B. Didillon, J. M. Dominguez, I. Schiftef, G. Espinosa *Appl. Catal., A* 166 I (1994) 179

11 G. Espinosa, G. Del Angel, J. Barbier, P. Bosch, V. Lara, D. Acosta *J. Mol. Catal.* 164 (2000) 253

12 J. Margitfalvi, S. Szabo, F. Nagy, S. Gobolos, M. Hegedus "*Preparation of catalysis III*" Pub. Elsevier (1983)

13 C. Micheaud, P. Marecot, M.Guerin, J. Barbier *Appl. Catal., A* 171 (1998) 229

14 C. L. Pieck, P. Marecot, J. Barbier *Appl. Catal., A 141* (1996) 229

15 G. Del Angel, A. Bonilla, Y. Pena, J. Navarrete, J. L. G. Fierro, D. R. Acosta *J. Catal.* 219 (2003) 63

16 T. Mallat, Z. Bodnar, P. Hug, A. Baiker *J. Catal.* 153 (1995) 131

17 J. Barbier, P. Marecot, G. Del Angel, P. Bosch, J. P. Boitiaux, B. Didillon, J. M. Dominguez, I. Schiftef, G. Espinosa *Appl. Catal., A* 166 (1994) 179

18 P. Del Angel, J. M. Dominguez, G. Del Angel, J. A. Montoya, E. Lamy-Pitara, S. Labruquere, J. Barbier *Langmuir* 16 (2000) 7217

19 V. Ponec, G. C. Bond "*Catalysis by Metals and Alloys*" (ed. B. Delmon, J.T. Yates) *Studies in Surface Science and Catalysis*, Vol. 95, Pub. Elsevier, Amsterdam (1995)

20 H. Mehrer "*Diffusion in solid metals and alloys*" Vol 26 Pub. Springer Velarg (1990)

21 D. A. Porter "*Phase transformations in metals and alloys*" Ed. David A. Porter, Kenneth E. Easterling, Pub. Van Nostrand Reinhold, New York (1981)

22 J. C. Bertolini, P. Miegge, P. Hermann, J. L .Rousset, B. Tardy *Surf. Sci.* 331-333 (1995) 651

23 R. A. Van Santen, M. A. M. Boersma *Journal of Catalysis* 34 (1974) 13

24 J. L. Rousset, J. C. Bertolini, P. Miegge *Phys. Lett B* 53 (1996) 4947

25 J. F. Faudon, F. Senocq, G. Bergeret, B.Moravueck, G. Glugnet, C. Nicot, A Renouprez *J. Catal.* 144 (1993) 460

26 L. R. Bidwell, R. Speiser *Acta Crystallogr.* 17 (1984) 260

27 D. Briggs, M. P. Seah "*Practical surface analysis*" Pub. John Wiley and Sons (1990)

28 F. B. Rasmussen, J. Sehested, H. T. Teunissen, A. M. Molenbroek, B. S. Clausen *Appl. Catal., A* 267 (1-2) (2004) 165

29 M. Skotak, Z. Karpinski, W. Juszczyk, J. Pielaszek, L. Kepinski, D. V. Kazachkin, V. I. Kovalchuk, J. L. D'Itri *J. Catal.* 227 (2004) 11

30 A. Malinowski, W. Juszczyk, M. Bonarowska, J. Pielaszek, Z. Karpinski *J. Catal.* 177 (1998) 153

31 A. L. Bonivardi, M. A. Baltanas *J. Catal.* 138 (1992) 500

32 S. B. Ziemecki, G. A. Jones, J. B. Michel *J. Catal.* 77 (1986) 207

33 B. J. Joice, J. J. Rooney, P. B. Wells, G. R. Wilson *Discuss. Faraday Soc.* 41. (1966) 223-231

34 S. B. Ziemecki, J. B. Michel, G. A. Jones *React. Solids* 2 (1986) 187

35 M. Bonarowska, J. Pielaszek, V. A. Semikolenov, Z. Karpinski *J. Catal.* 209 (2002) 528

36 M. Boudart, H. S. Hwang *J. Catal.* 39 (1975) 44

37 J. Barbier "*Preparation of solid catalysts*" Ed. G. Ertl, H. Knoezinger, J. Weitkamp, Pub. Wiley-VCH Weinheim (1999) 526

38 I. Bakos, S. Szabo *J. Electroanal. Chem.* 344 (1993) 303

39 M. Albert Vannice, B. Sen *J. Catal.* 115, (1989) 65

40 J. C. Bertolini, P. Miegge, P. Hermann, J. L . Rousset, B. Tardy *Surf. Sci.* 331-333 (1995) 651

41 P. Miegge, J. L . Rousset, B. Tardy, J. Massardier, J. C. Bertolini *J. Catal.* 149 (1994) 404

Chapter 7

7 *In situ* characterisation of vanadium phosphate oxide catalyst

7.1 Introduction

As introduced in section 1.4 vanadium phosphate catalysts (VPO) has attracted the attention of both the industrial and academic world.[1,2,3] The oxidation of butane to maleic anhydride involves the abstraction of 8 hydrogen atoms and insertion of 3 oxygen atoms and is an elegant, complex and fascinating reaction.

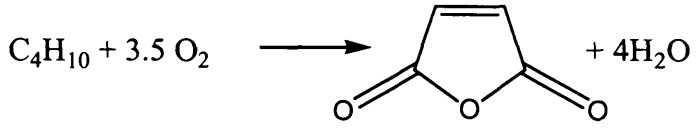

The most active phase for this reaction is reported to be $(VO)_2P_2O_7$ that has been largely studied. Another relevant phase is $VOPO_4$ that has been shown to enhance the efficiency of the catalyst in the production of maleic anhydride.[1,4,5,6,7] There are six well-known $VOPO_4$ phases: α_I, α_{II}, β, γ, δ and ε.[1,8] A seventh polymorph ω-$VOPO_4$ has been studied less as it is unstable at room temperature.[9,10] In this Chapter the investigation of ω-$VOPO_4$ using *in situ* techniques such X-ray diffraction and Raman spectroscopy is reported. The results revealed different, interesting aspects of this phase. ω-$VOPO_4$ under goes a reversible thermal transformation that makes it undetectable at room temperature, while under reaction conditions it is also unstable and shows a fast transformation to δ-$VOPO_4$ activated by the presence of specific gases such butane, acetic acid or hydrogen. Remarkably this transformation is reversible as the ω-$VOPO_4$ can be recrystallised from δ-$VOPO_4$ by heating in oxidising conditions. The *in situ*

transformations of the catalyst observed under reaction conditions can aid the understanding of the real form of the active catalyst and eventually how the catalyst works.

7.2 Results

7.2.1 Formation of ω-$VOPO_4$

Two samples of $VOHPO_4 \cdot 0.5H_2O$ were prepared (following the procedures previously reported[11,12]) from either V_2O_5 or $VOPO_4 \cdot 2H_2O$ and these are denoted VP-o and VP-d respectively (the samples were prepared by the Ph.D student Graham Laing). These $VOHPO_4 \cdot 0.5H_2O$ precursors form highly active catalysts when heated to 400°C under the reactant gas flow of 1.5% butane in air.[13] In the first experiment the hemihydrate was heated at 750°C for 3 h in dry N_2. The heating profile is characterized by steps of 25°C reached at 10°C/min and lasting 25 min. The powder X-ray diffraction was recorded *in situ* at these 25°C intervals.

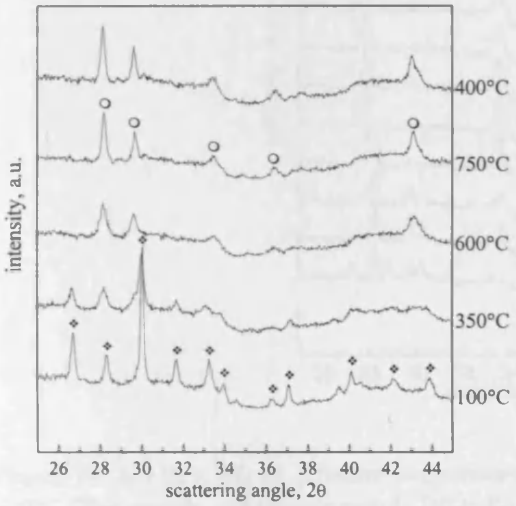

Figure 72. *In situ* XRD recorded at different temperatures during the thermal treatment of VP-O in N_2. VP-o (❖) transforms to pure $(VO)_2P_2O_7$ (❍) at high temperature.

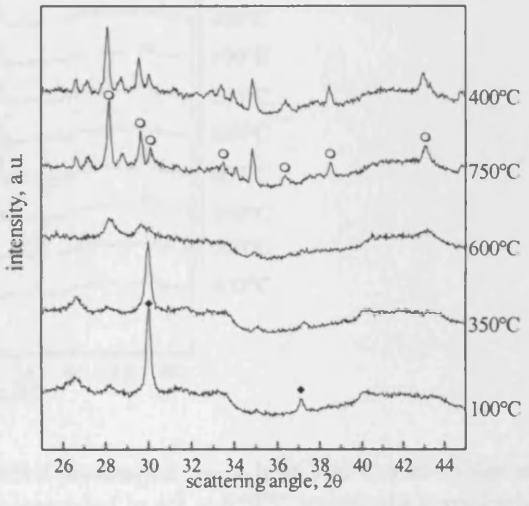

Figure 73. *In situ* XRD recorded at different temperatures during the thermal treatment of VP-d in N_2. VP-d (◆) transforms mainly to $(VO)_2P_2O_7$ (❍) at high temperature.

The VP-o transformed to $(VO)_2P_2O_7$ at 400°C and was stable up to 750°C. The VP-d precursors transformed over a broader range of temperature (350-450°C) to $(VO)_2P_2O_7$ containing a minor

amount of an unidentified phase. Cooling the samples (10°C/min) to 400°C did not result in any changes in the X-ray diffraction patterns obtained at 750°C (Figure 72 and Figure 73).

The samples were then heated in air from 400°C to 750°C with a similar heating program. The $(VO)_2P_2O_7$ derived from VP-o started to transform to ω-$VOPO_4$[14] at 575°C and the transition was complete at 650°C. The ω-$VOPO_4$ phase is stable only up to 675°C. The phases obtained from VP-d also transformed to ω-$VOPO_4$ between 550°C and 625°C, but the ω-$VOPO_4$ obtained from the VP-d sample is stable only up to 650°C (Figure 74).

7.2.2 Thermal stability of ω-$VOPO_4$

ω-$VOPO_4$ was prepared as described above from both VP-o and VP-d by heating in air at 650°C. The samples were then cooled to 100°C in air and the diffraction patterns recorded *in situ* every 50°C. Decomposition of ω-$VOPO_4$ at 350°C to a disordered material phase was observed (Figure 74).

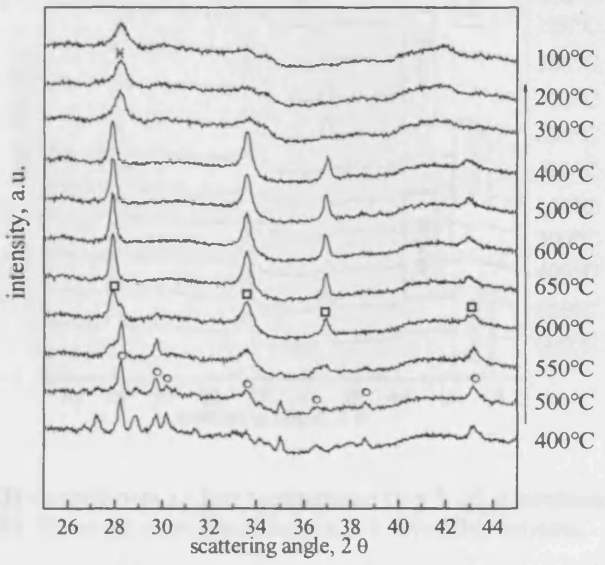

Figure 74. *In situ* XRD at different temperatures of VP-d pre-treated for 3 h at 750°C and cooled at 400°C. This sample, containing mainly $(VO)_2P_2O_7$ (❍), calcinied in air at 650°C transforms completely to ω-$VOPO_4$ (❑). Cooling ω-$VOPO_4$, the structure collapses to a disordered material (✳).

These transformations are summarized in Figure 75. By cycling the temperature between 650°C and 100°C, a reproducible transformation of ω-$VOPO_4$ to disordered material during the cooling steps and the recrystallization of ω-$VOPO_4$ during the heating steps was observed (Figure 76).

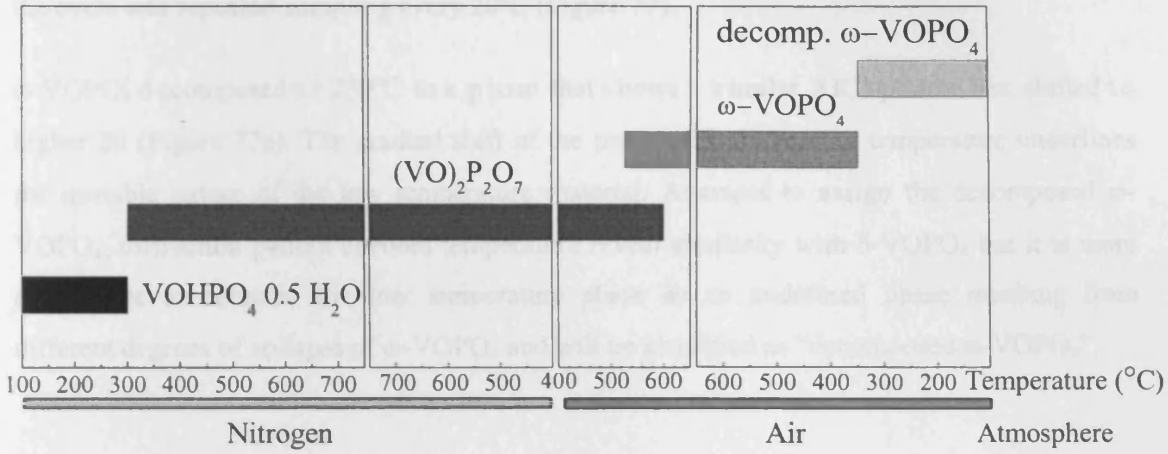

Figure 75. Scheme of the thermal treatment of VP-o. Formation and decomposition of ω-$VOPO_4$.

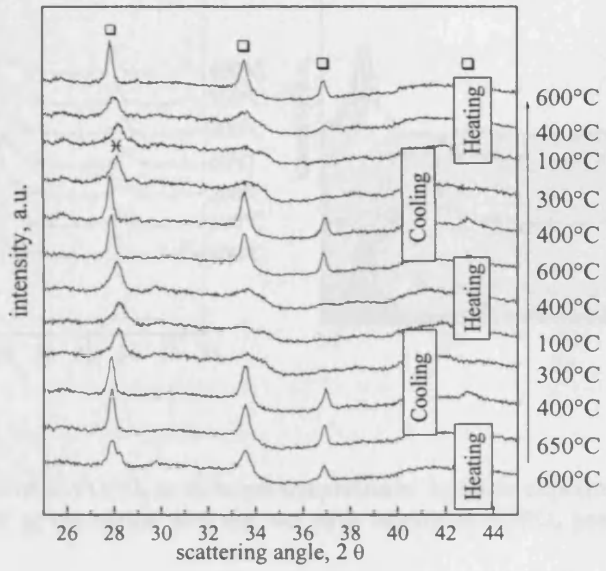

Figure 76. ω-$VOPO_4$ (❑) decomposes at low temperature to a high disordered structure that shows a single broad reflection (✳). However its recrystallization is a reversible process.

Interestingly, it was observed that the crystallization temperature of ω-$VOPO_4$ decreased (from 600°C to 500°C to 450°C) as the number of cycles was increased, while the decomposition temperature was always constant at 350°C. It is probable that, eventually, the system could reach a state where the crystallization and decomposition temperature are the same.

To study the thermal transition between ω-$VOPO_4$ and decomposed ω-$VOPO_4$ in more detail, the cycle was repeated[i] sampling every 20°C (Figure 77).

ω-$VOPO_4$ decomposed at 280°C to a phase that shows a similar XRD pattern but shifted to higher 2θ (Figure 77a). The gradual shift of the peaks with decreasing temperature underlines the unstable nature of the low temperature material. Attempts to assign the decomposed ω-$VOPO_4$, diffraction pattern at room temperature reveal similarity with δ-$VOPO_4$ but it is more appropriate to consider the low temperature phase as an undefined phase resulting from different degrees of collapse of ω-$VOPO_4$ and will be identified as "decomposed ω-$VOPO_4$".

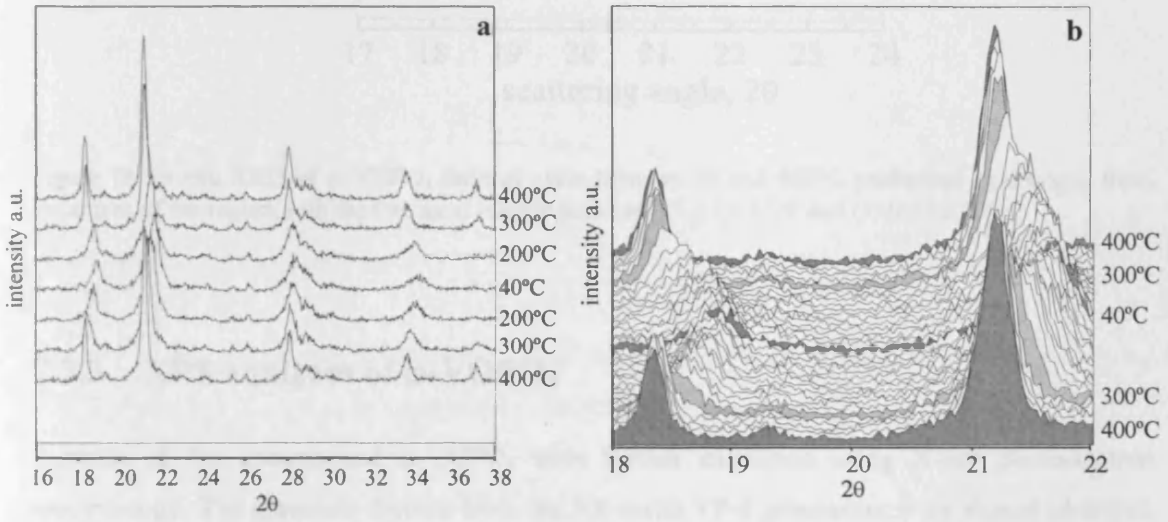

Figure 77 a) *In situ* XRD of ω-$VOPO_4$ at different temperatures. b) Same experiment performed acquiring short patterns every 20°C of the region with the two most intense ω-$VOPO_4$ peaks, (111) at 21.2°2θ and (110) at 18.3°2θ.

The stability of ω-$VOPO_4$ was examined under an inert atmosphere performing a similar cycle of temperature in N_2. The results (Figure 78) show that the transformation also occurs in the absence of oxygen.

[i] This experiment was performed with a similar *in situ* XRD cell mounted on a θ-θ gonimetre located in the Fritz-Haber-Institut in Berlin.

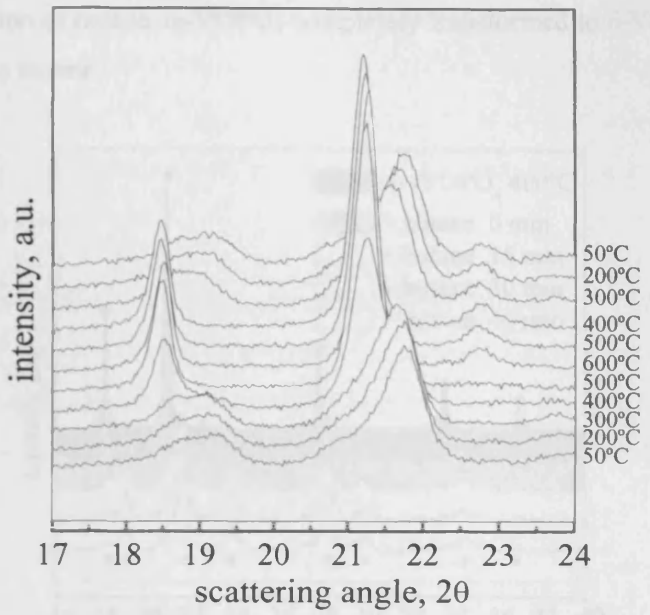

Figure 78. *In situ* XRD of ω-$VOPO_4$ thermal cycle between 50 and 600°C performed in nitrogen flow. Enlargent of the region with the two most intense peaks at (111) 21.2°2θ and (110)18.3°2θ.

7.2.3 XPS analyses of ω-$VOPO_4$

Samples of the decomposed ω-$VOPO_4$ were further examined using X-ray photoelectron spectroscopy. The materials derived from the VP-o and VP-d processors were almost identical, the V(2p) spectra indicating that the surface region of the VP-d (VP-o) derived samples was composed of 78% (73%) V^{5+} species the remainder being present as V^{4+}, no V^{3+} states were observed.[ii]

7.2.4 Stability of ω-$VOPO_4$ to butane

The next experiment was planned to study ω-$VOPO_4$ under reaction conditions adding 1.5% butane to the airflow at 400°C. The *in situ* XRD apparatus in Berlin, where the experiment was undertaken, had on line a mass spectrometer analysing the gases after the reaction. The ω-

[ii] X-ray photoelectron spectra were recorded on the Scienta ESCA 300 instrument at the NCESS facility at Daresbury Laboratory, Cheshire, UK. A monochromatised AlKα rotating anode source was operated at 5 kW and spectra recorded at a pass energy of 150 eV. Samples were mounted mainly as powders using double-sided adhesive tape and sometimes as pressed discs; there were no significant spectral differences observed when both methods of mounting were employed.

$VOPO_4$ sample was prepared from the VP-o $VOHPO_4 \cdot 0.5H_2O$ and held at 400°C in 80ml/min airflow. After the addition of butane, ω-$VOPO_4$ completely transformed to δ-$VOPO_4$ in the first 15 min after exposure to butane.

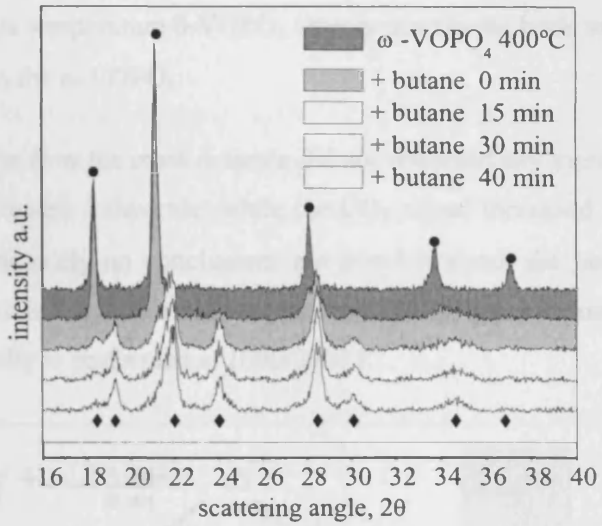

Figure 79. *In situ* XRD of ω-$VOPO_4$ (●) at 400°C in air and effect of the addition of 1.5% butane. ω-$VOPO_4$ transformed to δ-$VOPO_4$ (♦)

In order to define the time scale of the transformation the experiment was performed a second time acquiring a shorter pattern centred at about 21.5°2θ every 2 min (Figure 80).

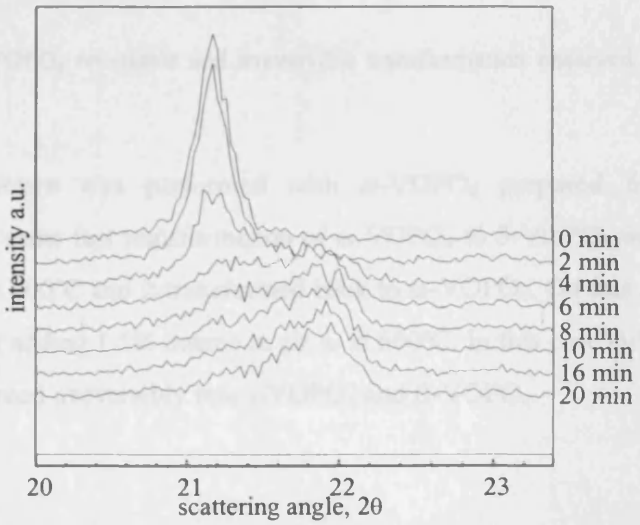

Figure 80. Time-resolved *in situ* XRD. Effect of 1.5% butane in air on ω-$VOPO_4$. The (111) ω-$VOPO_4$ signal transform into the (111) δ-$VOPO_4$.

The transition is advanced after 4 min and complete after 6 min. This is a remarkably fast transformation considering the low concentration of butane involved and the time required to completely fill the dead volume of the cell (about 5 min). Once butane was removed from the flow δ-$VOPO_4$ remained stable. The sample was then cooled to room temperature in air and reheated at 600°C. At this temperature δ-$VOPO_4$ largely transforms back to ω-$VOPO_4$. Cooling to 400°C has no effect on the ω-$VOPO_4$.

After adding butane to the flow the mass detector did not observed any increase of the 98 and 54 masses associated with maleic anhydride, while the CO_2 signal increased suggesting that total oxidation occurs. Unfortunately no conclusions are possible about the possible activity of ω-$VOPO_4$ as the experiment in the *in situ* cell was performed with space velocity of about 8000 h^{-1} while the reaction normally is performed at 1000/2000 h^{-1}.

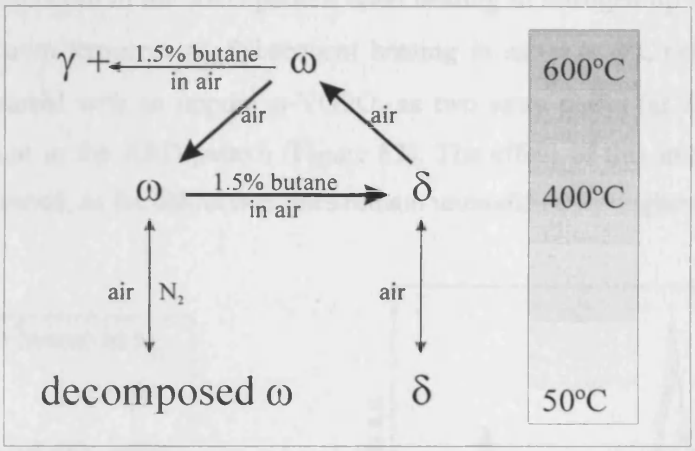

Figure 81. Summary of ω-$VOPO_4$ reversible and irreversible transformation observed between 50 and 600°C.

A similar butane experiment was performed with ω-$VOPO_4$ prepared from the VP-d $VOHPO_4 \cdot 0.5H_2O$, and the same fast transformation of ω-$VOPO_4$ to δ-$VOPO_4$ was observed. δ-$VOPO_4$ was then heated at 600°C and it transformed back to ω-$VOPO_4$. On this sample another experiment was performed adding 1.5% butane in air to at 600°C. In this case ω-$VOPO_4$ reacted with butane and it transformed irreversibly into γ-$VOPO_4$ and β-$VOPO_4$.

7.2.5 Effect of different gases on ω-$VOPO_4$

The structural change of ω-$VOPO_4$ observed under reaction condition offers an opportunity to investigate the role of the atmosphere, and the molecule involved in the catalytic reaction, in modifying the catalyst.

The next series of experiments were designed to study the reactivity and stability of ω-$VOPO_4$ at 400°C with different gases. In all the *in situ* XRD experiments ω-$VOPO_4$ was prepared by heating $VOHPO_4 \cdot 0.5H_2O$ (VP-o) in N_2 at 5°C/min to 550°C. The $(VO)_2P_2O_7$ obtained was cooled down to room temperature and heated in a 60 ml/min airflow at 5°C/min up to 625°C. The ω-$VOPO_4$ formed was cooled to 400°C ready for the tests.

Butane in nitrogen. The first experiment studied the effect of butane on ω-$VOPO_4$ in the absence of O_2. The airflow was switched to N_2 flow (60 ml/min) and left for 2h. 6 ml/min butane was then added to the stream. The XRD results show that the time scale for the transformation is similar to the previous experiment and the transformation is complete after 6 min but, in absence of O_2, δ-$VOPO_4$ is not stable and decomposes after 40 min. Therefore the effect of butane on ω-$VOPO_4$ is the decomposition of the structure to a XRD amorphous phase. No changes were observed in the XRD pattern upon heating in nitrogen up to up to 700°C and cooling down to room temperature. Subsequent heating in air at 600°C reformed ω-$VOPO_4$. This experiment started with an impure ω-$VOPO_4$ as two extra peaks (at 2θ = 22.7 and 28.3 degree) were present in the XRD pattern (Figure 82). The effect of this impurity is, however, considered to be limited, as the diffraction lines remain unmodified throughout all the steps.

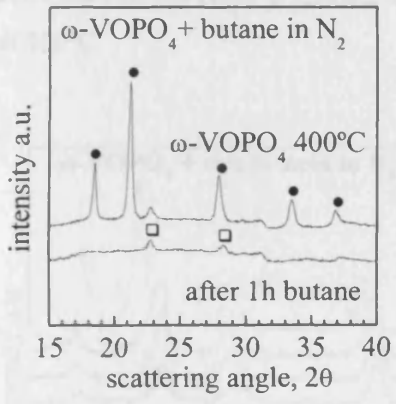

Figure 82. *In situ* XRD of ω-$VOPO_4$ at 400°C in N_2 and effect of the addition of 5% butane.

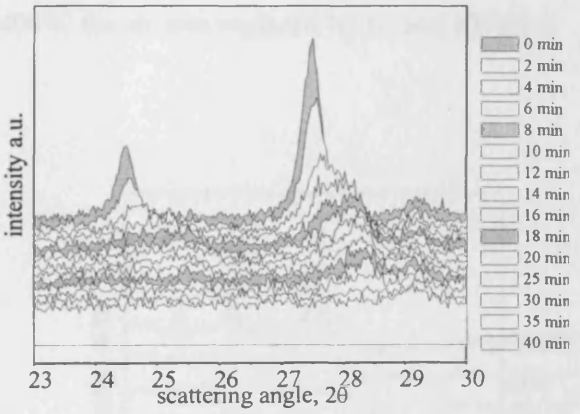

Figure 83. Time-resolved *in situ* XRD. Effect on ω-$VOPO_4$ of 5% butane in N_2 at 400°C. The (110) and (111) ω-$VOPO_4$ signals transform into to the (002) and (111) δ-$VOPO_4$ signals and then disappear.

Acetic acid in air. The next experiment investigated the stability of ω-$VOPO_4$ exposed to acetic acid, a possible by-product of the oxidation of butane. The acetic acid was added by flowing the carrier gas (60 ml/min) through a saturator at 25°C. The amount of acid in the flow was estimated by assuming a stable dynamic equilibrium in the saturator of 3.2%.

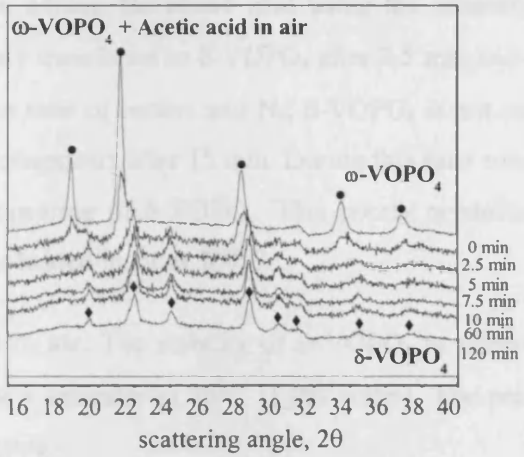

Figure 84. Time-resolved *in situ* XRD of ω-$VOPO_4$ at 400°C in air. Effect of the addition of acetic acid.

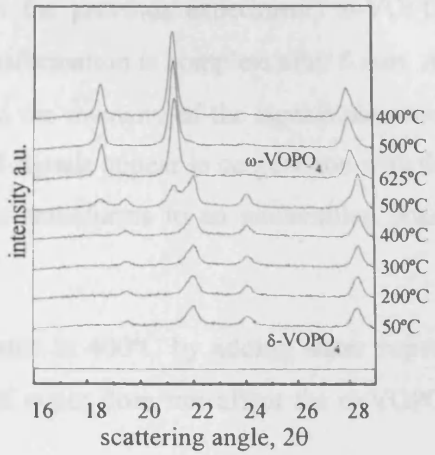

Figure 85. *In situ* XRD of δ-$VOPO_4$ heated at 650°C in air and cooled to 400°C.

Using air as the carrier gas, ω-$VOPO_4$ totally transformed to δ-$VOPO_4$ in less than 5 min (Figure 84). Cooling to room temperature in air and heating to 625°C, transforms δ-$VOPO_4$ back to ω-$VOPO_4$ (Figure 85). On cooling to 400°C ω-$VOPO_4$ remains stable. In a second experiment δ-$VOPO_4$ was heated at 600°C in N_2 and the transition to ω-$VOPO_4$ was not observed.

Acetic acid in N_2. After preparing ω-$VOPO_4$ at 400°C the air was replaced by N_2 and left for 2 h at 400°C.

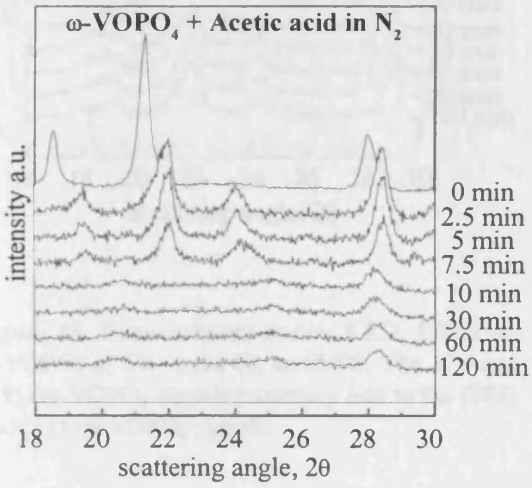

Figure 86. Time-resolved *in situ* XRD of ω-$VOPO_4$ at 400°C in N_2 and effect of the addition of acetic acid.

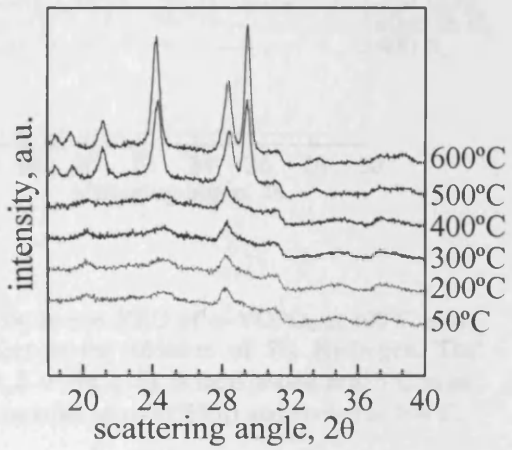

Figure. 87 *In situ* XRD of the poorly crystalline material produced by the reaction between ω-$VOPO_4$ and acetic acid in N_2 (heated in air from 50 to 600°C).

Upon adding the acetic acid using the saturator (as in the previous experiment) ω-$VOPO_4$ largely transforms to δ-$VOPO_4$ after 2.5 min and the transformation is complete after 5 min. As in the case of butane and N_2, δ-$VOPO_4$ is not stable and the intensity of the signals decreases and disappears after 15 min. During this time some broad signals appear in conjunction with the disappearing of δ-$VOPO_4$. This poorly crystalline phase transforms to an unidentified phase when heated in air at 500°C.

H_2O in air. The stability of ω-$VOPO_4$ to water was tested at 400°C by adding water vapour using a saturator at 25°C (1.0% water). The presence of water does not affect the ω-$VOPO_4$ structure.

H_2 in N_2. Introducing 5% H_2 in the N_2 stream (at 400°C), the transformation of ω-$VOPO_4$ into δ-$VOPO_4$ was observed as for the butane and acetic acid experiments. However, the time scale is completely different and the transition starts only after 10 min and requires about 2h to complete (Figure 88). The δ-$VOPO_4$ obtained, however, is the same as in the previous cases and is able to transform back to ω-$VOPO_4$ when heated at 600°C in air (Figure 89).

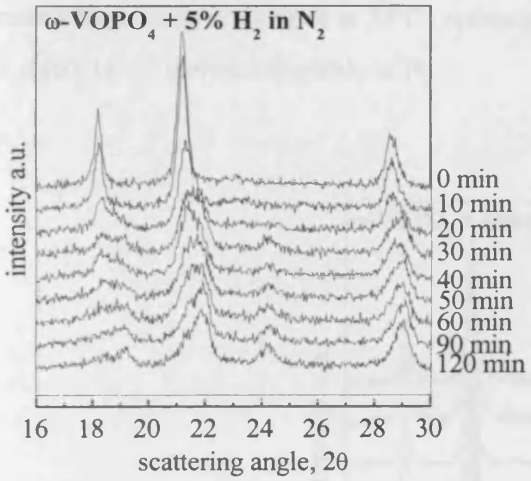

Figure 88. Time-resolved *in situ* XRD. Effect on ω-$VOPO_4$ of 5% H_2 in N_2 at 400°C. The 110 and (111) ω-$VOPO_4$ signals transform into to the (002) and (111) δ-$VOPO_4$ signals.

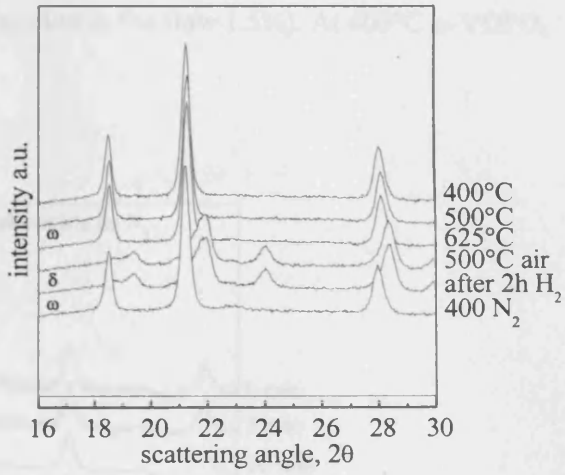

Figure 89. *In situ* XRD of ω-$VOPO_4$ at 400°C in N_2 and effect of the addition of 5% Hydrogen. The product, δ-$VOPO_4$ (δ), is then heated at 625°C in air (transformation to ω-$VOPO_4$) and cooled at 400°C.

CO in Ar. Testing the reactivity of ω-$VOPO_4$ to CO (10%) in Ar we observe that CO activates the transformation of ω-$VOPO_4$ to δ-$VOPO_4$ in 1 around hour (Figure 90). δ-$VOPO_4$ transforms back to ω-$VOPO_4$ at 600°C in air (Figure 91).

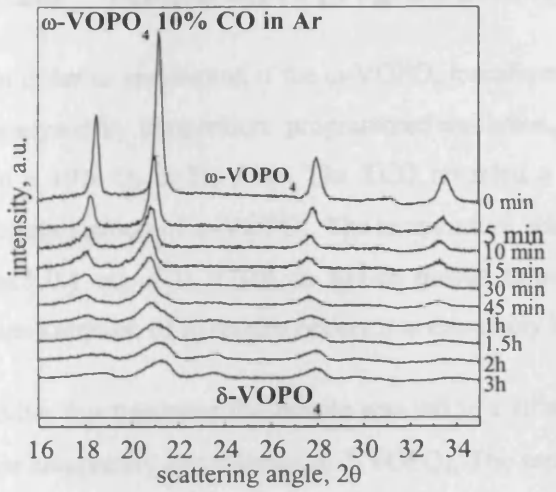

Figure 90. Time-resolved *in situ* XRD. Effect on ω-$VOPO_4$ of 10% CO in Ar at 400°C. The (110) and (111) ω-$VOPO_4$ signals transform into to the (002) and (111) δ-$VOPO_4$ signals.

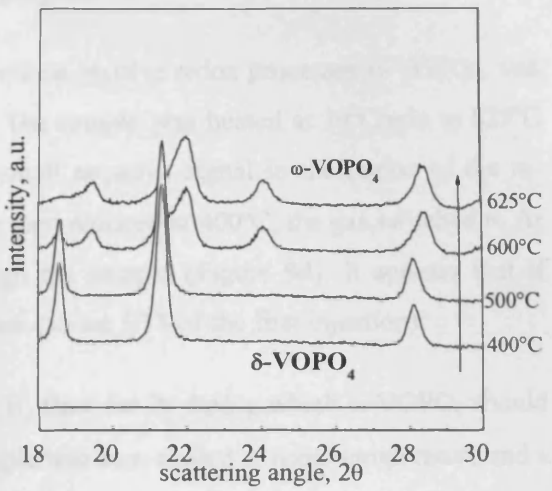

Figure 91. XRD pattern of δ-$VOPO_4$ (400°). Heated in air at 600°C transforms to ω-$VOPO_4$.

Maleic anhydride in N_2. Maleic anhydride is a relatively volatile solid. We introduced it in the carrier flow using a saturator at 55°C (estimated amount in the flow 1.5%). At 400°C ω-$VOPO_4$ is stable to the maleic anhydride in N_2.

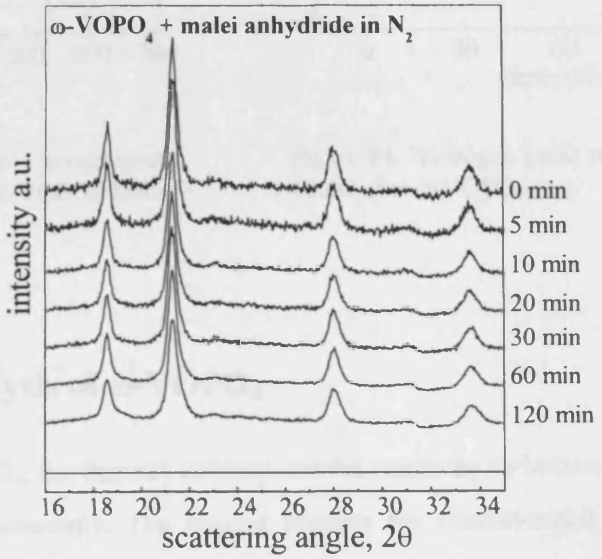

Figure 92. *In situ* XRD of ω-$VOPO_4$ at 400°C (0 min). The sample exposed tomaleic anhydride in N_2 for different times remains stable.

7.2.6 Temperature programmed analysis

In order to understand if the ω-$VOPO_4$ transformations involve redox processes ω-$VOPO_4$, was analysed by temperature programmed oxidation. The sample was heated at 10°C/min to 525°C in a 10% O_2 in He flow. The TCD revealed a small negative signal in the region of the re-crystallisation of ω-$VOPO_4$. The temperature was then reduced at 400°C, the gas switched to Ar and 0.1 ml of H_2 (10% in Ar) as pulsed through the sample (Figure 94). It appears that if consumption of hydrogen occurs it is extremely low (about 1/15 of the first injection).

After this treatment the sample was left in a 10% H_2 flow for 2h during which ω-$VOPO_4$ should be completely transformed to δ-$VOPO_4$. The sample was then cooled to room temperature and a second TPO was performed between room temperature and 700°C. This time a large positive signal is observed that starts at 550°C and reaches a maximum close to 700°C. This consumption of O_2 occurs in the region where δ-$VOPO_4$ transforms to ω-$VOPO_4$.

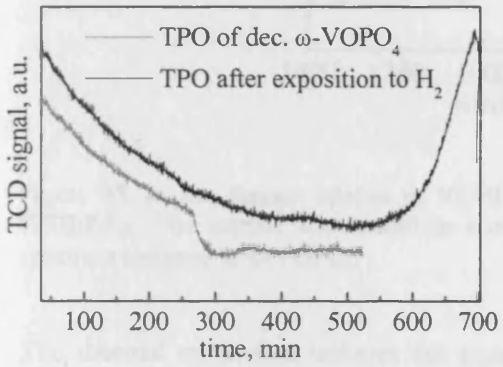

Figure 93. Temperature programmed oxidation of decomposed ω-$VOPO_4$ before and after exposure to H_2.

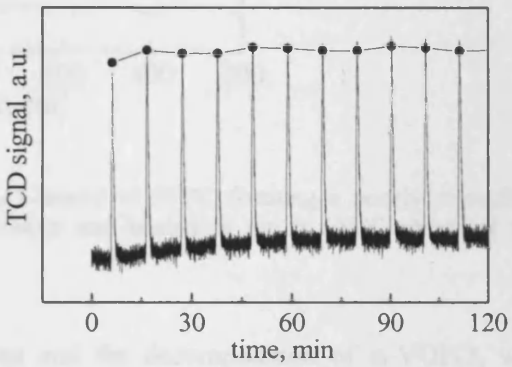

Figure 94. Hydrogen pulse reaction performed a 400°C over ω-$VOPO_4$.

7.2.7 Raman analysis of ω-$VOPO_4$

The formation of ω-$VOPO_4$, the thermal stability and the reactivity to butane, were investigated with *in situ* Raman spectroscopy. The heating profiles are characterized by steps of 25°C reached at 10°C/min.

ω-$VOPO_4$ was prepared in the Raman *in situ* cell starting from $VOHPO_4 \cdot 0.5H_2O$ VP-o. $VOHPO_4 \cdot 0.5H_2O$ was heated at 550°C in N_2 (60 ml/min) and transformed to $(VO)_2P_2O_7$. The comparison of these results with reference spectra,[15,16] confirm the formation of poorly crystalline $(VO)_2P_2O_7$ at 500°C. The sample was cooled to room temperature and heated in air

(60 ml/min) up to 625°C. A transition was observed at 550°C, approximately the same temperature at which $(VO)_2P_2O_7$ transformed to ω-$VOPO_4$ in the *in situ* XRD cell. The new ω-$VOPO_4$ Raman spectra was compared with published Raman spectra and a strong similarity with the spectrum for δ-$VOPO_4$ was found. The main difference was the presence of a single peak at 1084 instead the two peaks at 1090 and 1075 cm^{-1}. The sample was cooled to 50°C and the spectrum was compared with a fresh sample prepared in the *in situ* XRD cell. The two patterns were identical.

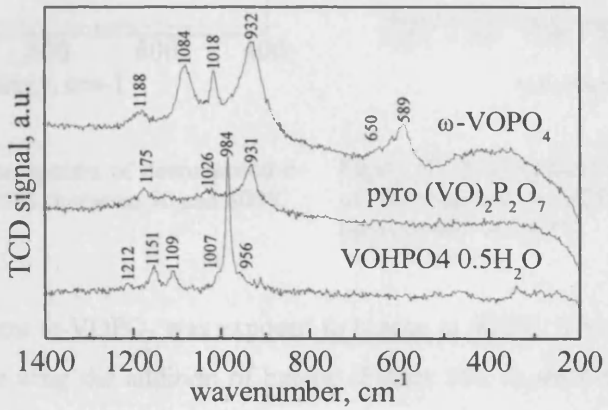

Figure 95. *In situ* Raman spectra of $VOHPO_4 \cdot 0.5H_2O$ heated at 550°C forming a poorly crystalline $(VO)_2P_2O_7$. The sample was cooled to room temperature and heated in air at 625°C obtaining the spectrum assigned to ω-$VOPO_4$.

The thermal cycle that induces the crystallisation and the decomposition of ω-$VOPO_4$ was reproduced in the *in situ* Raman cell. ω-$VOPO_4$ was heated from 50 to 600°C (Figure 96) and cooled to 50°C (Figure 97). The temperature ramp is characterized by steps of 50°C reached at 5°C/min.

Detailed analysis revealed some small difference between the spectra. The signal at 1085 cm^{-1} in the spectrum at 600°C shifts to 1080 cm^{-1} at low temperature (Figure 97). This shift is very small but important as it appears to be reversible and it occurs between 200 and 375°C. In the same range of temperature the peak at 975 cm^{-1} disappears as the temperature increases.

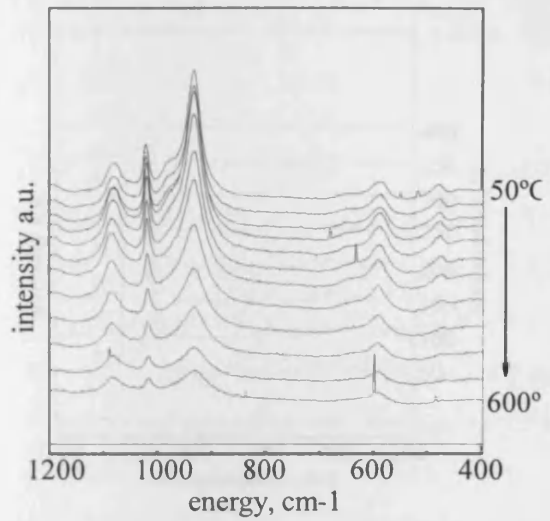

Figure 96. *In situ* Raman spectra of decomposed ω-$VOPO_4$ collected every 50°C between 50 and 600°C.

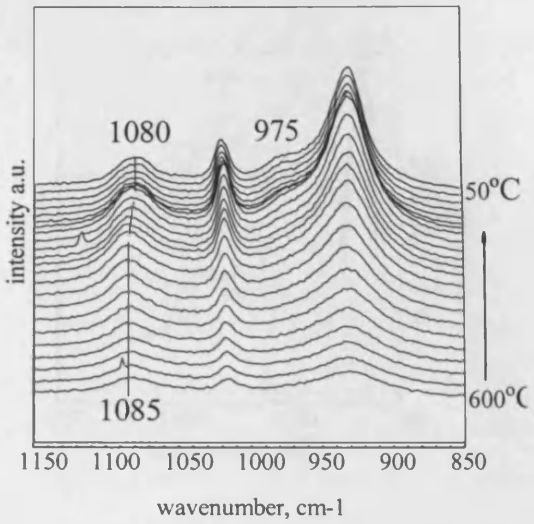

Figure 97. Enlargement of the *in situ* Raman spectra of decomposed ω-$VOPO_4$ collected every 25 °C between 600 and 50°C.

In the next experiment ω-$VOPO_4$ was exposed to butane at 400°C. The Raman spectrum shows very little difference after the addition of butane (Figure 98). A shift of the 1081 cm^{-1} peak to 1079 cm^{-1} (Figure 99) was observed.

When the sample was cooled down (Figure 100) it showed a change in the spectrum, with the 1080 cm^{-1} peak dividing in two parts centred at 1073 and 1088 (Figure 101). This new spectrum can unequivocally be assigned to δ-$VOPO_4$.

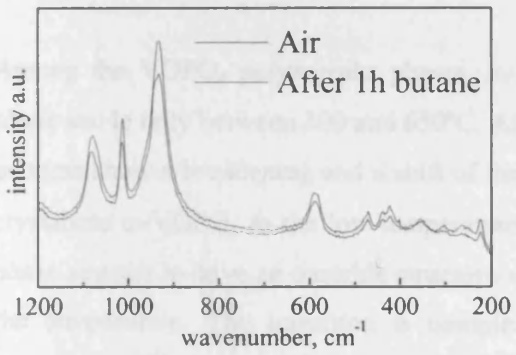

Figure 98. Raman spectra of ω-$VOPO_4$ at 400°C collected in an air flow before and after the exposition to butane 1.5%.

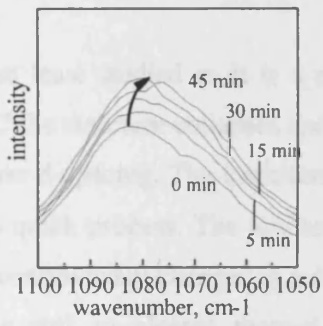

Figure 99. Enlargement of the Raman ω-$VOPO_4$ peak at approximately 1080 cm^{-1} recorded at different times after the addition of 5% butane to the air flow.

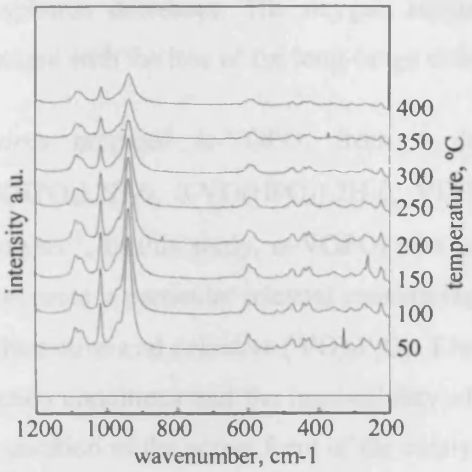

Figure 100. Raman spectra recorded at different temperature (from 400 to 50°C) of the product of reaction between ω-$VOPO_4$ and butane at 400°C.

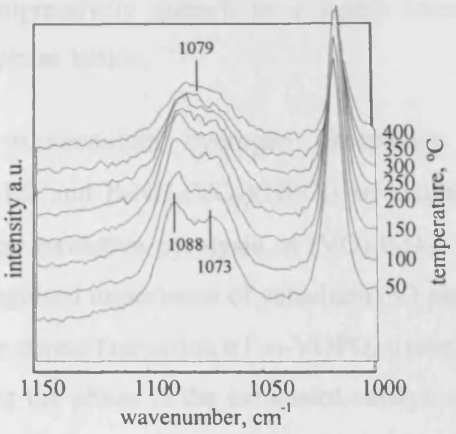

Figure 101. Enlargement of the peak at 1080 cm^{-1} during the cooling step described in Figure 100.

The fast and marked transformation between ω-$VOPO_4$ and δ-$VOPO_4$ observed in the XRD patterns analysis corresponds to very small variations in the Raman spectra. However, the Raman analysis reveals that the butane is active in changing the structure of the sample from ω-$VOPO_4$ to δ-$VOPO_4$.

7.3 Discussion

Among the $VOPO_4$ polymorphs phases, ω-$VOPO_4$, is the least studied as it is a metastable phase stable only between 300 and 650°C. At around 300°C the structure collapses and the XRD patterns show a broadening and a shift of the signal to lower d-spacing. The transition from the crystalline ω-$VOPO_4$ to the low temperature material is a quick process. The low temperature phase appears to have an unstable structure as the pattern continuously changes as a function of the temperature. The transition is completely reversible and an elegant thermal cycle of formation and decomposition, where the crystallinity is perfectly restored at high temperature, can be observed.

The only reference in the literature about ω-$VOPO_4$ are the JCPDS database[14] (where the peaks have been assigned but not the space group) and the work of *Amoros et al.*[9,10] (that concentrates on studying the crystallographic structure). He proposed a dynamic model involving an 'elastic glassy" transition structure containing corner chained VO_6 octahedral units and a two position

twistable phosphate group.[10] At low temperature the movement of the O_2 atoms around the phosphorus decreases. The oxygen atoms will progressively quench in a highly stressed structure with the loss of the long-range order of the phase lattice.

Amoros prepared ω-$VOPO_4$ from 4 different oxovanadium hydrogen phosphates: α-$VO(HPO_4).2H_20$, β-$VO(HPO_4).2H_20$, $VO(HPO_4).4H_20$ and β-$NH_4(VO_2)(HPO_4)$ by oxidative pyrolysis[10]. In this study, ω-$VOPO_4$ was prepared by oxidative pyrolysis of $(VO)_2P_2O_7$. This novel route is particular relevant considering the recognised importance of vanadium (V) phases in the active and selective $(VO)_2P_2O_7$. The possible direct formation of ω-$VOPO_4$ under the reaction conditions and the impossibility of detecting the phase in the exhausted catalyst raise the question of the active form of the catalyst under reaction conditions. Furthermore this route appears highly efficient in producing pure ω-$VOPO_4$ as confirmed by the absence of extra signals in the XRD patterns. This is achieved by heating the $(VO)_2P_2O_7$ to 610°C for 1 h. This temperature prevents the transformation of ω-$VOPO_4$ into α_{II}-$VOPO_4$ and allows the $(VO)_2P_2O_7$ to completely transform to ω-$VOPO_4$. If some $(VO)_2P_2O_7$ remains a second purifying cycle at the same temperature will complete the transformation.

The cycle performed in nitrogen reveals that no extra reagents are needed for the transformation, suggesting that it is a thermally controlled transition. This is confirmed by the differential scanning calorimetric measurement (DSC)[10] that, despite the transition is kinetically quick, does not record any thermal effect.

Once pure ω-$VOPO_4$ has been formed with a good degree of purity the transition temperature occurs in the range 330 and 270°C with a difference of 20-40°C between the heating (formation) and cooling (decomposition) step as the crystallization occurs at slightly higher temperature.

In the experiment reported in section 7.2.2, we observed the transition of decomposed ω-$VOPO_4$ to crystalline ω-$VOPO_4$ at higher temperature (500 and 450°C). This phenomenon was observed also in other samples containing impurity. The decrease of the transition temperature after the cycles at 600°C can be explained by a progressive purification of ω-$VOPO_4$.

The observation of ω-$VOPO_4$ during the catalyst preparation underlines the value of *in situ* techniques in the characterization of a catalyst. Since ω-$VOPO_4$ is generated from $(VO)_2P_2O_7$ the possibility that it plays a role in the performance of the catalysis is real. *Ex situ* analysis would fail to notice this phase and consequently would have provided incomplete information on the actual form of the catalyst.

7.3.1 Effect of different gas on ω-$VOPO_4$

Flowing butane in air (the feedstock for the maleic anhydride) at 400°C over ω-$VOPO_4$ induces the transformation of ω-$VOPO_4$ to δ-$VOPO_4$. The transition occurs in about 4 min that, considered the time for the butane to completely fill the dead volume (5-6.5 min depending from the flow rate), suggests an immediate reaction between the two species. It is remarkable that the surface interaction between the solid catalyst and the butane gas has a profound effect on the bulk structure of the catalyst. This transition occurs between two $VOPO_4$ (V^V) polymorph species and no stoichiometric red-ox processes are expected. When the butane flow is stopped the new phase, δ-$VOPO_4$, is stable in air below 400°C but it transforms back to ω-$VOPO_4$ when heated in air at 600°C completing the cycle (1).

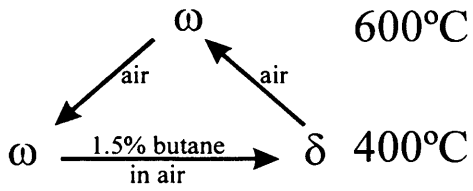

(1)

The *in situ* transformation of ω-$VOPO_4$ under reaction conditions provides an extraordinary opportunity to study the interaction between the reagent gas and the solid catalyst. Understanding the dynamics of the transformation would help in understanding the role of the gaseous reactants (and products) in forging the real form of the catalyst under reaction conditions.

The reactivity of ω-$VOPO_4$ to various gases was tested at 400°C using air or N_2 as carrier gas. After 2-3 h of gas stream, the catalyst was cooled in air at room temperature and heated to 600°C in order to check the possibility of reforming the starting ω-$VOPO_4$ phase. The results are summarized in Table 5. At 400°C ω-$VOPO_4$ is stable both in air and N_2 and also water vapour and maleic anhydride does not alter the delicate structure. But as a small amount of reducing species is added to ω-$VOPO_4$, the transformation to the δ-$VOPO_4$ polymorph is observed. Four different reagents have promoted this transformation. Butane and acetic acid promote the transformation more efficiently as it occurs in just 4 min, while CO and H_2 are less efficient and require about 1-2 h to induce the complete transition. In all the experiments, ω-$VOPO_4$ has transformed to δ-$VOPO_4$ but a further transformation can occur obtaining a non-crystalline material. This second process is possible only in absence of O_2.

Reagent	Carrier gas	
	Air	Inert gas
Butane	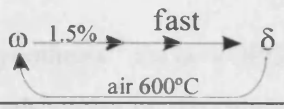	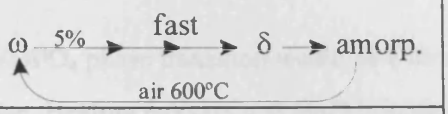
Acetic acid	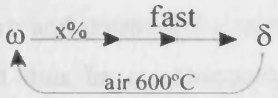	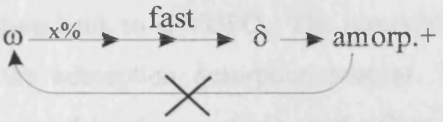
H_2		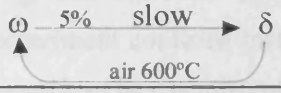
CO		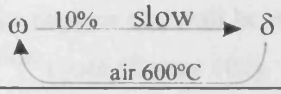
H_2O	ω Stable	
Maleic anhydride		ω Stable

Table 5. Schemes of the reactivity of ω-$VOPO_4$ (ω) with different reactants. It is also indicated if the modified catalyst (δ-$VOPO_4$ (δ), amorphous (amorp.), or amorphous plus a not very crystallite unidentified phase (amorp.+)) can transform back to ω-$VOPO_4$ when heated in air at 600°C.

The reverse conversion of δ-$VOPO_4$ to ω-$VOPO_4$ also yield interesting results. δ-$VOPO_4$ has transformed into ω-$VOPO_4$ every time it has been heated in air at 600°C. Similarly the amorphous material obtained from the butane in N_2 experiment crystallized in air to ω-$VOPO_4$ at 600°C. When reheated in N_2 the amorphous phase was stable up to 700°C.

This suggests that O_2 plays a central role in the formation of the amorphous phase and in its re-transformation to ω-$VOPO_4$. In fact, in the butane and acetic acid experiments, the presence of O_2, stabilizes δ-$VOPO_4$ preventing the possible successive degradation to an amorphous material. In absence of oxygen the lattice oxygen is consumed by the reagents inducing a collapse of the structure. This is confirmed by the need for O_2 to perform the successive re-crystallization of ω-$VOPO_4$.

From these results we can try to define the nature of the gas surface interactions that induces the observed phase transitions. Two different scenarios appear possible:

- The adsorption of the gas on the catalyst could "template" the surface inducing some modification that lead to the atom rearrangement and consecutive phase transition.

- The oxidation of adsorbed species on the catalyst surface (catalytic reaction) may modify the catalyst structure and induce the phase transition.

In the case of the first hypothesis[17] the ω-$VOPO_4$ to δ-$VOPO_4$ phase transition would be a direct consequence of the gas adsorption on the catalyst surface. Heating δ-$VOPO_4$ at 600°C (in air or N_2) the gas would desorb and promote the transformation back to ω-$VOPO_4$. The reversibility of the transition would thus be a consequence of the adsorption desorption process. The decomposition of δ-$VOPO_4$ to amorphous material observed in absence of O_2 in the flow is a consequence of O_2 being consumed by the reagent during the oxidation reaction. The observation of CO_2 in the mass spectrometer in the butane experiment confirms that oxidation processes occur on the $VOPO_4$ catalyst. The oxidation proceeds by the chemisorption of the reactant on the surface and the reaction with the catalyst lattice oxygen that will be replaced by gas phase/adsorbed oxygen following a Mars Van Krevelen[18,19,20] cycle (Figure 102).

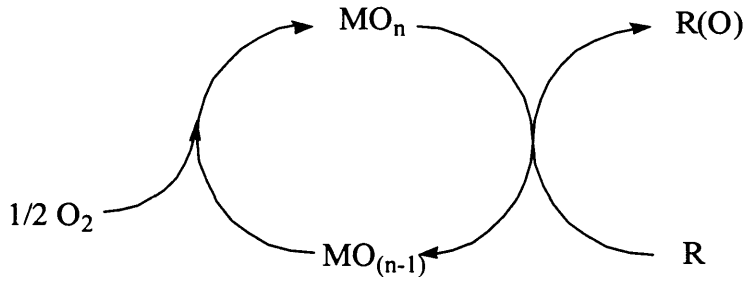

Figure 102. Mars Van Krevelen mechanism. M is a metal in the catalyst and R is the reactant.

In presence of oxygen in the carrier gas the lattice oxygen vacancies can be replaced while in a N_2 atmosphere they cannot. The collapse of δ-$VOPO_4$ into an amorphous structure is thus due to the oxygen vacancies not refilled by the gaseous oxygen. In the butane experiment the amorphous phase (similarly to δ-$VOPO_4$) transformed into ω-$VOPO_4$. This observation leads to the definition of "amorphous with memory" and to important implications. It suggests that the collapsed material has lost the lattice periodicity but still contained some kind of order to preserve the memory of the crystalline phase. The oxygen vacancies have produced disorder without destroying the short range order. Upon heating the amorphous material in N_2 it remains stable, while in air it transforms to ω-$VOPO_4$. Therefore at high temperature in presence of oxygen is possible to re-establish the long-range order by occupying the oxygen vacancies. In the acetic acid N_2 experiment ω-$VOPO_4$ is transformed to δ-$VOPO_4$ that subsequently collapses. In this case an extra phase was observed. The new phase compromised the reversibility of the transformation.

The second hypothesis attributes the transformation from ω-$VOPO_4$ to δ-$VOPO_4$ to the oxidation of the reactant on the catalyst surface that can occur by a Mars Van Krevelen mechanism. As explained above this mechanism implies the mobility of the lattice oxygen. This movement would generate the ω-$VOPO_4$ instability and the transition to δ-$VOPO_4$ (Figure 103).

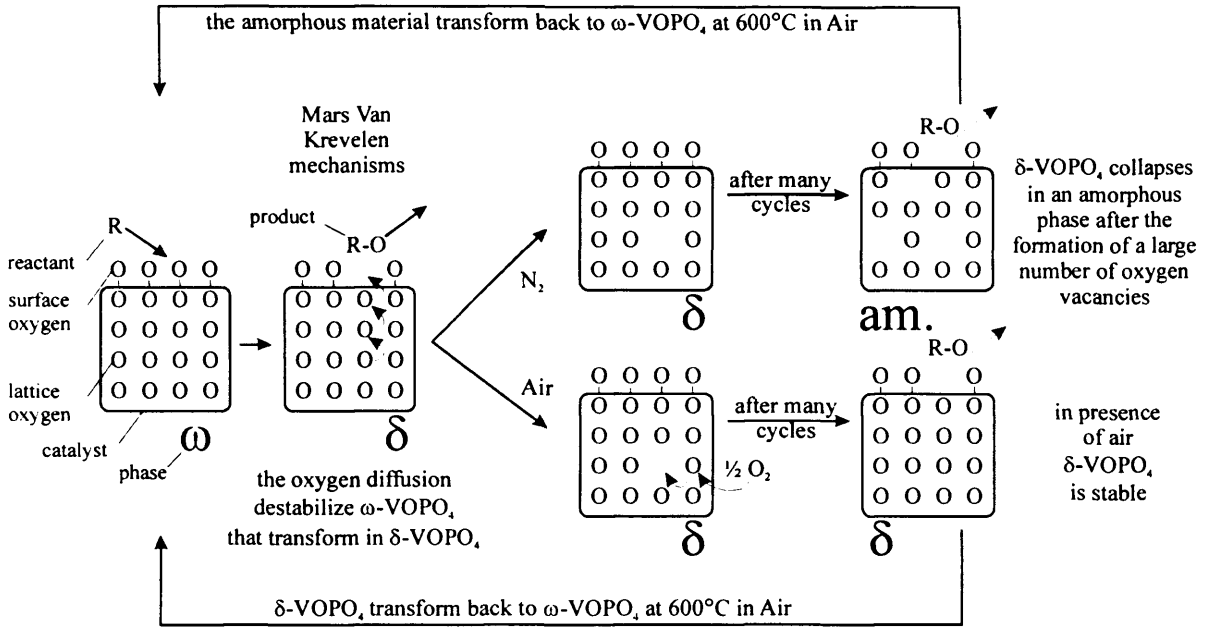

Figure 103. Scheme that correlates the phase transition observed in the experiments with the activity of the catalyst and the mobility of the lattice oxygen following a Mars Van Krevelen mechanism.

In this case, the back transformation from δ-$VOPO_4$ to ω-$VOPO_4$ at 600°C has to be considered a thermal transition. This explanation is in agreement with the observation that δ-$VOPO_4$ when heated in air always transforms to ω-$VOPO_4$ at the same temperature (600°C). The formation of the amorphous material and its re-crystallization can be explained as formation and reoccupation of oxygen vacancies as reported above. The two hypotheses are both possible but the important results from the H_2 and CO analysis cast some doubt on the template mechanism. The addition of H_2 and CO to ω-$VOPO_4$ promotes (as in the butane and acetic acid experiment) the transition to δ-$VOPO_4$. It is difficult to imagine that the adsorption of the small molecules of H_2 or CO induce the same alteration of the ω-$VOPO_4$ structure induced by butane and acetic acid. Moreover, because the adsorption is normally a fast process the explanation of the observed slow transition (1 h) would require the introduction an unlikely milder templating effect. With the second hypothesis the slow transformation can be explained simply by a slower oxidation rate in agreement with the fact that VPO is selective for partial oxidation and so very active for oxidation of C-H bond but not for C=O or H-H bond. These considerations explain also the stability of ω-$VOPO_4$ to maleic anhydride. Since maleic anhydride is the selective product of oxidation of hydrocarbon on VPO we do not expect further oxidization. The absence

of reaction implies the absence of oxygen extraction that, according to the second hypothesis, explains the stability of ω-$VOPO_4$ to maleic anhydride.

In conclusion the data appears to support the second hypothesis better (Figure 103). The ω-$VOPO_4$ to δ-$VOPO_4$ transformation is due to the reorganization of the ω-$VOPO_4$ structure induced by the mobility of the lattice oxygen and the reverse transformation is due to a thermal transition. The formation of the amorphous material depends on formation of lattice oxygen vacancies. The instability of ω-$VOPO_4$ has provided a tool for detecting the mobility of the lattice oxygen during the oxidation reaction. The experiments highlight that this mobility is induced, in a smaller scale, by the oxidation of CO and H_2.

7.3.2 Raman analysis of ω-$VOPO_4$

Raman VPO spectra present two distinct parts: below 700 cm^{-1} and between 850 and 1200 cm^{-1}. The first part is related to the crystal lattice bending modes, coupled vibration and collective modes of the crystal lattice. The second region is related to the vibrational modes of P-O, V-P-O and V-O bonds. Raman bands are rarely attributable to a unique vibration but involve coupling.

ω-$VOPO_4$ was prepared in the *in situ* Raman from $VOHPO_4 \cdot 0.5H_2O$ (obtained from VP-o) following the same thermal path used in the XRD analysis (heating in N_2 at 550°C and successive calcination in air at 630°C). The ω-$VOPO_4$ Raman spectrum reveals an extraordinary similarity with the δ-$VOPO_4$ spectrum. When ω-$VOPO_4$ is cooled to room temperature an important subtle change is recorded, differently from the XRD patterns where strong changes were observed. The main change is the small shift of the 1080 cm^{-1} peak (Figure 97). This shift is very small and it would be normally neglected when comparing spectra collected at 600°C temperature difference. It became relevant as it occurs exactly in the range of temperature where we expect the transition of ω-$VOPO_4$ to decomposed ω-$VOPO_4$ suggesting that the bond associated to this vibration are directly involved in the ω-$VOPO_4$ collapse. The peaks of δ-$VOPO_4$ are compared with those of ω-$VOPO_4$ and decomposed ω-$VOPO_4$ (Table 6).

δ-$VOPO_4$	1200 vW	1090 M	1075 M	1020 M	977 W	936 S	655 W	590 M	482 W	444 vW	428 vW	376 vW	352 W
decomposed ω-$VOPO_4$	1196 W	1081 M		1021 M	974 W	932 S	653 W	586 M	480 W	443 vW	423 vW	372 W	349 W
ω-$VOPO_4$ 400°C	1190 W	1086 M		1019 M		931 S	651 vW	590 M	476 vW	443 vW	420 vW		355 vW

Table 6. Position of the Raman peak (cm^{-1}) of δ-$VOPO_4$, ω-$VOPO_4$ (collected at 400°C) and decomposed ω-$VOPO_4$ (collected at room temperature). S = strong, M = medium, W = weak, vW = very weak.

The main difference between the decomposed ω-$VOPO_4$ and δ-$VOPO_4$ spectra is that the 1081 cm^{-1} ω-$VOPO_4$ signal corresponds to two peaks, 1090 and 1075 cm^{-1}, in the δ-$VOPO_4$ spectrum. *Volta et al.*[15] assigned these two δ-$VOPO_4$ peaks to the same V-$O_{equatorial}$–P coupled because the signals exhibited the same dependence from the temperature. This assignment indicates that the main modification between ω-$VOPO_4$ and decomposed ω-$VOPO_4$ occurs in the V-O-P bonding. The shift of the XRD signal to smaller d-space suggests that a more compact structure is formed. From the Raman result we expect that the VO_6 and PO_4 groups remain substantially unmodified during the collapse while their reciprocal distance and position changes. The model proposed by *Amoros et al.*,[10] consistent of mobile VO_6 and PO_4 groups that quench a low temperature, is in agreement with these results.

The addition of butane to ω-$VOPO_4$ produces the small shift of the 1080 cm^{-1} peak. When the catalyst is cooled to room temperature this signal splits into two peaks, 1088 and 1073 cm^{-1}. This new spectrum fits totally with δ-$VOPO_4$. This means that the butane has induced the transition from ω-$VOPO_4$ to δ-$VOPO_4$ as observed in the XRD. This transition did not occurred as fast as observed recorded in the XRD analysis probably because of the different design of the two *in situ* cells. While in the XRD cell the flow is forced through the powder sample in the Raman cell the gas flow only over the surface of the catalyst. The splitting of the 1080 cm^{-1} signal supports the assignment of *Volta* of 1090 and 1075 cm^{-1} to the same vibrational bond (V-O-P). It also clearly indicates that the instability of ω-$VOPO_4$ and the transformation to δ-$VOPO_4$ are directly connected with the change of V-O-P bond while the VO_6 and PO^4 remain substantially unmodified.

7.4 Conclusions

The ω-$VOPO_4$ study led to interesting results and considerations on three different fronts:

- the study of the metastable ω-$VOPO_4$ phase itself,
- the role of ω-$VOPO_4$ phase in the maleic anhydride production,
- the information on the reaction mechanism obtained exploiting the characteristic transformation of ω-$VOPO_4$ when exposed to different environments and treated at different temperatures.

About the first point we found a new route for the formation of ω-$VOPO_4$. The preparation starts from the active $(VO)_2P_2O_7$ and is very efficient, as in the XRD pattern ω-$VOPO_4$ was the

only phase present. The reversible decomposition of the phase at low temperature was studied *in situ* using narrow intervals of temperature and identifying a precise temperature range of transition. The Raman analysis provided a specific indication that the difference between ω-$VOPO_4$ and the low temperature form involves a variation in the V-O-P bond while the VO_6 and PO_4 groups remain unchanged. The remarkably fast transformation of ω-$VOPO_4$ into δ-$VOPO_4$ induced by the oxidation of the reactant (on the surface of the catalyst) suggests a similarity of the two phases. This was strongly supported by the Raman analysis that showed extraordinary similar ω-$VOPO_4$ and δ-$VOPO_4$ spectra. The only difference was found to be again in the V-O-P bond. In particular δ-$VOPO_4$ showed two different V-O-P coupled stretching vibrations signals while ω-$VOPO_4$ showed only one mode correspondent to the merged δ-$VOPO_4$ signals. This leads again to a model where the VO_6 and PO_4 groups remain unmodified while the V-O-P corner bond change. This information can be useful for the calculation of the unknown structure of both ω-$VOPO_4$ and δ-$VOPO_4$.

ω-$VOPO_4$ was prepared from $(VO)_2P_2O_7$ in air at 450°C. The reaction conditions for the maleic anhydride production are very similar to the conditions necessary for the formation of ω-$VOPO_4$. Therefore the formation of ω-$VOPO_4$ during the industrial process is likely. Obviously ω-$VOPO_4$ cannot be involved in the main catalytic process as it fast transforms to δ-$VOPO_4$ in presence of the reactant but it could play an important role in the activation of the catalyst. For example ω-$VOPO_4$ could be an unknown route for the formation of a certain amount of V^V recognised to be important to increment the catalyst performance. The understanding of the formation and transformation of ω-$VOPO_4$ could contribute to solve the uncertainty concerning the nature of the active sites.

Finally the characteristic transformations of ω-$VOPO_4$ appear as an exceptional opportunity to study the mechanism of reaction. Thanks to results obtained using feedstock with and without oxygen and to the discovery of the reversibility of the transition process, it was possible to correlate the phase transformation from ω-$VOPO_4$ to δ-$VOPO_4$ (and to the amorphous phase) with the oxidation of the reactant on the surface. It was shown how the consumption of surface oxygen and the consequent mobility of the lattice oxygen (predicted by the Mars Van Krevelen) activates the transformation from ω-$VOPO_4$ to δ-$VOPO_4$. Consumption of the lattice oxygen was observed in the absence of oxygen in the feedstock leading to the collapse of ω-$VOPO_4$ and the formation of an amorphous phase. The process was found to be reversible as adding O_2 at 600°C ω-$VOPO_4$ was reformed.

References

1 G. Centi *Catal. Today* 16 (1993) 5

2 G. J. Hutchings *Appl. Catal.* 72 (1991) 1

3 G. Centi, F. Trifiró, J. R. Ebner, V. M. Franchetti *Chem. Rev.* 88 (1988) 55

4 G. W. Coulston, S. R. Bare, H. Kung, K. Birkeland, G. K. Bethke, R. Harlow , N. Herron, P. L. Lee *Science* 275 (1997) 191

5 G. J. Hutchings, J. A. Lopez-Sanchez, J. K. Bartley, J. M. Webster, A. Burrows, C. J. Kiely, A. F. Carley, C. Rhodes, M. Hävecker, A. Knop-Gericke, R. W. Mayer, R. Schlögl, J. C. Volta, M. Poliakoff *J. Catal.* 208 (2002) 197

6 C. J. Kiely, A. Burrows, G. J. Hutchings, K. E. Bere, J. C. Volta, A. Tuel, M. Abon *Faraday Dicuss.* 105 (1996) 103

7 K. Aït-Lachgar, A. Tuel, M. Brun, J. M. Herrmann, J. M. Krafft, J. R. Martin, J. C. Volta, M. Abon *J. Catal.* 177 (1998) 224

8 S. M. Lim, J. T. Vaughey, W. T. A. Harrison, L. L. Dussack, A. J. Jacobson J.W. Johnson *Solid State Ionics* 84 (1996) 219

9 P. Amorós, M. D. Marcos, A. Beltrán, D. Beltrán *Curr. Opin. Sol. State Mater. Sci.* 4 (1999) 123

10 P. Amorós, M. D. Marcos, M. Roca, J. Alamo, A. Beltram-Porter, D. Beltram-Porter *J. Phys. Chem. Sol.* 62 (2001) 1393

11 J. W. Jonson, D. C. Johnston, A. J. Jacobson, J. F. Brody *J. Amer. Chem. Soc* 106 (1984) 8123

12 G. J. Hutchings, D. Lee *J. Chem. Soc. Chem. Commun.* (1994) 1095

13 C. J. Kiely, A. Burrows, S. Sajip, G. J. Hutchings, M. T. Sananes, A. Tuel, J. C. Volta, *J. Catal.* 162 (1996) 31

14 37-809 JCPDS-ICDD – PC PDF database, PA 19073 U.S.A.

15 F. B. Abdelouahab, R. Olier, N. Guilhaume, F. Lefevre, J. C. Volta *J. Catal.* (1996) 134, 151

16 V. V. Guliants, J. B. Benziger, S. Sundaresan, I. E. Wachs, J. M. Jeheng, J. E. Roberts *Catal. Today* 28 (1996) 275

17 G. J. Hutchings, A. Desmartin-Chomel, R. Oliver, J. C. Volta *Nature* 386 (1994) 41

18 P. Schneider, G. Emig, H. Hofmann *Ind. Eng. Chem. Res.* 26 (1987) 11

19 C. Doornkamp, M. Clement, X. Gao, G. Deo, I. E. Eachs, V. Ponec *J. Catal.* 185 (1999) 415

20 P. L. Mills, H. T. Randall, J. S. McCracken *Chem. Eng. Sci.* 54 (1999) 3709

Chapter 8

8 Conclusions

The work in this thesis has dealt with problems concerning the preparation and the characterization of catalysts. The main aim of the project was to understand catalyst preparation and to establish how particle size can be controlled for supported alloy metal catalysts. As a PhD project this is a vast topic that needed to be focused on one of the numerous possible approaches to the problem (sec. 1.3.1). The work was intentionally designed in this way to encourage an original contribution to the research instead of developing and adding to existing ideas. On this basis, the actual research was defined as the study progressed and delineating the strategy was a major objective.

The strategy chosen for the bimetallic catalyst preparation involves the preparation of a single metal parent and the selective reduction of a second metal on the surface of it. Successive thermal treatments were then planned to alloy the particles. This is a novel approach in the panorama of supported alloy preparation. In fact while the selective deposition methods are slowly developing and acquiring importance for the preparation of uniform composition bimetallic supported particles, no previous study had specifically targeted to investigate the possibility to exploit this technique to prepare real alloy particles by thermal treatment.

The work started with the characterisation of the parent catalysts. This preliminary study has occupied a large part of this work leading to interesting results on the Pd-Al_2O_3, Ni-Al_2O_3 and Co-Al_2O_3 single metal catalysts. After the single metal study the deposition of Ni over Pd and of Pd over Ni were attempted. Only the latter system led to the successful preparation of core-shell particles where the Pd covered the Ni. The Pd-Ni-Al_2O_3 bimetallic catalyst was then reduced at different temperature in order to alloy the particle. The results revealed that alloy can be formed at relatively low temperature (300°C).

In the last part of the thesis is presented the *in situ* characterization of ω-$VOPO_4$ (detailed conclusions of this part have been drawn in section 7.4). The study started with the *in situ* XRD characterization ($(VO)_2P_2O_7$ (active catalyst for the oxidation of butane to maleic anhydride). The observation of the little known metastable phase ω-$VOPO_4$ during the process that leads to the oxidation of butane to maleic anhydride defined the start of research focused on the investigation of this phase. The discovery of the reversible quick solid-state transformation between ω-$VOPO_4$ and δ-$VOPO_4$ activated by butane under reaction conditions was found to be an original investigative tool for studying the catalytic process. The study of the transformations of these phases, under a variety of reactant gases, led to important considerations about the reaction mechanism and about the role of the reactants and products in forging the active catalyst. In particular, the transformation from ω-$VOPO_4$ to δ-$VOPO_4$ was found to be directly dependent from the mobility of the lattice oxygen activated by the oxidation of the reactants that proceed by a Mars Van Krevelen mechanism. Different speeds of transition were related with the kinetic of the reaction. In the absence of oxygen in the stream (exclusion of the Mars Van Krevelen cycle) ω-$VOPO_4$ transforms initially into δ-$VOPO_4$ and subsequently into an amorphous phase. This second transformation was induced by the formation of lattice oxygen vacancies generated by the oxidation process. Remarkably, by adding oxygen at 600°C the vacancies can be reoccupied and the original ω-$VOPO_4$ structure reformed.

Figure 104 reports the main steps of this research in its entirety listing the most relevant results obtained in every section of the work. A summary of the results is below reported.

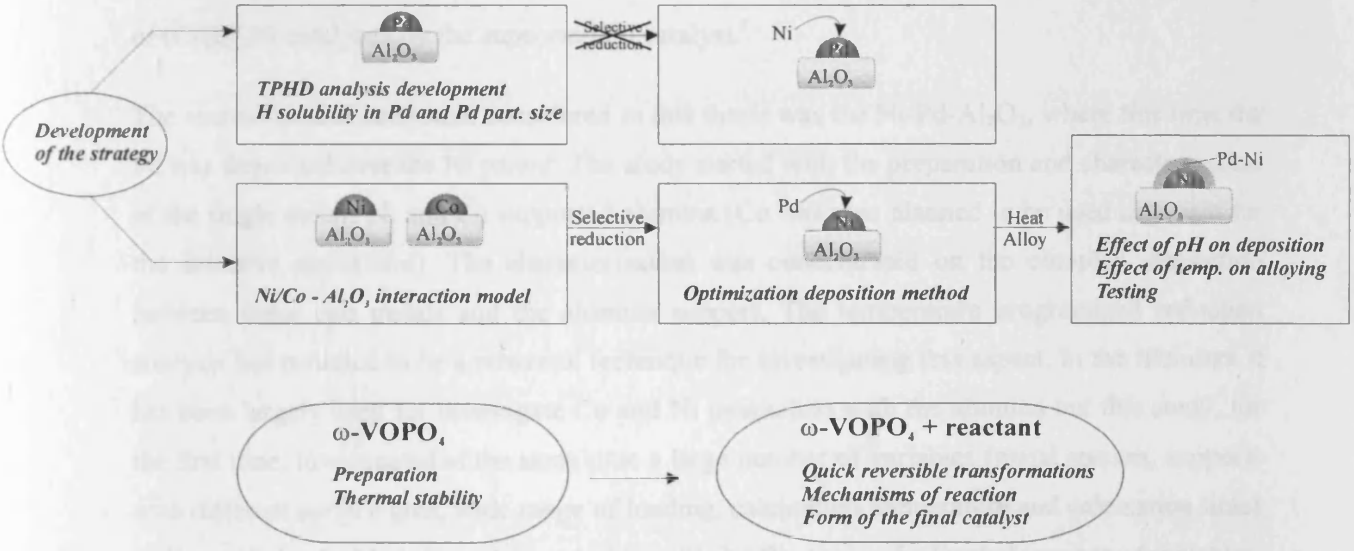

Figure 104. Scheme of the main results reported in this thesis.

A series of single metal Pd-Al_2O_3 catalysts with different dispersion were prepared using different preparation methods. From the *in situ* XRD we have obtained precise information

about the sintering process indicating that in order to avoid large sintering of the Pd particles the thermal treatments have to be performed below 500°C. The temperature programmed hydride desorption analysis used to for the measurement of the amount of hydrogen absorbed into the Pd was developed adding a second step where the hydride adsorption was measured. This allowed the precise measurement of the amount of absorbed hydrogen. The pulse H_2 (and CO) chemisorption was then used to measure the amount of surface Pd from which the fraction exposed and the average particle size could be estimated. The combination of absorption and chemisorptions measurements allowed to well define the solubility of the hydrogen into the bulk Pd as a function of the particle size. The hydrogen solubility also decreases when a second metal was inserted in the Pd crystal structure forming an alloy. The knowledge and skills achieved in measuring the solubility of hydrogen in Pd are thus very important because they can be directly exploited for the difficult characterization of small particles of Pd-based alloy.

The selective deposition of Ni over Pd described in Chapter 5 would have provided an ideal situation to extend the study of the hydrogen solubility and the quantitative correlation with the degree of alloying. Unfortunately, the selective reduction of Ni over adsorbed hydrogen did not occur at any of the examined pH conditions. More investigations were required to define the precise location of the deposited Ni (respect to the Pd) and the role of the adsorbed hydrogen during the deposition step. However, the amount of deposited Ni in presence of the "reducing" hydrogen was very similar to the amount deposited in absence of hydrogen suggesting that the reductive (and selective) mechanism was not operating. An alternative way, that in the future could be used for the selective deposition of Ni over the Pd and is the selective decomposition of $(C_5H_5)_2Ni$ catalysed by the supported Pd catalyst.[1]

The second bimetallic system considered in this thesis was the Ni-Pd-Al_2O_3, where this time the Pd was deposited over the Ni parent. The study started with the preparation and characterization of the single metals Ni and Co supported alumina (Co was also planned to be used as parent for the selective deposition). The characterization was concentrated on the complex interaction between these two metals and the alumina support. The temperature programmed reduction analysis has revealed to be a powerful technique for investigating this aspect. In the literature it has been largely used for investigate Co and Ni interaction with the alumina but this study, for the first time, investigated at the same time a large number of variables (metal species, supports with different surface area, wide range of loading, calcination temperature and calcination time) and provided valuable information not obtainable by the study of a limited number of variables. An overall view on the effect of the different variables was acquired and we were able to propose a general model (valid for both Ni and Co) that describes the formation and the transformation of three reducible species. The understanding of the formation and reduction of

these oxide precursors is an important step for the optimisation of the condition for the preparation of the metal catalyst.

Ni-Al_2O_3 was finally used as parent for the reduction of Pd over selectively adsorbed hydrogen. The use of Ni as metal parent is not reported in the literature, as noble metals were normally preferred. The results shown that the selective deposition is possible and Ni particle with Pd deposited on its surface were prepared in two different acid conditions. The bimetallic particles were then reduced at different temperature to promote alloying. The characterisation of nano-particles supported alloy is notoriously difficult. In this study the combination of XPS, *in situ* XRD and temperature programmed hydride desorption provided useful information for the evaluation of the degree of alloying as a function of the reduction temperature.

Surprisingly the different acid conditions lead to the formation of very different core-shell bimetallic particles. The Pd-Ni-Al_2O_3 prepared using an HNO_3 solution at pH 3 and reduced at high temperature did not formed alloyed particles but large pure Pd particles. The Pd-Ni-Al_2O_3 prepared using an HCl solution at pH 1 produced a bimetallic catalyst with a strong metal-metal interaction. These bimetallic particles formed Ni-Pd alloy when reduced at 300°C or higher temperature. The Pd diffusion into the Ni at such low temperature was possible because of the nature of the system constituted by a layer of Pd atoms over a small particle. The alloy composition calculated by the XRD indicates that alloy reach in Pd was formed suggesting that the alloying at lower temperature do not involve the core of the Ni particle. Finally the hydrogenation of crotonaldehyde to butyraldehyde showed that alloyed particles were more active than the one containing pure Pd.

The work performed demonstrates how the selective deposition method can be used for the preparation of supported alloy nano-particles. The control of the alloy particle size is directly dependent from the dimension of the metal parent particles and the uniformity of the composition of the alloy particle is ensured by the nature of the selective deposition method itself. In the Ni-Pd system alloy particles were prepared using relatively low reduction temperature. The measurements of the solubility of the hydrogen in Pd revealed to be very useful in studying the bimetallic system especially when the particle were too small for an X-Ray diffraction analysis.

In the literature, it is reported that the thermal treatment of Pt-Au bimetallic particles, prepared by selective deposition,[2] led to the aggregation of the deposited metal in pure metal particles. We have observed that the acid conditions during the Pd reduction were crucial in promoting the formation of pure Pd particles or activating the alloy formation. This is a very important observation as it can lead to progress in the preparation of small alloy particles at low

temperature. Further investigations are necessary to define the deposition mechanism that produced bimetallic particles that can be alloyed by thermal treatment. For this purpose two main steps were identified: 1) the transmission electron microscopy analysis of the samples before and after the thermal treatment, 2) the preparation of Pd-Ni-Al_2O_3 by direct redox reduction and successive characterization for the comparison with the Pd-Ni-Al_2O_3 catalysts described in this work.

Another important aspect that will be developed is the catalytic test of the samples. The crotonaldehyde hydrogenation did not offered the ideal conditions to study the Pd-Ni system because of the large difference in activity of Ni and Pd and because the catalysts were active only to the hydrogenation of the C=C group. The hydrogenation of acetylene was selected for further catalytic tests (sec 1.3.5).

The next bimetallic catalyst of interest is Co-Pd-Al_2O_3. A preliminary TPHS analysis suggested that alloy could be formed after reduction at 300°C.

The work on ω-$VOPO_4$ will proceed with *in situ* EPR analysis and catalytic test for the oxidation of butane to maleic anhydride. Furthermore, the structural similarities emerged between ω-$VOPO_4$ and δ-$VOPO_4$ will be the starting point for an EXAFS and XRD study designed to solve the structure of the two phases.

References

1 J. F. Faudon, F. Senocq, G. Bergeret, B. Moravueck, G. Glugnet, C. Nicot, A. Renouprez *J. Catal.* 144 (1993) 460

2 P. Del Angel, J. M. Dominguez, G. Del Angel, J. A. Montoya, E. Lamy-Pitara, S. Labruquere, J. Barbier *Langmuir* 16 (2000) 7217